INVESTIGATION OF CAMKII ACTIVATION:

A MODEL OF SELF-REGULATION

By

Laurel Hoffman

Dissertation

Submitted to the Faculty of the

Graduate School of Vanderbilt University

in partial fulfillment of the requirements

for the degree of

DOCTOR OF PHILOSOPHY

in

Molecular Physiology and Biophysics

December, 2011

Nashville, Tennessee

Approved:

Aurelio Galli, Ph.D.

Albert Beth, Ph.D.

Sharron Francis, Ph.D.

Walter Chazin, Ph.D.

To my family;

David, Sue Ann, Nathan, Adam, Sarah, Lily, Ben,

and my Nashville family of friends

ACKNOWLEDGEMENTS

I would like to thank the National Institutes of Health for my funding my pre-doctoral fellowships through the Vanderbilt Vision Research Center training grant as well as the National Institute of Mental Health individual Ruth L. Kirschstein National Research Service Award. There are so many who helped me along the journey of becoming a scientist. I am grateful for the mentoring and insight of my committee members, Aurelio Galli, Al Beth, Walter Chazin, and Sharron Francis. Our discussions were invaluable as they generated new ideas while keeping my project on track.

I am also very thankful for the past and present members of the Mchaourab laboratory. The diversity of our group not only brought knowledge and new scientific perspective to the table, but also culture from all corners of the world. I value the friendships I have made and the camaraderie and support they offered. I would like to especially thank Hanane for teaching me her molecular biology secrets and Derek for training me on all the instruments. This project would not be possible without the support of our collaborator Roger Colbran. Not only is he a CaMKII expert, but he must know every paper and experiment ever published on CaMKII. Needless to say he was a tremendous resource as we embarked on this new to our lab project. And most importantly, I would like to thank my mentor Hassane Mchaourab. I feel lucky that I got to work under a fantastic scientist and that he agreed to let me work on a project of my choosing. He values the educational aspect of graduate school above all and made it a true learning experience for me. Finally I would not have survived with out the love and support of my family and friends. This achievement belongs to all of us.

TABLE OF CONTENTS

LIST OF TABLES

LIST OF FIGURES

LIST OF ABBREVIATIONS

AC-2 ..... Autocamtide-2
AMPAR ..... α-amino-3-hydroxy-5-methyl-4-isoxazolepropionic Acid Receptor
AngII ..... Angiotensin II
BDNF ..... Brain Derived Neurotrohpic Factor
CaM ..... Calmodulin
CaMKII ..... Calcium/Calmodulin dependent Kinase II
CD ..... Circular Dichroism
CREB ..... Cyclic AMP-response Element Binding protein
CW ..... Continuous Wave
DEER ..... Double Electron-Electron Resonance
D135N ..... 10His CaMKII, residues 1-340 with inactivating mutation
D135N* ..... 10His CaMKII, residues 1-340 on cysteine-less background with inactivating mutation
EM ..... Electron Microscopy
EPR ..... Electron Paramagnetic Resonance
FID ..... Free Induction Decay
FFT ..... Fourier Transformation
GST ..... Glutathione S transferase
LTD ..... Long Term Depression
LTP ..... Long Term Potentiation
MOMD ..... Microscopic Order/ Macroscopic Disorder
MTSSL ..... (1-oxyl-2,2,5,5-tetramethylpyrroline-3-methyl) Methanethiosulfonate Spin Label
NMDAR ..... N-methyl D-aspartate type glutamate Receptor
PMCA ..... Plasma Membrane Ca^{2+}-ATPases
PP1 ..... Protein Phosphatase 1
PP2A ..... Protein Phosphatase 2A
PSD ..... Post Synaptic Density
RGCs ..... Retinal Ganglion Cells
SAXS ..... Small Angle X-ray Scattering
SDSL ..... Site Directed Spin Labeling
SDS-PAGE ..... Sodium Dodecyl Sulfate Polyacrylamide Gel Electrophoresis
SERCA ..... Sarco-Endoplasmic Reticulum Ca^{2+}-ATPase
T286E* ..... 10His CaMKII, residues 1-340 on cysteine-less background with inactivating mutation and 286 phosphorylation mimic
WT ..... 10His CaMKII, residues 1-340
WT* ..... 10His CaMKII, residues 1-340 on cysteine-less background

CHAPTER I

STRUCTURE AND FUNCTION OF CaMKII

Introduction

Calcium-calmodulin dependent protein kinase II, or CaMKII, has fascinated scientists for decades and many have spent their entire careers captivated by this enzyme. It is relevant to diverse disciplines due to the fact that it's found in all human cell types and mediates various biological processes. One of the most important aspects of CaMKII is the critical role it plays in memory. It's hard to imagine anything more essential to survival, preservation of culture, and emotional experience than memories. This is illustrated by the tremendous value we place on acquiring new information and concepts, safeguarding cultural traditions, documenting histories, and preserving a loved one's capacity to remember. Presently we do not completely understand how memories are able to store, retain, and recall information and experiences. The investigation is underway and proteins key for the biochemical processes associated with memory are currently being identified and characterized. CaMKII has been deemed one of the "memory molecules" and with every new discovery, the significance of this enzyme is confirmed. Investigation of CaMKII not only aids in understanding memory and other biological processes, but also contributes to establishing the global properties of proteins in general. For instance, the knowledge gained from studying this protein also helps answer fundamental scientific questions applicable for proteins, such as how a protein's

structure defines its function. In the case of CaMKII, its unique features and structure endow the enzyme with a sophisticated mechanism that is truly remarkable.

CaMKII is integral in long term potentiation

In the brain CaMKII is critical for the normal regulation of synaptic transmission (reviewed in [1]). Brain regions such as the hippocampus, amygdala, striatum, and mammillary bodies are involved in memory, each integral in a specific type of memory. For example the amygdala is thought to govern emotional memory while the hippocampus is largely responsible for spatial learning and declarative learning. These brain regions are made up of complex networks of neuronal cells connected by synapses which provide a system for inter-cell chemical communication. Learning and memory are attributed to chemical changes in these synapses, thought to be mediated by long-term potentiation (LTP) and long-term depression (LTD) [2,3]. While LTP describes a long enhancement in signal transmission resultant from synchronous stimulation between neurons [2], LTD is an activity-dependent reduction in the neuronal synapse efficacy, which can last for hours [3]. These mechanisms underlie the ability of synapses to change their strength, a phenomenon referred to as synaptic plasticity [4].

Signal sensitivity is strengthened by increasing the number of neurotransmitter receptors on the postsynaptic cell [5]. The mechanisms by which this occurs requires a cascade of molecules working together through protein-protein regulatory interactions, and cross talk with other signaling pathways [6]. In the case of a glutamatergic synapse, neuronal excitation allows cells to communicate by release of glutamate neurotransmitter. Receptors on the postsynaptic neuron, such as N-methyl D-aspartate type glutamate

receptors (NMDAR) and α-amino-3-hydroxy-5-methyl-4-isoxazolepropionic acid receptors (AMPAR), receive chemical signals by binding neurotransmitters released from presynaptic neurons (Figure 1.1). In turn this causes depolarization of the membrane and influx of calcium (Ca^{2+}) through NMDA receptors into the dendritic spine, which contains the postsynaptic density (PSD), a region where signaling and scaffolding molecules are closely packed. The Ca^{2+} cation, being extremely potent and highly reactive, is arguably the most utilized second messenger in signaling. Therefore, the influx of this molecule into the PSD is tightly regulated to mediate a myriad of diverse responses. In the case of LTP and many other instances, Ca^{2+} transients are sensed by ubiquitous calmodulin (CaM), a Ca^{2+}-dependent protein that binds and activates numerous enzymes [7]. Of its targets, calmodulin notably activates the family of Ca^{2+}-calmodulin dependent protein kinases, including CaMKII. CaMKII activity is therefore tightly coupled with Ca^{2+} transients, serving to propagate and interpret signals through the phosphorylation and assembly of several substrates [8,9,10].

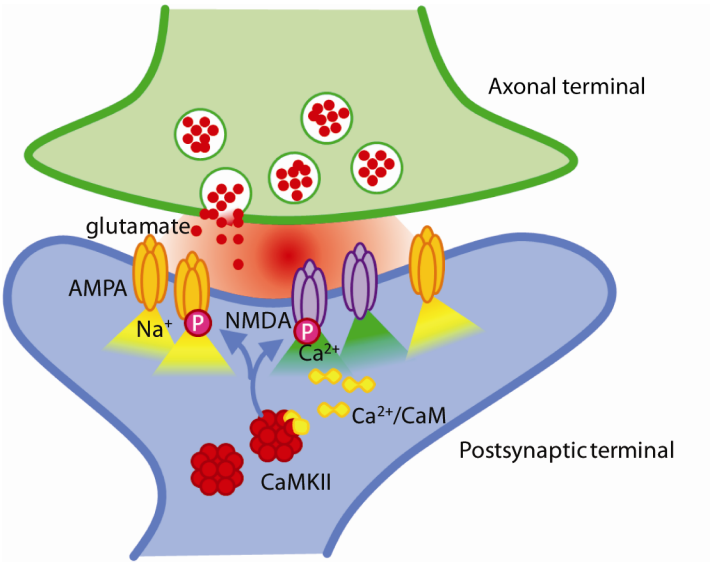

Figure 1.1 CaMKII involvement in long term potentiation of glutamatergic synapses. This figure was adapted from Sheng et al., 2007 [11]. Chemical signals traverse synapses between the axonal terminal (green) and postsynaptic terminal (blue) by release of glutamate neurotransmitter (red dots) into the synapse. Receptors including AMPAR (gold) and NMDAR (purple) bind glutamate and cause the influx of sodium and calcium during depolarization of the membrane. Increases in calcium in the postsynaptic density are sensed by ubiquitous calmodulin (yellow) which activates CaMKII (red clusters) in turn. Once active, CaMKII phosphorylates numerous substrates including AMPA and NMDA receptors to modulate calcium signaling.

Phosphorylation is a highly specific modification which incorporates a negatively charged phosphate from ATP onto a phospho-accepting amino acid, frequently modifying the activity of the substrate protein. This is the way in which CaMKII is able to propagate signaling cascades to modify function of downstream proteins and produce biochemical consequences. The phosphorylation of substrates is an event that is tightly regulated as proteins need to be activated and inhibited at appropriate times in appropriate places. Phosphorylation reactions are reversed by phosphatases to induce the opposite effect on substrate activity. Synaptic plasticity requires this buffering of phosphorylation and therefore a balance between kinases and phosphatases must be maintained for normal cellular function. This is but one of many cellular and biochemical mechanisms in place to regulate the effect of CaMKII activity.

Among the proteins which undergo phosphorylation modifications are the NMDA and AMPA receptors. In this manner CaMKII-mediated phosphorylation can serve as a positive modulator of receptor function, modifying the very signals which activated the enzyme initially. CaMKII is also one of the critical proteins for the trafficking of receptors in and out of the PSD, although the molecular mechanism by which the number of neurotransmitter receptors increases is not completely understood [1,12,13]. Through trafficking and phosphorylation of neurotransmitter receptors, CaMKII has been shown to be critical for regulation of synaptic transmission and integral in complex cognitive behavior like learning and memory [1,14,15,16,17,18,19].

CaMKII plays a role in diseases with excitatory synaptic transmission abnormalities

Much of the current knowledge of the role of CaMKII in these cascades has come from studying memory and learning disorders. For example, alterations in CaMKII activity are observed in a mouse model of Angelman Syndrome, a complex mental disability characterized by intellectual and developmental delay [20]. Research on the disease model showed that behavioral phenotypes of these mice are corrected by knock-in mutations that compensate for CaMKII hypoactivity [21]. CaMKII activity is also misregulated in dopamine-depleted rodent striatum, and the associated Parkinsonian symptoms can be corrected by CaMKII inhibition [22,23]. Furthermore, this enzyme plays roles in mental health disorders and drug addiction since glutamate signaling interfaces with dopamine pathways. Antidepressants desipramine and reboxetine have been shown to up-regulate CaMKII, acting through a complex mechanism suggested to affect CaMKII expression and localization [24,25,26]. Additionally the enzyme plays a

role in cocaine addiction through reward pathways [27]. Because CaMKII is implicated in numerous diseases, it is a promising target for drug development.

With approximately 40 known substrates [1,28,29,30,31], CaMKII plays pivotal roles in several signaling pathways beyond learning and memory. In one example, CaMKII has been implicated to regulate a neuroprotective mechanism associated with glaucoma, a disease characterized by the death of retinal ganglion cells (RGCs) (reviewed in [32]). The permanent loss in vision caused in glaucoma has been linked to an excessive activation of glutamate receptors, causing high intracellular concentrations of calcium [33,34]. Extreme levels of Ca^{2+} devastate the ionic balance critical for normal cellular function and induce neurotoxicity, activate apoptosis, and cause eventual death of RGCs [35]. However, cell survival mechanisms induce the production of brain derived neurotrophic factor protein (BDNF) which promotes cell survival by inhibiting apoptosis [36]. It is the interplay of these signaling cascades which decide cell fate.

CaMKIIα_B contains a nuclear localization sequence which aids in the translocation to the nucleus where CaMKII has been shown to be involved in the survival response of RGCs [37]. Previously it has been shown that NMDA receptor activation stimulates transcription of this particular nuclear form of CaMKII [38] and although the mechanism is not entirely clear, it is hypothesized that excessive glutamate signaling kindles this pathway. Indeed, specific knock down of CaMKIIα_B by RNAi was shown to significantly enhance glutamate induced death of RGCs [37]. In the nucleus CaMKII plays a role in Ca^{2+} mediated transcriptional regulation of genes through phosphorylation of transcription factors including CREB (Cyclic AMP-response Element Binding protein) [39,40,41,42]. CREB is thought to act as a neuroprotective protein against glutamate

receptor induced neurotoxicity by promoting expression of pro-survival genes including BDNF [43].

While nuclear CaMKII has been shown to regulate the expression of BDNF, cytoplasmic CaMKII is involved in secretion of BDNF [32]. It has been suggested that since CaMKII has been shown to be associated with presynaptic vesicles, it may serve as a regulator of neurotransmitter as well as BDNF release [44,45]. In this case, when CaMKII becomes activated in the presence of high intracellular Ca^{2+}, it promotes cell death by inhibiting the release of BDNF [32]. At low concentrations, BDNF will no longer help support the survival of existing neurons nor stimulate the growth and differentiation of new neurons [46,47,48,49]. Cytoplasmic CaMKII is additionally linked to eventual activation of the apoptotic caspase-3 protein, which promotes the execution phase of programmed cellular death [50,51]. Evidence for this destructive pathway shows that inhibition of cytoplasmic CaMKII reduces glutamate-induced cell death [38,52,53,54]. In these pathways, CaMKII plays a pivotal role in both the cell death and survival mechanisms determining the fate of RGCs. Thus specific modulation of CaMKII or its nuclear counterpart may be a possible neuroprotective strategy for glaucoma and other diseases with glutamate excitotoxicity.

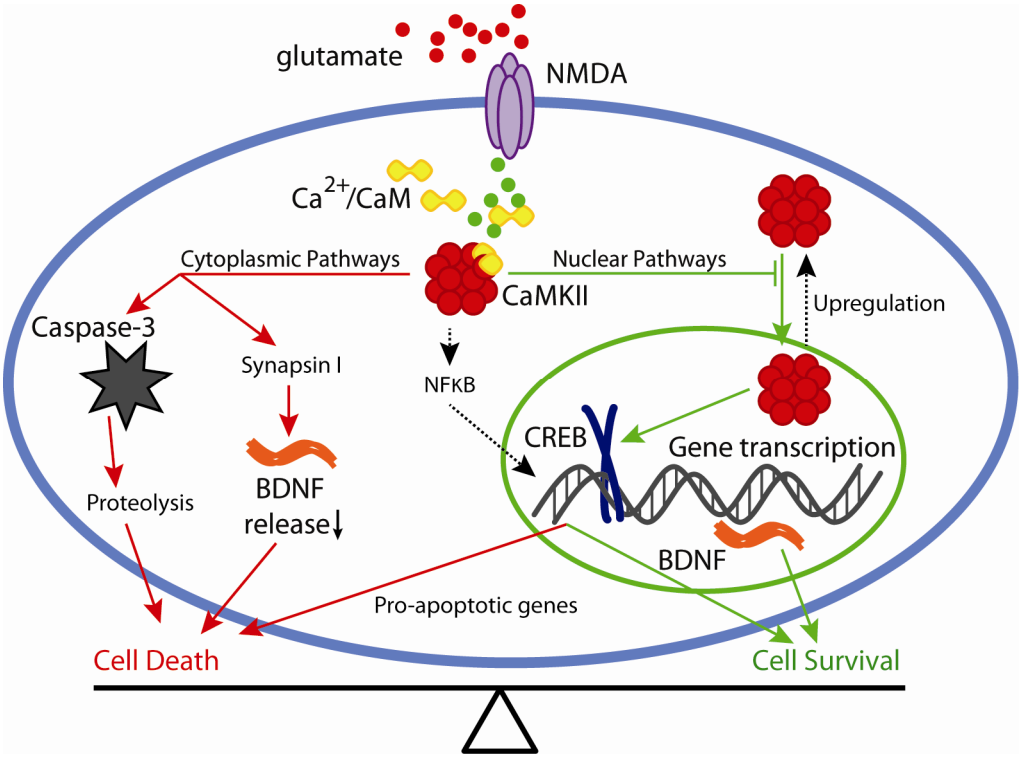

Figure 1.2 The role of CaMKII in cell death and survival pathways of retinal ganglion cells. This figure adapted from Cooper et al., [32] illustrates CaMKII involvement in cytoplasmic (red arrows) and nuclear (green arrows) signaling pathways. Excessive glutamate activation (red dots) leads to increased levels of Ca^{2+} (green dots) which activate CaMKII (red clusters). Cytoplasmic CaMKII promotes cellular death by downstream activation of the apoptotic caspase-3 protein (grey) as well as the decreased release of cell survival neurotrophic factor, BDNF (orange). In contrast NMDA (purple) activation promotes the transcription of nuclear CaMKII which aids in cell survival. Here CaMKII phosphorylates transcription factors like CREB (blue) to increase expression of pro-survival genes incldluing BDNF.

Although cellular death via glutamate excitotoxicity was first demonstrated in retinal neurons [34], a comparable mechanism was subsequently observed in brain neurons affected by cerebral ischemia [55,56]. In the case of focal cerebral ischemia (stroke), a decreased oxygen supply causes cellular death to explicit regions of the brain and also creates a surrounding penumbra where secondary cell loss occurs (for review see [57]). In this case, the ischemic conditions trigger anoxic depolarization of neurons, causing massive release of glutamate [58,59,60]. This excitotoxic glutamate signaling parallels the pathways observed in glaucoma induced RGC death, where CaMKII activation plays a critical role in cell fate. The toxic effects of excessive glutamate and

abnormal CaMKII activity are not just thought to be responsible for neuronal cell death after a stroke-related brain injury, but also are critical in the case of some neurodegenerative diseases [61,62,63].

CaMKII plays important roles in regulating normal heart function

For regular electrical activity of the heart, contractile function must be properly maintained through Ca^{2+} cycling. Ca^{2+}-dependent facilitation of Ca^{2+} channels serves to potentiate influx through L-type channels. This facilitation is a plastic event critical for regulation of excitable cells and in the case of cardiac cells, regulates the force and frequency of the cardiac contraction [64]. The enzyme modulates Ca^{2+} influx by phosphorylation of the α and/or β subunits of voltage-gated Ca^{2+} channels [65,66,67]. The interaction of CaMKII with the carboxy-terminus of the channel $Ca_v\alpha1.2$ has been shown to be essential for this process of facilitation [68,69] and subsequently is was shown that targeting of CaMKII to the channel requires binding to the beta(2a) subunit [70]. The protein-protein interaction allows for CaMKII-mediated phosphorylation of channel gating and once established, the interaction may persist even after Ca^{2+} levels drop [68]. CaMKII not only regulates Ca^{2+} levels through the modification of channels, but is also integral in the sequestering of free Ca^{2+} into intracellular stores [71]. In these mechanisms, CaMKII is required for the maintenance of Ca^{2+} homeostasis. When Ca^{2+} homeostasis is misregulated, myocardial dysfunction may be initiated along with electrical instability and arrhythmias [72]. CaMKII is central in regulating homeostatic proteins and in the cases of hypertrophy and heart failure, CaMKII activity is upregulated or is found to have increased expression [73,74]. Inhibition of this enzyme has been

shown to prevent myocardial infarction and restore excitation-contraction coupling making it a promising therapeutic strategy for cardiac diseases [75]. Inhibition of CaMKII may also be translated to other diseases with excitatory synaptic transmission abnormalities.

CaMKII is sensitive to dynamic calcium transients

Cytosolic Ca^{2+} concentrations are dynamically regulated by hormonal and electrical signals to generate spatially localized intracellular calcium transients. Since Ca^{2+} influx generates specific but diverse physiological responses and misregulation is often detrimental to cellular function, it is essential that cells have mechanisms in place to regulate levels of intracellular Ca^{2+}. Ca^{2+} signals are therefore transient, having varied concentrations, gradients, and localization in the cell depending on the specific cellular events. This gives rise to signaling microdomains such as neuronal postsynaptic spines and presynaptic termini which can have concentrations that differ from the main cell body [76,77]. Ca^{2+} transients last from milliseconds to minutes but prolonged elevations, such as in the case of excitotoxicity, can promote cell death. The differences in amplitude, frequency, and location encode which signals will be turned on and where [76]. Concentrations of free intracellular Ca^{2+} range from 10-50 nM in the resting basal state to 10 μM in a stimulated state [6,76,78]. Since concentrations of Ca^{2+} are millimolar in the extracellular space and in organelles, the cell uses mechanisms employing ligand and voltage-gated ion channels, Ca^{2+} pumps, and exchangers to carefully regulate Ca^{2+} levels spatially and temporally [6]. While these proteins regulate the influx of Ca^{2+}, the cell also utilizes cytosolic proteins to bind Ca^{2+} and reduce its

effective concentration. Some are buffers which bind with low affinity to limit the Ca^{2+} diffusion while others bind with high affinity to produce biochemical changes and physiological responses [6]. In order to terminate signals, there are several mechanisms for removal of cytosolic Ca^{2+}. Plasma membrane Ca^{2+}-ATPases (PMCA) powered by ATP hydrolysis pump Ca^{2+} out of the cell [79], and intracellular Ca^{2+} is replenished by Sarco-Endoplasmic Reticulum Ca^{2+}-ATPase (SERCA) activity [80]. In this way, Ca^{2+} signaling does not serve as an all or nothing switch, but rather undergoes a complex and sophisticated allocation mechanism. Since CaMKII responds to Ca^{2+} influx, regulation of Ca^{2+} signaling is central to the mechanism in which CaMKII activity is controlled.

CaMKII isoform diversity

CaMKII or CaMKII-like proteins are found in numerous living organisms and are highly conserved across species, especially in mammals. For example, the coding region of rat CaMKIIα mRNA is 93% identical to the human sequence and their translated protein products are identical in amino acid composition. CaMKII proteins of lower organisms like *Drosophila melanogaster* and *Caenorhabditis elegans*, also play a pivotal roles in behavior and cognitive function like in the case of mammals. In *Drosophila melanogaster*, inhibition of CaMKII was shown to disrupt learning of courtship behavior and acoustic priming [81,82] and also altered short-term plasticity in synaptic transmission of the insects [83]. In *Caenorhabditis elegans* CaMKII has been shown to regulate transport and recruiting of GLUR-1 receptors to postsynaptic structures [84], implicating its role in synaptic activity. Additionally, a gain-of-function CaMKII mutation was able to reduce locomotor activity and alter muscle excitation properties

[85]. These behavioral phenotypes associated with misregulation of CaMKII suggest higher and lower organisms may have similar CaMKII mechanisms. The conservation of the sequence and function over an impressive range of species illustrates the importance of this enzyme.

CaMKII function is attributed to a family of isoforms derived from four alternatively spliced genes referred to as alpha [86,87,88,89], beta [90,91,92,93,94,95], gamma [96,97,98,99,100,101], and delta [73,99,102,103]. The gamma and delta isoforms are expressed in most tissues and are the abundant isoforms implicated in cardiac function. In contrast alpha and beta are most prominent in neuronal tissue and make up to 2% of total protein in the hippocampus [6]. While CaMKII isoforms are predominantly cytosolic, some alternative splice variants of alpha, delta, and gamma contain a nuclear localization sequence which aids translocation to the nucleus where CaMKII likely plays a role in Ca^{2+}-mediated gene transcription [16,88,104,105,106]. The translated protein products for all isoforms contain three functionally distinct domains (catalytic, regulatory, and association) with the exception of one unique splice variant which lacks the catalytic domain, αKAP [89]. There are four variable regions within the gene that are alternatively spliced to make up 30 mammalian isoforms. Figure 1.3, recreated from a review written by Hudmon and Schulman [28], illustrates the diversity of isoforms and lists their linear structures as annotated by Tombes and Krystal [101].

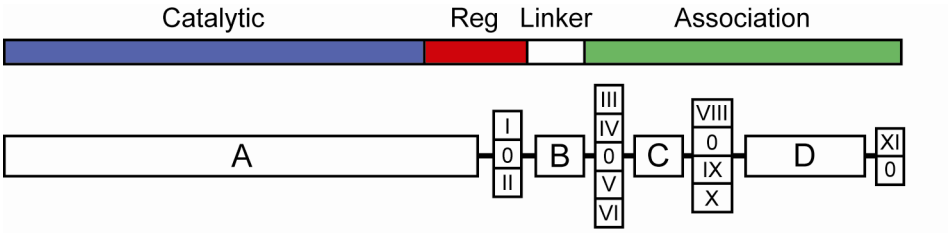

α =	A-B-C-D		δ_A =	A-B-IV-V-VI-C-D-XI	(δ1)
α_B =	A-B-III-C-D		δ_B =	A-B-III-C-D-XI	(δ3)
α_{KAP} =	I-B-III-C-D		δ_C =	A-B-C-D-XI	(δ2)
			δ_D =	A-B-IV-V-C-D-XI	(δ4)
β =	A-II-B-IV-V-VI-C-D		δ_E =	A-B-IV-V-VI-C-D	(δ5)
β' =	A-II-B-IV-V-C-D		δ_F =	A-B-III-C-D	(δ7)
βe =	A-B-IV-V-VI-C-D		δ_G =	A-B-C-D	(δ6)
βe' =	A-B-IV-V-C-D		δ_H =	A-B-VI-V-C-D	(δ8)
β_3 =	A-B-IV-V-C-2X-D		δ_I =	A-B-VI-C-D-XI	(δ9)
β_M =	A-II-B-IV-V-VI-C-3X-D		δ_J =	A-B-VI-C-D	(δ10)
			δ_K =	A-B*-C-D-XI	(δ11)
γ_A =	A-B-III-VI-C-D		δ_L =	A-B*-C-D	(δ12)
γ_B =	A-B-IV-V-VI-C-D		δ_M =	A-B-III-IVC-D-XI	(δ11a)
γ_C =	A-B-VI-C-D				
γ_D =	A-B-IV-VI-C-VIII-IX-D				
γ_E =	A-B-IV-V-VI-C-VIII-IX-D				
γ_F =	A-B-VI-C-VIII-IX-D				
γ_G =	A-B-IV-VI-C-IX-D				

Figure 1.3 Diversity of CaMKII isoforms (adapted from [99]). Mammalian CaMKII consists of three domains; catalytic (blue), regulatory (red) and the most C-terminal association domain (green) which is connected through a linker region (white). The core of all isoforms and splice variants contains segment A, consisting of the catalytic and regulatory domains, B, conserved linker region, and C and D, constituting the association domain except for αKAP which does not contain the catalytic domain. Inserts, labeled by Roman numerals I-XI, are incorporated at variable positions V1-V4. The asterisk denotes a single amino acid deletion resulting from an alteration in the splicing junction. The linear sequence of all the variants is denoted according to isoform (bottom).

The core sequence includes the catalytic and regulatory domains (A), a stretch of linker region which connects regulatory and association domains (B), and two regions of the association domain that are highly conserved (C and D). Between core regions, alternative splicing takes place in the variable segments which are implicated in SR-membrane targeting (V1), nuclear localization (V2), SH3-binding (V3), or unknown function (V4). Although all isoforms except αKAP have conserved sequence and capacity to function as a Ca^{2+}/CaM-dependent kinase, these variations introduce slight

yet unique differences. For example studies showed that sensitivity to Ca^{2+} oscillations is dependent on alternative splicing of the linker region, different splice variants having variable CaM activation constants and rates of autophosphorylation [107].

The catalytic domain of CaMKII is responsible for catalyzing the phosphorylation reaction, the transfer of the γ-phosphate of ATP to the hydroxyl group of a serine or threonine in a substrate protein. The function of all Ser/Thr kinases is to catalyze this same reaction and therefore the CaMKII catalytic domain has a similar structural scaffold to other kinases (Figure 1.4A). Although substrates must also enter the catalytic cleft, other portions of the catalytic domain are often necessary to help anchor specific substrates.

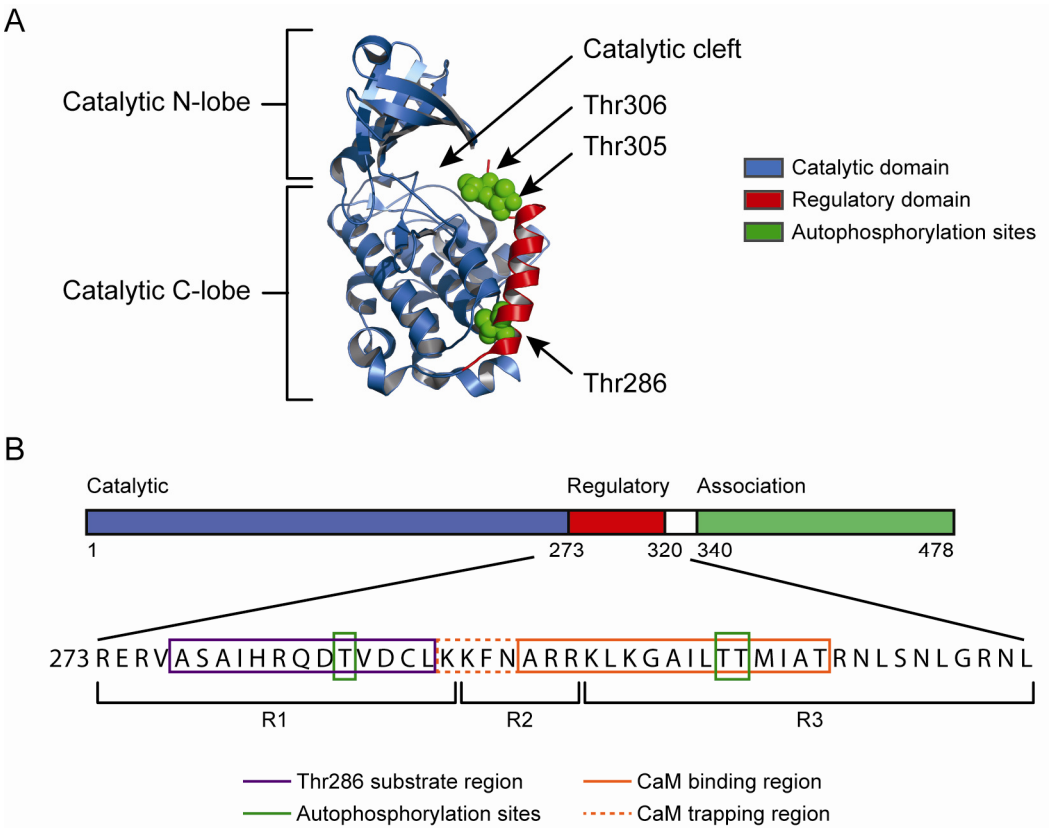

Figure 1.4 CaMKII domains and autoregulatory features. A) An illustration of an atomic resolution crystal structure of human CaMKIIδ [108] exhibits classic kinase architecture with catalytic N- and C-lobes (blue), between which lies the catalytic cleft where ATP binds. B) The regulatory domain contains at least three autophorylation sites, Thr286, Thr305 and Thr306 (highlighted in green), a Thr286 substrate sequence (purple), and a calmodulin binding segment (orange). Also highlighted are the R1-R3 classifications that were annotated previously to designate structurally relevant portions of the regulatory domain [109].

Catalytic activity is highly controlled by the adjacent regulatory domain through Ca^{2+}/CaM binding (Figure 1.4B, orange) and autophosphorylation of several residues (Figure1.4A, green). These autophosphorylation sites include Thr286, which endows the enzyme with constitutive activity when phosphorylated, and sites Thr305 and Thr306 which prevent CaM binding. In addition, this domain contains a "substrate" sequence containing site Thr286 (Figure 1.4B, purple) which is sequestered to the catalytic domain under inhibited conditions and is thought to prevent substrate binding [110,111]. Unique among protein kinases, CaMKII assembles into a dodecameric holoenzyme via the C-terminal association domain [112,113,114]. CaMKII is the only oligomer of the

calcium/calmodulin dependent kinase family and its subunit composition can contain a heterogeneous mixture of isoforms (reviewed in [1,6,28]) although holoenzymes made of only α subunits have also been identified [115]. The sensitivity of CaMKII to CaM activation is dependent on its subunit composition which is stochastically determined by the relative abundance of each isoform [116]. Mixed populations of holoenzymes have been purified from rat forebrain with varying α:β ratios, the most active of which was protein containing a 3:1 ratio [117,118,119]. Isoforms comprised of other ratios only contributed an estimated 5-10% of activity [119]. The variable activities of heterozygous holoenzymes illustrate that there are consequences of isoform composition which may contribute to differential tuning to Ca^{2+} signals. Assembly of different isoforms into the same molecule produces composite holoenzymes that may display a combination of individual properties, like sensitivity to Ca^{2+}. Isoforms differ in their response to Ca^{2+} suggesting each isoform has evolved to encode oscillations in subtly different ways [107].

CaMKII exists in several discrete intermediates each with their own level of activity

CaMKII responds to changes in the amplitude and frequency of calcium transients by undergoing a controlled transition from an autoinhibited basal intermediate to an autonomously active phosphorylated intermediate [120]. The activity of each intermediate is dependent on intricate interdomain interactions where binding and phosphorylation of specific residues communicate instructions for both inhibition and activation (for review see [28]). CaMKII can become constitutively active independent of Ca^{2+} concentration [121], but can also exist in an inactive state which is unable to bind

Ca^{2+}/CaM, thereby preventing activation [122,123]. Figure 1.5 depicts a hypothetical biochemical activation pathway, predicting six discrete, stable intermediates that make up a cycle of activation. One subunit, taken out of the context of the holoenzyme is depicted for simplicity. In a short overview of this pathway, the basal, apo state (A) is held inactive by an autoinhibitory interaction between catalytic (blue) and regulatory (red) domains. CaM (yellow) binding to the regulatory domain disrupts this interaction to activate the enzyme (B). Once bound to CaM, CaMKII can undergo an autophosphorylation reaction at Thr286 (C) which causes the enzyme to retain activity even in the absence of CaM (D). Autophosphorylation reactions at Thr305 and Thr306 prevent CaM binding making the activity of CaMKII independent of Ca^{2+}/CaM (E). Thr286 must be dephosphorylated before autoinhibition can reinstate (F) and Thr305 and Thr306 must be dephosphorylated (A) before reactivation by CaM is possible. This proposed mechanism leads to four active (B-E) and two inactive intermediates (A and F).

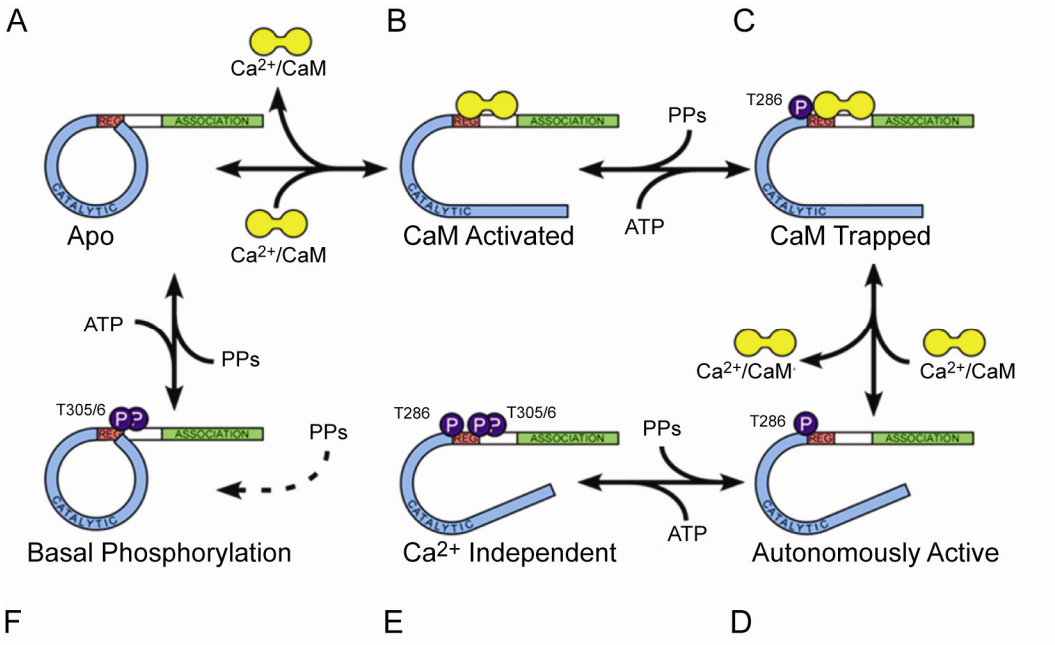

Figure 1.5 Biochemical intermediates of CaMKII activation (adapted from [124]). A) Apo CaMKII is expected to employ an autoinhibitory interaction between catalytic (blue) and regulatory (red) domains. B) The enzyme becomes active upon CaM (yellow) binding and C) subsequently undergoes an autophosphorylation reaction at Thr286. D) Thr286 retains activity in the absence of CaM and E) becomes Ca^{2+} independent upon Thr305 and Thr306 autophosphorylation. F) Dephosphorylation is required for the reinstatement of autoinhibition.

This general hypothesis for activation of CaMKII is a compilation of a wealth of biochemical predictions that are described in more detail in the following sections.

Many interactions occur between the catalytic and regulatory domains. The inactive enzyme is predicted to employ an autoinhibition mechanism where its regulatory domain binds the catalytic domain to block activity (Figure1.5A). This interaction ensures that during resting Ca^{2+} concentrations, the kinase activity is 100-1000 fold lower than under maximum Ca^{2+} stimulation [125]. Regulatory domain deletion results in a constitutively active kinase suggesting that removal of the regulatory domain exposes the substrate-binding site and generates a conformation permissive for ATP binding and phosphate transfer [126,127,128,129,130,131]. CaMKII is therefore hypothesized to be intrinsically active, but substrate binding is blocked during autoinhibition. Additional

supporting evidence reports that regulatory domain peptides are able to compete not only with substrates, but with ATP binding as well [110,111,132]. This model is compatible with structures of inactive conformations of CaMKII homologs, which show regulatory domains bound to substrate-binding sites as well as ATP-binding domains [133,134]. The Ca^{2+}/CaM-binding event required for activation is predicted to abolish autoinhibition sterically by separating the regulatory domain from the catalytic domain (Figure 1.5B). The regulatory domain is consequently thought to contain a flexible region which allows it to disengage from the catalytic domain to accommodate Ca^{2+}/CaM binding. Ca^{2+}/CaM activation is thought to release autoinhibition, exposing the active site [135,136]. Subsequent to Ca^{2+}/CaM binding, CaMKII undergoes a rapid autophosphorylation at site Thr286 which confers autonomous activity [137] (Figure1.5C). Thr286 is burried in a hydrophobic pocket in inactive CaMKII, and presumably becomes exposed upon CaM activation [138]. Autophosphorylation of Thr286 is not required for kinase activity [139,140], but endows the enzyme with a unique mechanism to retain activity when Ca^{2+} levels drop and Ca^{2+}/CaM dissociates.

Autophosphorylation allows for CaM trapping

CaM consists of two sets of EF hand motifs, referred to as lobes, which can bind four Ca^{2+} ions and are connected by a flexible linker [141]. This promiscuous protein shows considerable conformational plasticity when interacting with its many target proteins [142]. This property helps select for binding partners and also allows for the possibility of interacting with a single protein substrate in multiple ways. Such is the case for CaMKII. When bound to CaMKII, Ca^{2+}/CaM has been shown to exist in at least

two conformations with interlobe distances of 40 and 26 Å [143], with the shorter distance presumably corresponding to a more compact state. Because incubation with ATP facilitates the assumption of the compact state [143], these data are thought to correlate to the well established CaM trapping phenomenon, were CaMKII-bound Ca^{2+}/CaM adopts a low affinity conformation when initially bound and a high affinity "trapped" conformation when Thr286 is autophosphorylated [143,144,145,146,147,148,149,150,151]. Autophosphorylation at Thr286 has been shown to cause a 20- to more than 1000-fold decrease in the dissociation rate of CaM depending on Ca^{2+} concentration [143,147,150,151]. Interestingly, the change in binding equilibrium was shown to be almost exclusively due to changes in the off rate [151].

The trapping phenomenon has been characterized using a peptide model system. Peptides representing varying lengths of the CaM binding region of the CaMKII regulatory domain were created and the CaM-binding affinities were measured. Regulatory domain peptides consisting of residues 291-312 bind CaM 2500 fold more potently than peptides consisting of residues 296-312 indicating the N-terminal residues of the peptide contribute significantly to CaM binding [150]. Correspondingly, the differences in affinities for the shorter and longer peptides compare to the affinities observed for unphosphorylated and Thr286-phosphorylated CaMKII respectively [143,146]. The difference in affinities of peptides was contributed mainly to binding enthalpies including hydrogen bond and van der Waals interactions while entropy contributions were not significant [150]. In other studies, residues 293-295 were shown to be necessary but insufficient for high affinity CaM binding, indicating that these residues promote CaM interaction with residues 296-298 [151]. It is suggested that 293-

295 facilitate 296-298 binding because electrostatic interactions of 296-298 are not fully established with the 296-312 peptide [151]. Figure 1.4B depicts the regulatory domain sequence of the CaM binding region (residues 295-310, orange box) and trapping region (residues 291-294, dotted orange box) as defined by these and other studies. Overall, these studies suggest that the interaction of trapping residues (291-294) with CaM may contribute little to binding directly, but the presence of these residues may indirectly facilitate high affinity CaM binding to neighboring residues 295-312.

This hypothesis was investigated by many groups who completed mutagenesis studies to determine the role of CaM trapping residues. The region was characterized by measuring CaM dissociation rates under the conditions of charge elimination or reversal. For example, phosphorylated kinase with F293A mutation was shown to have a faster CaM dissociation rate than phosphorylated kinase with native Phe293 under conditions of either high or low Ca^{2+}, implicating the residue in high affinity trapping. Furthermore, the mutation does not significantly change rates for unphosphorylated CaMKII indicating that it is relatively unimportant in the case of low affinity binding [147]. These studies also showed that a N294A mutation results in deficient trapping confirming these sites are necessary for high affinity binding [147]. Results from other groups who also measured dissociation rates indicate CaM interactions with Phe293 and Asn294 are weak or absent without Thr286 phosphorylation, but strengthen upon phosphorylation of Thr286 [144,149]. Additionally Asn294 was shown to be disordered in the CaM-bound peptide structure indicating that it does not make direct contacts with CaM [152]. Other studies showed that a peptide comprised of residues 294-312 has a 40-fold higher affinity for CaM than a peptide of 296-312 [151], and a peptide of residues 293-312 has a 100-

fold greater affinity for CaM than 296-312 [151]. Overall, these studies serve to confirm that residues 291-294 promote CaM trapping.

These biochemical studies led the way for investigation of CaM structure, which was expected to adopt different conformations when bound to CaMKII with and without Thr286 phosphorylation. In complex with unphosphoryated CaMKII, two CaM interlobe distances were observed at 44 and 26 Å [143]. With Thr286 phosphorylation or in complex with 294-309 there was one distance of 22 Å [143]. These studies indicate that CaM may adopt a "semicompact" conformation upon CaMKII binding, and a "fully compact" conformation upon autophosphorylation of Thr286. Both lobes of CaM were found to be engaged in both conformations, but the compact conformation made critical contacts with 291-294 which are believed to be readily available for binding interactions only when Thr286 is phosphorylated [150]. Interestingly, ATP binding to CaMKII induces a conformational change in CaMKII-bound CaM facilitating the more compact conformation [143].

These studies beg the question, what is the regulatory advantage of trapping? Since Thr286 phosphorylation imparts autonomous activity, why is there a mechanism in place to sequester the CaM molecule that is no longer needed to sustain activity? One theory suggests that trapping impacts the free Ca^{2+} concentration, as high affinity binding of Ca^{2+}/CaM keeps Ca^{2+} sequestered from the cytosol. CaMKII binding decreases the rate of Ca^{2+} dissociation from CaM and autophosphorylation of Thr286 causes a further decrease [9].

CaMKII activity in the absence of CaM

Autophosphorylated CaMKII will have a high affinity for CaM, but when Ca^{2+} becomes depleted, CaM will dissociate (Figure 1.5D). Although Ca^{2+} levels are transient, autophosphorylation at Thr286 eliminates the requirement of Ca^{2+}/CaM binding [121,153] and allows for Ca^{2+}-independent activity which is 30-60% that of CaM-bound CaMKII thereby promoting prolonged kinase activity [76]. Thr286 phosphorylation is predicted to prevent the reinstatement of autoinhibition in the absence of Ca^{2+}/CaM via charge repulsion. The phosphorylated CaMKII then maintains exposure of substrate and ATP binding sites without the steric constraints imposed by Ca^{2+}/CaM. Through autonomous activity CaMKII retains a conformational memory of prior activation.

In contrast, autophosphorylation at Thr305 or Thr306 abrogates CaM-binding and generates a Ca^{2+}-desensitized form of the kinase [122,123]. Phosphorylation at Thr305/Thr306 occurs in the CaM binding portion of the regulatory domain and serves to prevent CaM binding interactions presumably through addition of negative charges, although whether or not the additional bulk of the phosphate group plays a part has not been determined. Thr305/Thr306 phosphorylation can occur in protein already modified at Thr286, or in unphosphorylated protein, resulting in two Ca^{2+}-desensitized conformers. In the case of Thr286 phosphorylated autonomously active protein, phosphorylation of Thr305/Thr306 produces an intermediate which retains its activity. In this sense, the protein is truly Ca^{2+} independent because it was activated in the presence of Ca^{2+} and retains activity despite not being able to bind CaM (Figure 1.5E). However, phosphorylation at Thr305/Thr306 does not require prior CaM activation. CaMKII has been shown to undergo basal phosphorylation at low Ca^{2+} concentrations (Figure 1.5F).

In this circumstance, the protein is held inactive due to lack of Thr286 phosphorylation and prevention of CaM association. This particular intermediate must undergo dephosphorylation at Thr305/Thr306 by phosphatases before CaM activation can occur. CaMKII is thought to be dephosphorylated by protein phosphatase-1 (PP1) and protein phosphatases 2A (PP2A) [154]. Overall, this wealth of biochemical research indicates that there are at least six intermediates which are controlled by regulatory interactions with the catalytic domain and phosphorylation reactions. The maintenance and balance of activating and inactivating factors illustrates another level of the intricacies of CaMKII regulation.

Kinetic advantages of holoenzyme structure

The self-regulating abilities of CaMKII become even more intricate when considering that twelve functional domains oligomerize to form a dodecameric holoenzyme [112,113,114,155,156]. When truncated from the association domain and supramolecular holoenzyme structure, a polypeptide consisting of catalytic and regulatory domains can be activated and interact with protein substrates independently. If monomer units do function individually as kinases, why then is the highly conserved multimeric structure exploited by evolution? There are several theories as well as more substantial lines of evidence that suggest the holoenzyme structure provides key kinetic advantages, introducing a level of regulatory complexity which makes this protein more than the sum of its parts.

CaMKII can propagate even rapid calcium signals, on the order of 100 ns, due to its oligomeric assembly. The kinase subunits are concentrated to an unusual extent in the

holoenzyme (estimated at 3 mM [138]), facilitating cooperative Ca^{2+}/CaM binding [112,138,147] and the activity-dependent intersubunit autophosphorylation at Thr286 [157]. This raises the conceptual questions about how intersubunit interactions occur and how autonomous activity is controlled. It has been shown that CaMKII has the ability to escape calcium dependence at high Ca^{2+} frequencies [120] and the Thr286 autophosphorylation reaction required for this autonomous activity is an intersubunit interaction between adjacent kinase domains in the holoenzyme [157]. The clustering of functional domains provides a favorable arrangement for autophosphorylation because kinases "finding" each other is not diffusion limited. This is an ideal scenario for quick responses. The Thr286 phosphorylation reaction requires both the "phosphorylating" kinase and the "substrate" kinase to be bound to Ca^{2+}/CaM simultaneously. CaM binding has also been observed to be cooperative indicating that binding of one Ca^{2+}/CaM molecule facilitates subsequent binding of other Ca^{2+}/CaM molecules. The explanation of how this occurs is a subject of controversy as conflicting models have been proposed from varying Hill coefficients and crystal structures. Initially, CaM binding was thought to be non-cooperative, with stochastic, but uncorrelated CaM binding associated with increases in intracellular calcium concentration [158]. Since adjacent kinase domains must bind CaM independently for Thr286 phosphorylation to occur in this model, the non-cooperativity of binding induces a delay in onset of autonomous activation and provides an explanation of how acquisition of calcium independence is linked to the frequency of signaling. However, others have found CaM binding to be cooperative with apparent Hill coefficients ranging from ~2 [112,138] up to 4.3 [109] depending on the variant used. In order for the holoenzyme to be sensitive to frequency and not just

amplitude of calcium signals, there must be an explanation as to how uncontrolled Thr286 phosphorylation is prevented in this model. This is currently an unresolved question.

Stoichiometric Ca^{2+}/CaM binding produces maximal CaMKII activity, and the amount of substrate phosphorylation is directly dependent on the degree of this binding [30]. This illustrates the initial independent activity of individual subunits governed by the strength of the Ca^{2+} signal. However, the trans-autophosphorylation of CaMKII was found to be frequency dependent, where the resultant autonomous activity was sensitive to the frequency spikes [120]. For this investigation, CaMKII was immobilized on plastic tubing in vitro and subjected to various Ca^{2+} pulse frequencies by a computerized valve assembly. Autonomous activity was found to be sensitive to frequency, amplitude, and duration of the Ca^{2+} pulses, which varied among isoforms. It has been demonstrated in vitro that CaMKII responds not just to the strength of the Ca^{2+} activation signal, but also to its frequency. When CaMKII is stimulated by short Ca^{2+} pulses of 80 ms, it requires higher frequency oscillations of 10 Hz to achieve an increase in the Ca^{2+}-independent activity associated with Thr286 phosphorylation. To achieve the same level of autonomous activity with lower stimulation frequencies of 0.8 Hz, Ca^{2+} pulses of longer than 1000 ms are required [120]. This raises the question of how frequency is decoded by this structure.

Since autonomous activity does not occur every time a Ca^{2+} spike is detected, the molecule must have a mechanism in place to retain sensitivity. The prevailing mechanism predicts that at high frequency, the interval between Ca^{2+} pulses may be too short to allow full dissociation of CaM. This effectively increases the likelihood of CaM

binding to adjacent subunits to stimulate Thr286 phosphorylation and CaM trapping. CaM trapping then further potentiates the signal by ensuring that CaM will remain associated with CaMKII during future pulses. In contrast, between low frequency Ca^{2+} pulses, there may be insufficient time for the autophosphorylation reaction to occur before CaM dissociates. This would prevent autonomous activity and allow for deactivation of the kinase. In this manner, CaMKII responds not just to the amplitude of the activation signal, but also to its frequency. Ca^{2+}-independent activity allows CaMKII to function as a calcium detector and to grade is catalytic activity based on the frequency or duration of calcium exposure.

The holoenzyme structure allows for structural scaffolding

The structure of CaMKII not only serves to decode Ca^{2+} frequency, it also serves to target the kinase to regulatory proteins involved in Ca^{2+} homeostasis to maintain signaling fidelity. CaMKII has been shown to bind several proteins localized in diverse subcellular compartments and there, interactions may require its association domain [29,159]. The interactions of these diverse proteins can be non-competitive indicating that CaMKII can interact with multiple proteins simultaneously. This raises the likelihood that the multimeric CaMKII may nucleate formation of protein complexes or may act as a structural scaffold to maintain close proximity of binding partners. Protein-protein complexes can serve to amplify enzyme activity by creating spatial organization in specific location of the cell such as the PSD, and information can be relayed from one cellular location to another by assembly or disassembly of protein complexes (for review see [160]). For example protein-protein interactions with CaMKII have been shown to be

dynamically regulated by the state of activation. Thr286 phosphorylation positively modulates association with the PSD while Thr305/Thr306 phosphorylation acts as a negative regulator [18,20,161].

CaMKII interaction with the NMDA receptor is thought to mediate its co-localization to the PSD. CaMKII has been found to phosphorylate NMDA receptors and has also been observed to co-localize with NMDA receptor subunits NR2A and NR2B [162,163,164,165,166]. Co-localization is controlled by a variety of physiological conditions that promote Thr286 phosphorylation which stabilizes its interaction with NMDA receptor subunits. CaMKII can make simultaneous interactions with multiple subunits of the NMDA receptor as well as secondary interactions with other proteins, the assembly of which may play an important role in signaling. Several proteins have been shown to interact with CaMKII, the most abundant of which may be the postsynaptic density-enriched protein interaction with the Thr286 phosphorylated kinase [167] later identified as the NR2B subunit [154,164]. A complex of PSD95, CaMKII, and NR2A were found to co-purify suggesting a scaffolding role for CaMKII [168]. Some interactions with binding partners also serve to modulate the activity of CaMKII. For example NR2B has been shown to trap the autonomous form of CaMKII [169], potentially keeping the kinase localized at the PSD when Ca^{2+} levels are low.

Additionally CaMKII has been shown to dynamically interact with cytoskeletal proteins, the most crucial for protein organization. CaMKII binds actin filaments and interestingly Ca^{2+}/CaM promotes their dissociation [170]. Binding is tuned by isoform composition. For example CaMKIIβ, but not α, interacts with F-actin [171]. However heterozygous holoenzymes containing both α and β subunits are able to interact, allowing

CaMKIIα subunits to associate with F-actin through the β subunits of the holoenzyme. CaMKII also interacts with α-actinin, an actin-binding protein, and was found to form a ternary complex consisting of CaMKII, α-actinin, and densin-180 [159,172]. Densin-180 is believed to be involved in the formation of complex protein networks that maintain the architecture of cells by mediating specific adhesion between presynaptic and postsynaptic membranes at glutamatergic synapses [173]. These data suggest CaMKII has a regulatory role in a number of essential cellular functions associated with actin filaments. CaMKII also associates with cytoskeletal microtubules [174] and phosphorylation of MAP2 by CaMKII blocks its actin filament bundling activity [175]. The mechanisms of these proteins and their association with CaMKII suggest a role of CaMKII holoenzyme structure in maintaining the proper functions of intracellular transport and structural scaffolding.

These multiple and coincident binding partners function to provide stable anchors for CaMKII as well as promote formation of relevant protein complexes. The formation of protein assemblies is critical for the spatial and temporal organization of molecules within the cell, coordinating a high fidelity intracellular information transfer. Since CaMKII can be localized in different subcellular compartments, it may offer a flexible strategy for regulating, signaling, and achieving new responses from preexisting signaling components. These mechanisms, which are likely facilitated by CaMKII's oligomeric assembly, would allow protein relocalization and bringing together of the components needed to direct the flow of information, mediate complex signaling behaviors, and permit signal branching to other pathways.

CaMKII holoenzyme structure: form equals function

Currently there are several low resolution structures of the holoenzyme [112,155,156], but no atomic resolution structure was available during the studies presented in this document. However, very recently an atomic resolution structure became available [176] and will be discussed in Chapter 6, which details future directions for CaMKII studies. The 3D holoenzyme structure resolved from single particle images using transmission electron microscopy showed that domains come together in a dodecameric formation consisting of two stacked hexameric rings [155]. The central core of the rat CaMKIIα molecule is composed of association domains resembling a gear shape while the kinase domains make up foot-like appendages which connect by narrow density to the core. The kinase protuberances extend outward peripherally above and below the plane of the core in a radial fashion (Figure 1.6A). The structure has $6 \times 2 \times 2$ fold symmetry with six-fold radial symmetry from the "top" view looking down on the rings and the two two-fold symmetries evident from the "side" views. All four isoforms of CaMKII have been visualized at 21-25 Å resolution, and there are no apparent isoform differences in the ultrastructure of the holoenzyme [112].

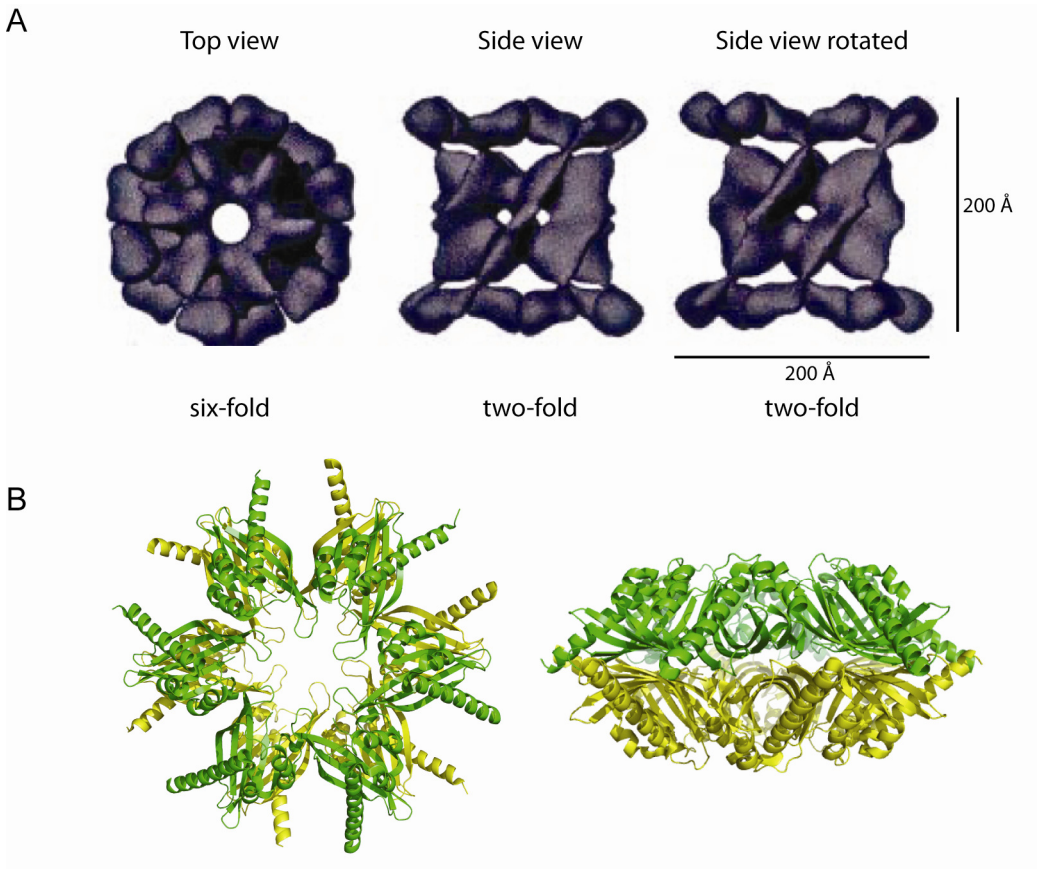

Figure 1.6 Oligomeric assembly of CaMKII. A) A three dimensional reconstruction of CaMKII holoenzyme shows a central gear shaped core consisting of association domains with surrounding kinase domains extending outward in foot-like appendages [155]. The oligomer is in a dodecameric assembly of two stacked hexameric rings featuring 2×6×6 fold symmetry. B) A crystal structure of the association domain lacking catalytic and regulatory domains illustrates a high resolution view of the core assembly (PDB 2UXO). Hexameric rings are shown in green and yellow from "top" and "side" views in the left and right panels respectively.

Interestingly, the holoenzyme has also been described with small angle X-ray scattering (SAXS) analysis to reveal quite a different holoenzyme model [138]. The model predicts the same central core of association domains with the same symmetry; however the kinase domains are arrayed out in parallel fashion in the same plane as the core. The assembly creates an outer ring of kinase domains, which alternate every other domain from the same hexameric ring. This produces a flat disk shaped holoenzyme with a height of approximately 50 Å in contrast to the 200 Å observed in electron microscopy (EM). In light of this discrepancy, the authors hypothesized that the disk conformation may be

representative of the autoinhibited kinase while the extended conformation could exist under activated conditions [138]. When Ca^{2+}/CaM was added to the kinase, SAXS analysis revealed a radius of gyration increase compatible with the EM structures. While this model is plausible, it does not account for the fact that the kinases observed in EM were not activated by CaM *in vitro*. If the model is correct, CaMKII must undergo dramatic changes in conformation to account for a ~150 Å increase in height. We can only speculate on how the consequences of this remarkable conformational change would impact cooperative activation, protein-protein interactions, and sensing of Ca^{2+} frequency.

The association domain core lacking catalytic and regulatory domains has been visualized by several atomic resolution structures of CaMKII variants as listed in Table 1.1.

PDB File	Description	Domains	Residues	Publication
2BDW	*C. elegans* CaMKII	Catayltic/Reg	1-318	Rosenberg et al., 2005 [138]
3KK8	*C. elegans* CaMKII	Catalytic/Reg	1-284	Chao et al., 2010 [109]
3KK9	*C. elegans* CaMKII	Catalytic/Reg	1-282	Chao et al., 2010 [109]
2VZ6	Human CaMKIIα	Catalytic/Reg	13-302	Rellos et al.,2010 [108]
3BHH	Human CaMKIIβ	Catalytic/Reg	11-303	Rellos et al.,2010 [108]
2V7O	Human CaMKIIγ	Catalytic/Reg	1-315	Rellos et al.,2010 [108]
2VN9	Human CaMKIIδ	Catalytic/Reg	1-301	Rellos et al.,2010 [108]
2WEL	CaM bound human CaMKIIδ	Catalytic/Reg	1-327	Rellos et al.,2010 [108]
3KL8	*C. elegans* CaMKII + CaMKIINtide	Catalytic	1-269	Chao et al., 2010 [109]
1HKX	Mouse CaMKIIα	Association	336-478	Hoelz et al., 2003 [113]
2F86	*C. elegans* CaMKII	Association	340-472	Rosenberg et al., 2006 [114]
2UX0	Human CaMKIIγ	Association	387-527	Pending publication
2W2C	Human CaMKIIδ	Association	334-475	Pending publication
3SOA	Human CaMKIIβ	All	7-444	Chao et al., 2011 [176]

Table 1.1 Atomic resolution structures of CaMKII variants

Although in one structure, the protein crystallized as a tetradecamer [113], the authors subsequently determined the assembly is dodecameric when kinase domains are present [114]. Thefore, the atomic resolution data is consistent with the dodecameric assembly postulated from low resolution EM reconstructions [113,114]. The interfaces between protomers of the same ring as well as the interface between the two rings are largely characterized by hydrophobic interactions. The rings are stacked in a symmetric fashion such that there is no stagger in the orientation of the two rings (Figure 1.6B). The residues located at the two interfaces are highly conserved with only minor amino acid substitutions between isoforms indicating the interfaces are similar.

Although the association domain is 15 kDa in size, assembly into the twelve subunit holoenzyme only requires short sequences on either end of the domain. Investigation of assembly by deletion mutants determined that residues 344-350 from the N-terminal region of the association domain as well as residues 350-478 from the C-terminus are necessary for multimerization [162]. Interestingly, the residues required for oligomerization are also isoform dependent suggesting subtle variation in assembly contacts. The minimum region for assembly of α homomers was found to differ from β homomers as well as mixed α/β heteromers [177].

Structure of the catalytic domain

CaMKII catalytic domain adopts a similar fold to other kinases, which contain a highly conserved core of approximately 300 amino acids [178,179,180]. The general fold for kinases was first established for cAMP-dependent protein kinase [181,182] and CaM-dependent kinases have similar bilobate architecture with the active site located in

the cleft between the two lobes [108,109,134,138,176] (Figure 1.4 illustrates CaMKIIδ catalytic and regulatory domains [108]). ATP binds to the smaller N-lobe which consists primarily of antiparallel β-sheets while the C-lobe is mainly α-helical and contains residues implicated in substrate recognition. Previously Goldberg et al. compared the structure of autoinhibited CaMKI with that of a cAPK/ATP/inhibitor complex and found differences in the orientation of catalytic lobes [134]. While the "active" cAPK/ATP/inhibitor complex was found to be in a "closed" conformation, the catalytic lobes of the autoinhibited CaMKI structure were rotated toward an "open" conformation, with an 18° separation relavitve to the "active" complex. Similarily, "open" conformations were observed in other low activity or inactive kinases including MAP kinase ERK2 [183], the insulin receptor tyrosine kinase [184], twitchin kinase [133], and nucleotide-free cAPK [185]. These were the first structural inferences that catalytic lobes rotate toward "closed" conformations upon activation of kinases and the inactive "open" conformation may be stabilized by regulatory domain interactions with the N-lobe [134].

Structures of monomeric CaMKII lacking the association domain

Crystal structures of monomeric CaMKII, consisting of the kinase and regulatory domains and lacking the association domain, have led to conflicting models of autoinhibition. In an inactive *C. elegans* CaMKII structure (PDB 2BDW), the regulatory domains from two subunits form an antiparallel coiled coil [138] (Figure 1.7A). Although it partially blocks the substrate binding site, the regulatory domain does not contact the ATP-binding lobe as postulated from biochemical data [110,111,126,127,128,129,130,131,132,135,186,187,188] and from structures of the

homologous and monomeric CaMKI (PDB 1A06) [134]. This structure would suggest a unique mode of activation seemingly inconsistent with previous biochemical data. It is noted that a plausible model was proposed based on the crystal structure of CaMKII for the mechanism of resting state inhibition [138]. The authors present a novel hypothesis explaining how autoinhibition occurs with an unobstructed nucleotide-binding pocket. The positioning of the regulatory helix is predicted to anchor Glu96, a residue thought to participate in ATP coordination, away from the nucleotide-binding pocket thus preventing ATP coordination and activation [138]. The regulatory domain coiled coil has been proposed to pair kinase domains in the holoenzyme stabilizing CaMKII in an inactive conformation and to explain cooperative activation by Ca^{2+}/CaM binding [109]. In this model, the CaM binding segments of regulatory domains are sequestered by the coiled-coil interaction between adjacent domains. When a Ca^{2+}/CaM molecule succeeds in binding one regulatory domain, it facilitates cooperative binding of a second Ca^{2+}/CaM molecule to the freely available CaM binding region of the partner regulatory domain. Previous studies support the notion that kinase domains form a dimer within the holoenzyme [189,190], but there is no direct evidence that dimerization is mediated by the regulatory domain. Whether the regulatory domain position and dimerization are physiologically relevant or are the result of crystal packing constraints is an open question.

During the progress of the studies presented in this document, several crystal structures of monomeric human CaMKII were published. These proteins, which are 77% identical to the monomeric *C elegans* CaMKII, did not show the coiled-coil dimers (PDBIDs 2VZ6, 3BHH, 2V7O, 2VN9) [108]. These structures are overlaid in Figure

1.7C and illustrate the high conservation of structure among the four isoforms of human CaMKII. They are monomeric and have catalytic domain conformations that agree largely with the catalytic monomer subunit of the *C. elegans* structure. However, the discrepancy arises in the conformation of the regulatory domain.

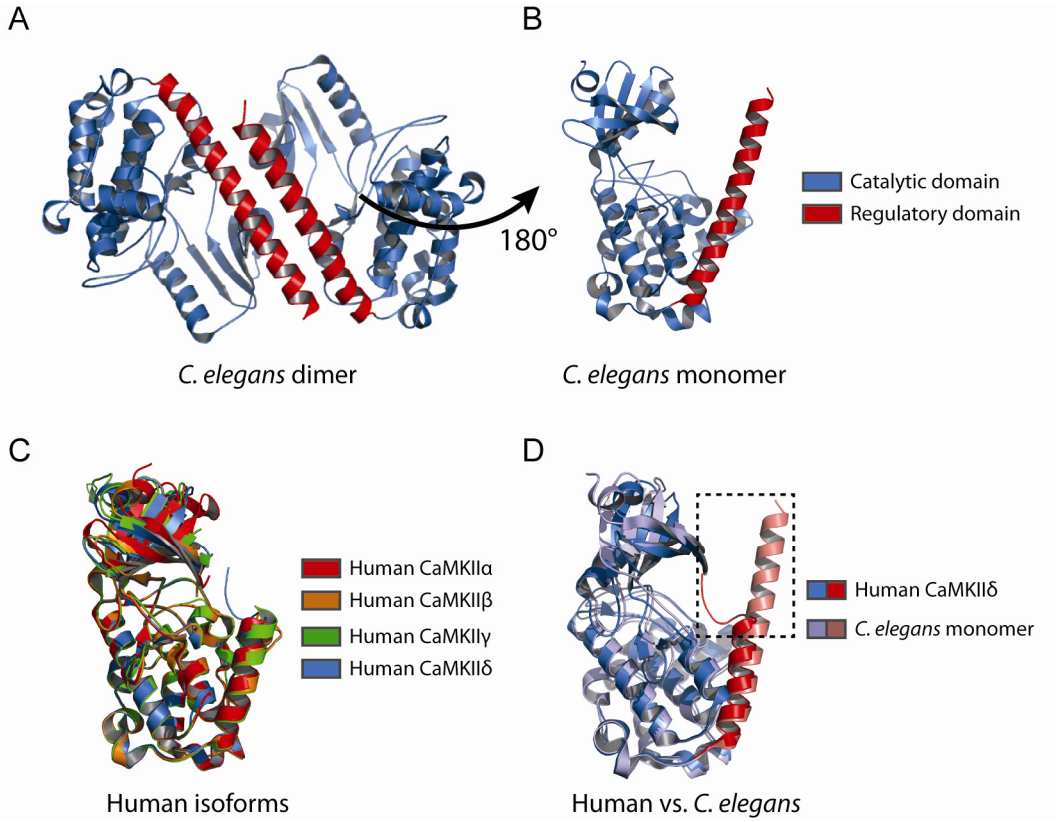

Figure 1.7 Comparison of CaMKII kinase domain structures. A) The C. elegans construct lacking the association domain crystallized as a dimer, with a coiled-coil interface between two regulatory domains of adjacent monomer subunits (PDB 2BDW). B) One subunit of the structure reveals classic catalytic kinase architecture and a long regulatory domain lacking contacts to the catalytic cleft. C) Human isoforms of CaMKII alpha (PDB 2VZ6), beta (3BHH), gamma (2V7O), and delta (2VN9) exhibit similar structures when compared to each other but the regulatory domain of the delta protein deviates from that of the *C. elegans* structure (D, boxed).

In the structure of human CaMKIIδ, the regulatory domain resolved through residue 308 appears docked against the catalytic cleft (PDB 2VN9). Figure 1.7D illustrates how this deviates from the regulatory domain of the *C. elegans* protomer. This structure supports the biochemical evidence for a pseudosubstrate sequence blocking the catalytic cleft.

However, this conformation may also be influenced by contacts between molecules in the crystal lattice. Furthermore, its mechanistic implications are confounded by the presence of an ATP-binding site inhibitor (not depicted in Figure 1.7). In all of the other structures of human CaMKII, the regulatory domain is not influenced by crystal contacts but the structures are only visible to residue 301. Thus, the conformation of the regulatory domain in the basal (apo) state is highly ambiguous. Structures may not be truly representative of the regulatory domain within the autoinhibited holoenzyme in solution.

As predicted by the biochemical activation hypothesis, the regulatory domain is expected to undergo conformational changes upon CaM activation. The CaM interaction was previously illustrated by a crystal structure of CaM in complex with a regulatory domain peptide of CaMKII (PDB 1CDM) [152] and more recently in a complex of Ca^{2+}/CaM with human CaMKII consisting of only catalytic and regulatory domains (PDB 2WEL) [108]. The CaM structure is more completely resolved in the latter, although CaMKII is cleaved at the end of the catalytic domain causing it to be disjointed from the remainder of the structure (Figure 1.8A). Figure 1.8 B and C illustrate from the "side" and "top" views respectively how residues 292-315 of the regulatory domain form a helical conformation, with CaM providing extensive stabilizing contacts on all sides. Because the CaM molecule surrounds the helix, the binding interaction likely necessitates a disruption of the regulatory and catalytic domains as predicted biochemically. In this case the conformation of the CaM bound regulatory region is unambiguous, as it is in agreement with the CaM-peptide structure (PDB 1CDM) [152] as well as a structure of CaM bound to a CaMKI peptide which shares high similarity to the CaMKII regulatory domain (PDB 1MXE) [191]. The structure, while it provides key information on CaM

binding contacts with the regulatory domain, does not reveal the corresponding catalytic domain conformation and any involvement it may or may not have in stabilizing CaM.

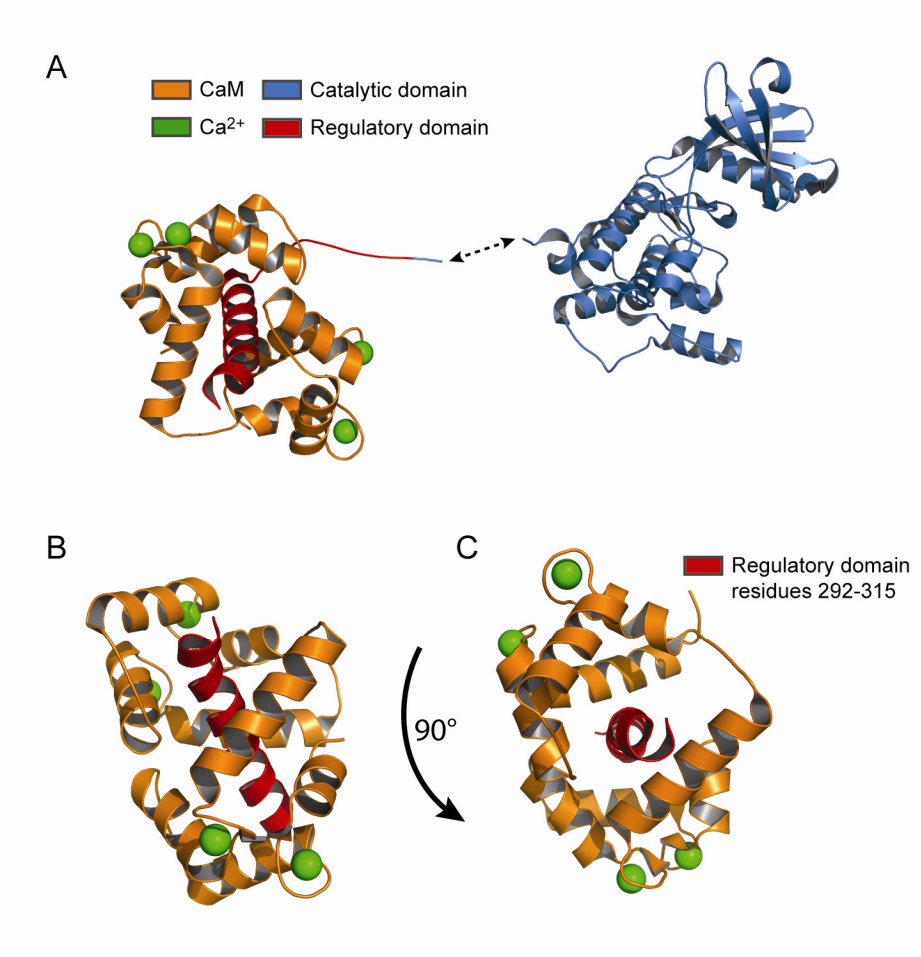

Figure 1.8 Crystal structure of CaM bound to CaMKII. A) A crystal structure illustrates CaM (orange) bound to CaMKII regulatory domain with the catalytic domain separated by unresolved data (PDB 2WEL). B) "Side" and C) "top" views of the CaM portion of the structure reveals how binding to CaMKII regulatory residues 292-315 (red) occurs.

The regulatory domain adopts a vastly different conformation in structures of *C. elegans* CaMKII partially truncated in the regulatory domain (PDB 3KK8 and 3KK9) [109]. The Thr286 autophosphorylation site of one protein is bound to the active site of another presumably mimicking a transphosphorylation intermediate.

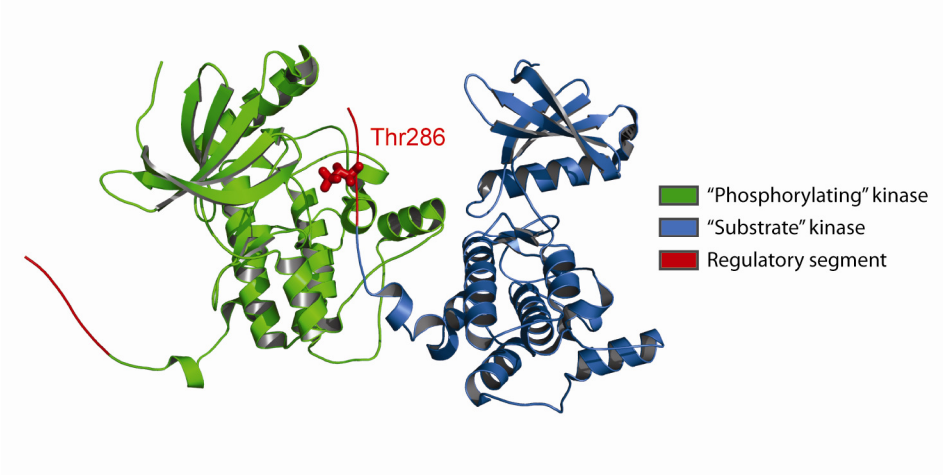

Figure 1.9 Structure of an enzyme-substrate complex. In a structure of a catalytic monomer lacking the association domain (PDB 3KK8), The R1 regulatory element is presented for phosphorylation at the active site of another monomer, presumably illustrating the transautophosphorylation reaction at Thr 286.

This structure shows the R1 regulatory segment of a "substrate" kinase extended into the catalytic cleft of a separate "phosphorylating" kinase. The proteins in this structure are positioned in a face-to-back orientation, with the interaction repeated in a chain throughout the crystal lattice. The electron density map also indicates that the Thr286 residue implicated in the acquisition of autonomous activity is unambiguously phosphorylated. Residues 276-291 of the R1 element make contacts with the catalytic C-lobe of the "phosphorylating" kinase in a random coil conformation. This is in contrast to the helical segment adopted in structures of autoinhibited CaMKII. Thus, the inference from functional and structural data is that regulation of CaMKII activity entails a complex series of conformational changes initiated at the regulatory domain and modulating its interactions with the kinase domain.

Outstanding questions and significance of structural investigations reported in this dissertation.

Currently a structural and dynamic framework to link CaMKII conformation with activation and conformational memory is not available. Although these initial structural studies provide valuable information of protein conformation, they do not describe the conformational rearrangements or dynamics of CaMKII's enzymatic intermediates in solution. These are snapshots of individual domains of subunits outside the context of the oligomeric assembly and are importantly, subjects of controversy. Therefore they represent only the initial phase of research needed to gain a complete picture of conformational rearrangements. Despite the wealth of biochemical information, so many questions remain unanswered. The foundation of an accurate activation mechanism relies on the identification and characterization of this enzyme's multiple intermediate states. However, there is no high resolution structure of the holoenzyme in all of the six proposed biochemical intermediates outlined in this document. Furthermore, there are a seemingly infinite number of possible intermediates when considering CaMKII's growing number of substrates and its role in scaffolding of multi-protein complexes.

Existing crystal structures of monomeric kinase domains have been extrapolated to mechanistic models of cooperative Ca^{2+} sensing and catalytic activation of the holoenzyme [108,109,138]. Experimental testing of these models in solution in the absence of constraints imposed by the crystal lattice is essential for an in-depth understanding of the complex landscape of holoenzyme activation. Motivated by these conflicting models and the dearth of available information about conformational changes associated with activation, this document describes analysis of regulatory domain

dynamics in solution using systematic spin labeling and electron paramagnetic resonance (EPR) spectroscopy [192,193] of monomeric *C. elegans* CaMKII. Using this spectroscopic approach, experiments can be designed to identify the structural characteristics of intermediates. The approach also captures protein dynamics, a property unresolved in the confines of a crystal lattice which may impose structural distortions on protein conformation. With limited structural data, it is difficult to decipher these complex mechanisms of self-regulation and activation. Developing a dynamic structural framework for CaMKII activation by CaM, for acquisition of conformational memory, and for interactions with protein partners will significantly impact the understanding of important biological processes and has the potential to inform new therapeutic strategies. This body of work describes the secondary structure, tertiary interactions, and backbone dynamics of the CaMKII regulatory domain in discrete catalytic intermediates that currently available data suggest are associated with activation.

CHAPTER II

ELECTRON PARAMAGNETIC RESONANCE SPECTROSCOPY

Introduction

Electron Paramagnetic Resonance (EPR) spectroscopy is a technique which detects transitions of unpaired electrons between discrete energy levels. The criterion for conducting an experiment is that the molecule possesses a permanent magnetic moment provided by an unpaired electron. Species that are readily detected by this method are free radicals and transition metals. However, for the study of proteins which do not contain such species, a paramagnetic probe containing a stable free radical must be experimentally incorporated. There are a variety of probes of this nature including the well characterized methanethiosulfonate spin label (MTSSL) [194,195] used in these studies. The label reacts with the protein via a cysteine disulfide linkage which is advantageous for investigations of protein structure since proteins can be engineered to contain cysteines at any desired position. Spin label side chains can therefore be placed in virtually any region of interest throughout the protein. These probes can report a multitude of parameters which describe the local environment of the side chain and provide information on protein structure and dynamics. In order to understand how these parameters are detected and interpreted, first the EPR experiment must be described.

[†]Denotes figures that were adapted or recreated from the Bruker Biospin website [177].

Electron spin orientation in an external magnetic field

An electron possesses the intrinsic physical properties of charge and spin angular momentum. Together these properties describe its magnetic moment, μ, which makes an electron behave like a magnet in an external magnetic field. The energy of the interaction between the electron and the magnetic field, H_0, can be described by the Hamiltonian operator, $\mathcal{H}$;

$$\mathcal{H} = -\mu_Z H_0$$

If the magnetic moment term is expanded to reveal its component parts, the Hamiltonian can be described in terms of S_Z, the electron spin quantum operator along the z axis, g, the electron g factor, and B, the electron Bohr magneton.

$$\mathcal{H} = -\mu_Z H_0 = g B H_0 S_Z$$

Together these terms describe the properties on which the total energy of the system is dependent and provide the set of possible outcomes. In brief, the g factor is a dimensionless proportionality constant of known value defined by the electronic configuration of the radical. It relates the observed magnetic moment to its corresponding angular momentum, quantum number, and the appropriate quantum unit of magnetism, in this case the Bohr magneton, B. The magnetic components for the S_Z operator yield eigenvalues of ±½ for an electron, giving rise to two solutions for the Hamiltonian. In general there will be 2S +1 ways in which the electron will interact with the magnetic field, meaning the electron will adopt one of two energy states. The negative lower energy state is referred to as α and the positive higher energy state is β. When placed in an external magnetic field, an electron of lower energy -½ gBH_0 will align parallel to the field while higher energy +½ gBH_0 will align in an antiparallel fashion (Figure 2.1). In

the absence of a field, there is no preference for orientation and all orientations of spins are of equivalent energy.

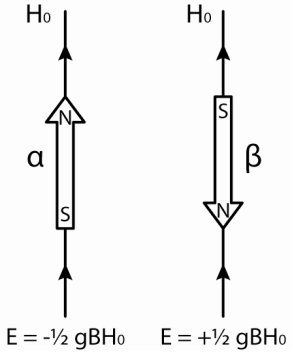

Figure 2.1† Minimum and maximum energy orientations of μ in a magnetic field. The lowest energy orientation, α, will align parallel to the field, H_0, while the highest, β, will align against the field [196].

Paired electrons occupying the same orbital cannot posses the same value of M_S [197,198] as a consequence of the Pauli Exclusion Principle. One electron will have a positive M_S value and the other a negative value, resulting in a cancellation of magnetic moments. This property makes paired electrons diamagnetic and EPR silent, and illustrates why an unpaired electron is necessary for EPR spectroscopy.

In the presence of an external magnetic field, the energy difference between the α parallel and β antiparallel spin orientations, ΔE, depends on the strength of the field, H_0.

$$\Delta E = gBH_0$$

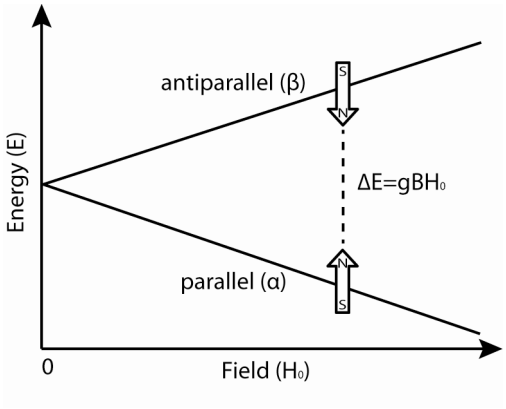

Figure 2.2[†] Separation of spin state energies as a function of applied magnetic field. The difference in energy between minimum and maximum spin orientations, ΔE, diverges linearly as the field strength increases.

As the field strength increases, the separation between energy levels increases. Figure 2.2 is a diagram illustrating an isolated electron in an external magnetic field where, at any given value for the field, H_0, there will be an energy separation, ΔE, between parallel and antiparallel states equal to gBH_0.

An EPR experiment detects energy transitions of unpaired electrons

Transitions between the low and high energy orientations of spins can be induced by adding energy to the system. An EPR experiment measures the absorption of photon energy during a transition event. The relationship is described by Planck's law, where ΔE is the difference in energy levels, h is Planck's constant, and ν is frequency of radiation:

$$\Delta E = h\nu$$

According to Planck's law, if electromagnetic radiation of proper frequency is applied to an electron, it will absorb the radiation and undergo a transition between energy levels. The corresponding frequency must match the energy separation, ΔE, between spin states and its value is in the gigahertz range for EPR experiments at X-band. Since the

difference in energy can also be described in terms of the g factor, Bohr magneton, and the magnetic field, the following relationship can be made:

$$\Delta E = h\nu = gBH_0$$

For the purposes of an EPR experiment, this mandates two important points: (1) measurements of transitions between energy levels must take place in a magnetic field and (2) energies of the spin states diverge linearly as the magnetic field increases.

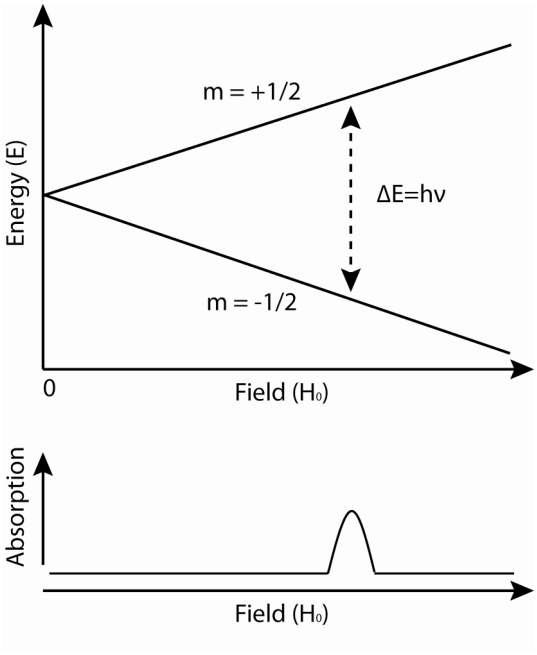

Figure 2.3† The field for resonance. Absorption of electromagnetic radiation will occur when the magnetic field is tuned so that its energy of radiation matches the energy difference in the two spin states.

The measurement of an electronic transition can be observed in one of two experimental methods. In one experiment, the magnetic field, H_0, is kept constant while the frequency, ν, is varied. An absorption of energy, E, will be observed at the frequency value that correlates to the separation of energy states, ΔE. Alternatively a transition can be observed in a constant frequency as the field is swept (Figure 2.3). The latter is the method of choice due to limitations of microwave electronics. With values of g = 2.0023 and $H_0 = 0.92731 \times 10^{-20}$ erg/gauss, the electronic transition will occur with an

electromagnetic radiation frequency of 9.5 GHz at a magnetic field strength of 0.34 Tesla (or 3400 Gauss). This frequency, known as X-band, corresponds to the microwave region (~3 cm wavelength) of the electromagnetic spectrum and is the predominant regime applied in EPR spectroscopy [198].

The signal is dependent on the spin population difference between energy states

The absorption signal arises from an average of many molecules, meaning ensembles of spins are detected in EPR experiments. In the presence of a magnetic field, spins will be in both high and low energy orientations; however the lower energy state will be slightly more populated as dictated by the Boltzmann distribution (Figure 2.4).

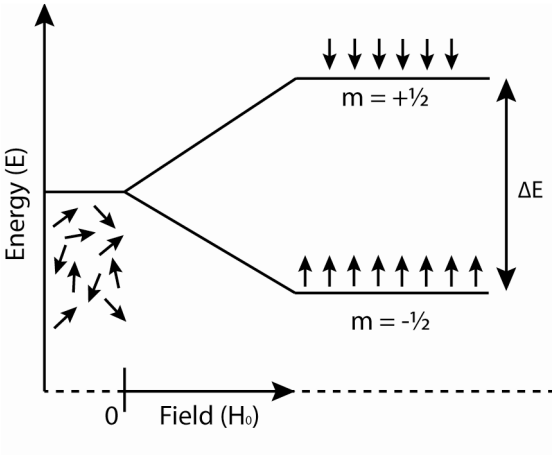

Figure 2.4 The Boltzmann distribution in a spin ensemble. In the absence of a magnetic field, spins will orient randomly with no difference in energy. When aligned in a field, the lower energy state will be slightly more populated than the higher energy state at thermal equilibrium.

There is an equal probability of a stimulated electron moving from α to β as from β to α; however, only the net excitation of spins will contribute to the absorption signal. As determined by the Boltzmann distribution, the spin population difference between the states is small and most of the spins are not detected. The spin population ratio of the states is temperature dependent and can be described by the following:

$$\frac{N_\alpha}{N_\beta} = e^{(\Delta E/kT)}$$

$$\frac{N_\alpha}{N_\beta} = e^{(gBH_0/kT)}$$

N values represent the populations of the α and β states, k is the Boltzmann constant and T is the absolute temperature [197,198]. If the ratio is calculated for a 293K temperature and a 1 Tesla magnetic field, the value is ~1.0046. Since this ratio is close to 1, the α state will only be slightly more populated. This relationship also illustrates that sensitivity can be improved by increasing the magnetic field strength or lowering the temperature.

Hyperfine interactions with neighboring nuclei determine the splitting of the signal.

The local environment of the unpaired electron will affect the influence of the magnetic field. The absorption pattern depends on the structure of the molecule containing the electron. The MTSSL molecule has been designed to make its free radical unusually stable even in the presence of some biological reductants (Figure 2.5). The gem dimethyl groups provide a steric hindrance for approaching redox reagents, offering protection for the N-O bond where the unpaired electron is localized.

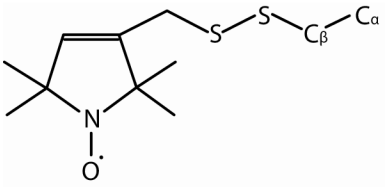

Figure 2.5 Diagram of the methanethiosulfonate spin label side chain. The unpaired electron necessary for the EPR signal is localized on the nitroxide portion of the molecule.

The electrons which give rise to the EPR signal, by way of their magnetic moments, will interact with nearby nuclear spins, resulting in additional energy states and multi-line spectra. The electron spin in MTSSL will therefore couple with the nuclear spin of the

adjacent ^{14}N due to their close proximity as illustrated in Figure 2.6. The electron M_s = -½ and +½ energy levels will be split by the nuclear I_S = -1, 0, and +1 spins resulting in six available energy levels for the nitroxide electron. Three allowable electronic transfers are possible when excited by electromagnetic radiation of three corresponding frequencies.

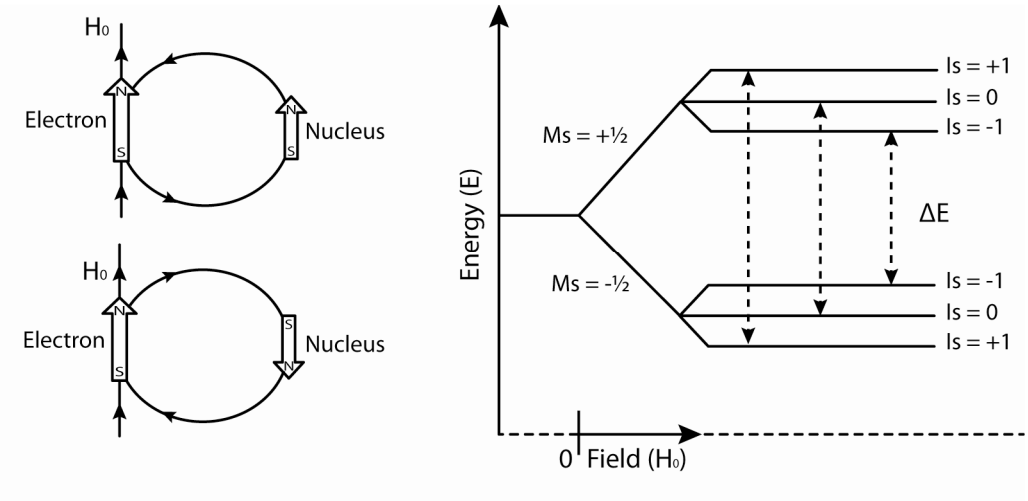

Figure 2.6† Hyperfine interactions between the electron and nucleus. The local magnetic environment of the neighboring ^{14}N nucleus interacts with the unpaired electron (left panel), increasing the number of spin states and allowing for three electronic transitions between energies (right).

These transitions result in three absorbance lines in an EPR spectrum of the nitroxide label and the field separation between them is dependent on the hyperfine coupling constant, A_0. A_0 indicates the degree of interaction between the unpaired electron and the perturbing ^{14}N nuclei and directly defines the spacing between spectral lines. Hyperfine coupling is just one factor which influences the spectrum. Spectra are also determined by spin label orientation and dynamics as well as relaxation processes.

The EPR lineshape is dictated by the orientation of the nitroxide in the magnetic field

In a hypothetical system where the unpaired electron is localized in a uniformly symmetric spherical orbital, the assumption can be made that all interactions with the

nucleus are uniform in all directions. In this case the hyperfine coupling constant, A_0, arises from only these isotropic interactions and the g factor is assumed to be the standard value given for a free electron. This would result in the three equally spaced absorption lines of equal intensity. In the actual case of all spin labels, the electron is occupying a non-symmetrical π orbital and the value for the g factor and A_0 depend on the orientation of the spin label in the field. They will have anisotropic contributions as the orbital angular momentum will experience the external magnetic field [198]. Therefore the net magnetic moment arises not only from the spin angular momentum, but from coupling to the orbital angular momentum as well. The overall field experienced by the electron can be expressed as

$$H_{eff} = H_0 + H_{local}$$

where the effective field, H_{eff}, is dependent on the external magnetic field, H_0, and the presence of a local magnetic field, H_{local}, such as the ^{14}N nuclear spin. The position of the field can be defined relative to the electron as illustrated in a three dimensional Cartesian coordinate system (Figure 2.7).

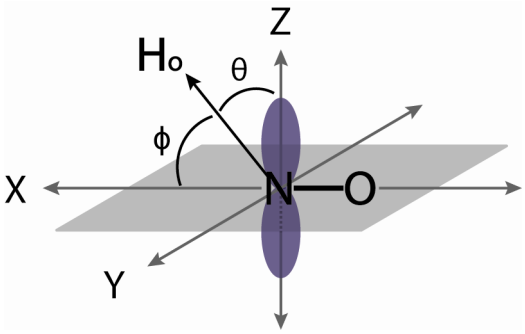

Figure 2.7† Relative orientation of the nitroxide spin label and magnetic field. The spin label N-O bond is placed along the X axis so that the π orbital (blue) aligns with the Z axis perpendicularly with the X-Y plane (gray). The magnetic field, H_0 is defined by angle θ from the Z axis and φ from the X-Y plane.

Here the π orbital containing the unpaired electron is aligned with the z axis of the coordinate system. The nitrogen-oxygen bond lies in the perpendicular x-y plane along the x axis. The field is represented by a vector and its position is conventionally defined by two spherical polar angles θ, its angle from the z axis, and φ, its angle to the x-y plane. Mathematically, both the g factor and A_0 can be represented as symmetric tensors. They describe the relationships between the magnetic field vector and the electron spin vector as well as between the electron spin vector and the nuclear spin vector. For example, g and A_0 can be divided into their component terms for each axis.

$$g = g_{xx} + g_{yy} + g_{zz}$$

$$A_0 = A_{xx} + A_{yy} + A_{zz}$$

In an isotropic system, all component parts would be equivalent.

$$g_{xx} = g_{yy} = g_{zz}$$

$$A_{xx} = A_{yy} = A_{zz}$$

In the nitroxide system, we can define these tensors anisotropically to include orientation dependence according to θ and φ.

$$g_{eff} = g_x \sin^2\theta\cos^2\varphi + g_y \sin^2\theta\sin^2\varphi + g_z\cos^2\theta$$

$$A_{eff} = [A_x^2 \sin^2\theta\cos^2\varphi + A_y^2 \sin^2\theta\sin^2\varphi + A_z^2\cos^2\theta]^{½}$$

The EPR spectrum represents the time averaged reorientation of the spin label ensemble

Only in a crystal lattice is it possible to have all labels in the same orientation with respect to the magnetic field. In most systems studied by EPR spectroscopy, each individual spin is orientated randomly within the field and makes its own contribution to the EPR spectrum. EPR spectra represent the ensemble of all spins, which, summed over

all molecules, represents many orientations [197]. One example of randomly orientated sample is spin labels in a crystalline powder. Although the molecules are randomly orientated, the nitroxide is held motionless. This gives rise to the "rigid limit" no motion EPR spectrum. For the rigid limit spectrum, the components are resolved along all directions in the magnetic field (Figure 2.8) and the spectrum can be predicted by adding up the individual spectra from all random orientations. In contrast, spin labels in solution will be constantly changing their positions due to molecular tumbling in addition to being randomly oriented. The rapid reorientation introduces a different level of complexity to the g and A_0 tensors. In this case the g_{eff} and A_{eff} are time-averaged.

$$g = \frac{g_x + g_y + g_z}{3}$$

$$A_0 = \frac{A_x + A_y + A_z}{3}$$

The resultant EPR spectrum is classified as the fast motion limit and illustrates that the rate of reorientation of spin labels influences its splitting resolution. The spectrum has an absorption pattern featuring three equally spaced peaks separated by the value for the A_0 tensor (Figure 2.8). Typically, EPR spectra are reported as the derivative of the absorption to more easily observe their features.

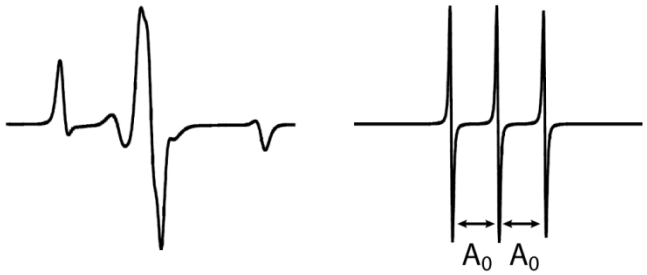

Figure 2.8 EPR spectra of motional extremes. The rigid limit EPR spectrum of MTSSL resolves all components along all direction in the magnetic field (left). The fast motion limit spectrum of MTSSL is time averaged (right).

The two derivative spectra in Figure 2.8 illustrate the extremes of spin label motion. They represent the difference between randomly oriented labels that are static (left panel) versus randomly orientated labels undergoing motion (right panel). Labels that are conjugated to proteins will have constrained motion and their spectra will fall within these extremes.

Relaxation influences EPR lineshape

As previously stated, the lower energy α state will be slightly more populated than the higher energy β state when a spin ensemble is placed in a magnetic field. These spins can be described by a bulk magnetic moment vector, M, which represents all spins collectively. Since spins have no preference for orientation in the absence of a magnetic field, M will be equal to zero. In the presence of a field, M is proportional to the population difference of spin states. Over time, a spin ensemble will return to thermal equilibrium as a function of relaxation which describes how spins "forget" the direction in which they are oriented. The two principle relaxation terms, T_1 and T_2, describe the physical properties responsible for the relaxation of the components of M.

T_1 involves redistribution of the different spin populations in order to achieve the thermal equilibrium distribution of the spin states. Spontaneous emission is very slow and contributes a negligible amount to spin distribution. Mainly equilibrium is reached when spins interact with their surroundings, exchanging energy to equilibrate spin populations. The surroundings are referred to as the lattice and gives rise to the T_1 pseudonym, spin-lattice relaxation. This transfer of energy from excited spin states to the lattice is non-radiative and decays exponentially over time. After the time T_1, the

population of spins will be described by the Boltzmann distribution and the net magnetization vector will align with the direction of the applied magnetic field. The T_1 value describing how fast M aligns with the field reflects the degree of coupling between all electron spins to the surrounding environment. The process of spin-lattice relaxation contributes to the magnetic moment vector M as described by the Bloch equation.

$$\frac{dM_Z}{dt} = \frac{M_0 - M_Z}{T_1}$$

M_Z is the bulk magnetization along the z-direction in the absence of a magnetic field and M_0 is the bulk magnetization at thermal equilibrium. The Bloch equation defines the interdependence between the net magnetization and the spin-lattice relaxation. Without T_1, the EPR experiment would be impossible. It is critical that the system achieves a ground energy state following microwave absorption. In the absence of spin-lattice relaxation, exciting microwave radiation would equalize the population of spin states and eliminate net polarization. As described previously, it is the net polarization of spins that contribute to the EPR signal. It is essential that the population be able to reach the Boltzmann equilibrium so that the bulk magnetization does not decay to zero.

Like any vector, M can be defined by its components relative to the x and y axes, M_x and M_y. But because M originates from the spin ensemble, it also possesses a bulk angular momentum resultant from individual electron spin angular momenta (Figure 2.9). The applied magnetic field will exert a torque on the bulk spin causing M to precess about the magnetic field like a gyroscope [197,198,199].

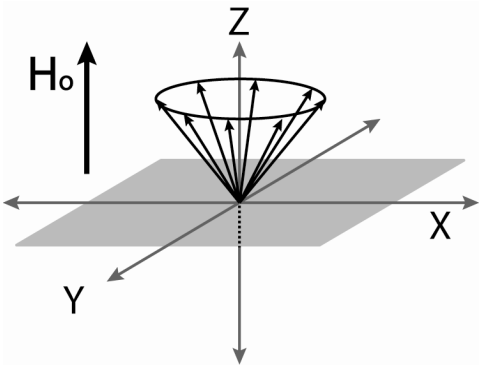

Figure 2.9[†] Precession of electron spin in the presence of a magnetic field. The external field interacts with the bulk angular momentum to cause precession of the spins about the z axis. The precession causes the x and y component s of the bulk angular momentum to average out to zero, leaving only the z component. The net magnetization along the z axis results from the net population of spins aligning with the field.

The precession results from time-dependent changes in the M_x and M_y components and its frequency is referred to as the Larmor frequency. The Bloch equations can be written to describe these transverse components.

$$\frac{dM_x}{dt} = \gamma H_0 M_y - \frac{M_x}{T_2}$$

$$\frac{dM_y}{dt} = \gamma H_0 M_x - \frac{M_y}{T_2}$$

Here γ is the electron gyromagnetic ratio, and T_2 is the spin-spin relaxation time. T_2 is the rate at which M_{xy}, the transverse component of the magnetization vector, exponentially decays towards zero. It does not include energy exchange with the lattice like T_1, but rather describes the relaxation from either dipolar interactions or collision with neighboring spins [197,198]. These energy transfers reorient or "flip" spins and alter their magnetic moments.

Both T_1 and T_2 relaxation mechanisms contribute to the EPR lineshape. In a continuous wave (CW) EPR experiment, continuous irradiation of microwaves is applied along the axis perpendicular to the magnetic field, H_0. This generates a steady state

magnetization behavior in the spin ensemble. The Bloch equations must also take into account the perturbing interaction of the oscillating microwave field and the absorption of the radiation is illustrated by a Lorentzian function. The function is the description of the spectral lines, which are subject to broadening depending on the interactions with the frequency. The width of a particular absorption peak is dependent on the value for T_2. At half height of the peak, the width is inversely proportional to T_2. Therefore, faster T_2 times lead to broader lineshapes. The T_1 relaxation process also contributes to the EPR signal because it establishes finite lifetimes for excited states and prevents absorption lines from becoming infinitely narrow.

The EPR lineshape is determined by the mobility of the probe

As mentioned previously, the orientation of the probe in a magnetic field will affect its EPR spectrum. The rate of motion of the nitroxide impacts the anisotropies of the g and A_0 tensors, and will ultimately determine the lineshape. These probe motions are incorporated into the qualitative EPR parameter of mobility. Mobility describes the motion of the probe which is dependent on how the surrounding environment restricts it. In the context of a labeled protein, the free electron is localized to a MTSSL probe, which in turn is conjugated to a protein tumbling through solution. A labeled protein is much more complex than a free probe and undergoes several types of additional motion, each occurring on a different time scale. Therefore, the EPR lineshape is reflective of the available degrees of motional freedom of the attached spin label as well as the dynamic properties of the tumbling macromolecule [200]. The various types of motion are summarized in Figure 2.10.

On a slow timescale the protein is tumbling randomly through solution, the rate of which is dependent on the size of the protein and the viscosity of the solvent. Typically for large proteins over 50 kDa, the rate is too slow to have an effect on the spectrum. Tumbling rates (10^{-7} s or slower) are outside the EPR timescale, which is in the nanosecond regime (10^{-11} – 10^{-9} s) [192,194]. Since tumbling offers little information on the structure of a protein, this is not disadvantageous. In fact for smaller soluble proteins, the viscosity of the solvent is often increased in order to eliminate any tumbling contribution to the EPR spectrum.

Proteins are not static molecules but are comprised of dynamic domains which move relative to each other. It is necessary for one protein to have the capacity to exist in several conformations so that it may complete its function, for example to recognize and bind its ligand. Domain rearrangements can be substantial, creating interdomain distance changes of tens of angstroms, or subtle, such as the twisting of domains where only a few angstroms change is observed. Either way, the rate of exchange between the conformations is typically too slow to contribute to the mobility of a spectrum (μs-ms). This is not to say that conformational rearrangements cannot be observed with EPR spectroscopy. There is an important distinction. Sets of spectra obtained under various conditions can be used to infer conformational changes. For example, a label in the active site of a particular protein may show high mobility in the absence of ligand. In a separate experiment, ligand is added to the system which causes immobilization of the site. The two spectra from these experiments can be compared to deduce that a conformational change has taken place. However, the actual transition between conformations was not observed directly.

Within each conformational state, the protein backbone can flux between a multitude of short lived substates, each having different torsional angles in the bonds of the backbone. The rate of backbone fluctuations depends on the stability of the local environment, and they exist on the nanosecond-picosecond timescale. For example, stabilized helicies in the center of a protein will remain relatively static and will not significantly increase the mobility. In comparison, loop regions where backbones are flexible and dynamic have faster rates and readily contribute to mobility increases.

The isomerization of the label about the chemical bonds attaching it to the protein backbone will also contribute to mobility. Each bond has a unique ability to isomerize which is dependent on steric restriction by neighboring atoms and the energy barrier for each rotamer conformation. Although there are several chemical bonds between the backbone of the protein and the free electron, it has been suggested that motion is largely restricted to rotation about the C_ε-C_ζ and the C_ε-S bonds [194]. Since the disulfide bond must cross a high energy barrier to rotate and the S-C_β bond is restricted by the C_α hydrogen, they are unlikely to contribute to probe mobility. Any bond may be further restricted by atoms of the protein backbone or neighboring amino acid side chains. The mobility of the probe therefore depends on its position within the protein as well. The EPR lineshape will depend on whether or not the spin label side chain is restricted in the core of a protein or freely rotating as a side chain facing the solvent.

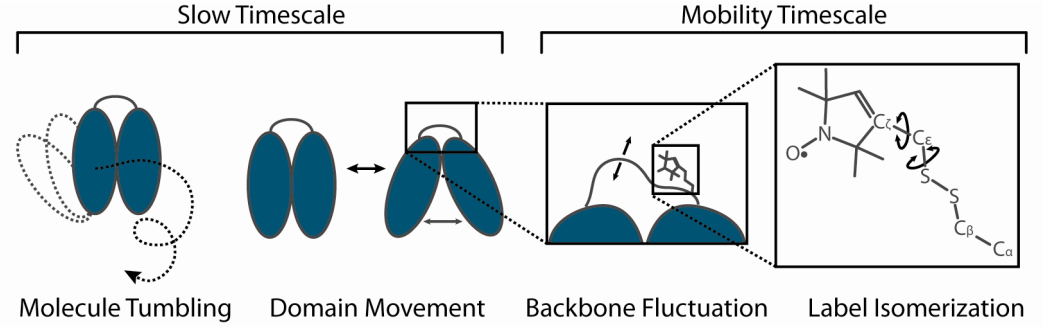

Figure 2.10 Types of protein motion. A hypothetical protein (blue) undergoes various types of motion including molecule tumbling through solution, domain movements, and backbone fluctuations. The MTSSL probe also undergoes rotation about the bonds conjugating it to the protein backbone.

Each of these types of motion will reposition the spin label with respect to the magnetic field but the motion of the spin label side chain is largely dictated by backbone dynamics and label isomerization (Figure 2.10). These motions have the potential to alter the spectral lineshape because they occur on the EPR relevant timescale. Since the EPR experiment does not observe just one motional transition, but many transitions of many molecules, the spectrum will report an average of all motions. Backbone dynamics and label isomerization can be distinguished from each other with a full simulation of the EPR lineshape [200,201].

Spin labeled sites can be classified by mobility and rotational correlation times

Due to the hyperfine interactions of the free electron with the neighboring ^{14}N nucleus, a sweep of the magnetic field under constant microwave irradiation will induce absorption at three resonance positions. These peaks vary according to the anisotropy of the label allowing for a range of lineshapes. For example, a site buried in the hydrophobic core of a protein will have a very different spectrum from a loop region due to their contrasting mobilities. However, spectra from one buried site versus another buried site will produce very similar lineshapes. Within a range of variability, buried,

surface, and loop sites all have signature lineshapes which can be used to classify residues. Additionally a numerical value referred to as its rotation correlation time, τ, can be assigned to spectra to define spin label mobility. This value represents the rate of spin label isomerization; a shorter timescale indicating faster rotation and higher mobility. Figure 2.11 illustrates simulated spectra of a MTSSL probe with preset rotational correlation times.

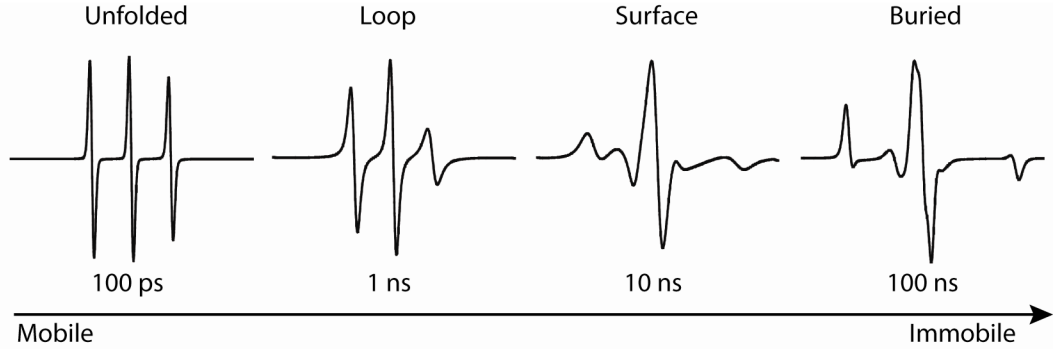

Figure 2.11 Spectral classification and rotational correlation times. Sites can be classified by their spectral lineshape, which is dependent on the rate of label isomerization. Slower reorientation rates of the label causes broadening of the resonance lines, which increases the breadth of the EPR spectrum as well as the peak widths. Rotational correlation times indicate rotation rate, with a shorter timescale indicating a faster rate. These spectra were simulated for MTSSL according to predefined correlation times.

For free label or label attached to unfolded proteins, the mobility will be highest because the label is the most unrestricted. Spectra will be characterized by three evenly spaced sharp, narrow lines with tight A_0 separation between peaks. A short rotational correlation timescale (100 ps) classifies these spectra suggesting the spin label has a fast rotational rate. Loop regions are less mobile and are broadened in comparison. They still possess a high degree of mobility because the label can freely isomerize and the protein backbone is flexible. They are classified by correlation times on the order of 1 ns. As the correlation time increases, lines become broader. Correlation times on the order of 10 ns describe surface sites which have stable, ordered backbones but freely rotating side chains. The most buried sites have the longest correlation timescale and show the most

spectral broadening. A 100 ns correlation time would be typical for a label placed in the hydrophobic core of a protein or at a protein-protein interface. In this case mobility is the lowest because the label is completely restrained. Thus the EPR lineshape is the interpretation of the spin label motion which can be used to characterize sites in loops, surface regions, or buried protein interiors. This informational is invaluable for structural studies.

Experimental spectra can be computationally simulated and rotational correlation times can be estimated with a microscopic order, macroscopic disorder method (MOMD) [202]. In this method, a set of simulation parameters and fitting procedures are incorporated to produce a hypothetical spectrum which has features similar to the experimental target. The correlation time describes the rotational nitroxide angles relative to its direction of motion. Variable parameters are used in this method to describe the motion of the nitroxide, which will dictate the resulting spectral lineshape. These parameters optimize the magnetic tensors, rotational diffusion rates, coefficient of the ordering potential, and diffusion tilt angles. Typically, standard nitroxide values are input for g-tensors and A-tensors which have been previously measured [203]. Otherwise parameters can be obtained from a simulation of a rigid limit, frozen solution spectrum. In general, fast isotropic motion is estimated by assuming the movement in the x, y, and z directions are equal to each other while restricted anisotropic rotation assumes these are not equivalent. Anisotropic motions require an ordering potential which serves to constrain the spatial extent of the motion. This term defines the orientation of the label by describing the potential of its movement, i.e. defining the space in which the spin label motion is occurring. The strength of this ordering potential is determined by its

coefficient which is user-defined. Diffusion tensor values are additionally varied to establish the diffusion rate as are diffusion angles which express the rotation of the diffusion. Spectral line broadening can also be estimated by defining either a Gaussian or Lorentzian function. For fitting of experimental spectra, starting values for these variables are chosen using a Monte Carlo algorithm. The appropriate simulated spectrum is reached when the parameters produce a simulation that converges with the experimental spectrum. The rotational correlation time, τ, for the motion is obtained from the resulting diffusion coefficient, R.

$$\tau = \frac{1}{6(R_x + R_y + R_z)^{1/3}}$$

While any specific simulation may converge to fit the experimental spectrum, the solution is not unique. However, correlation times will not vary greatly from one simulation to another.

Dipolar coupling is distance dependent

In addition to side chain mobility, the distance between two paramagnetic probes can be measured by various EPR methods. The information obtained can define the spatial relationship between structural elements which yields information on the global organization of the molecule. When two spin labels are in close proximity, spin-spin interactions between the two electrons are manifested in the CW-EPR spectrum through broadening of lines which are a function of inter-probe distance. The spin Hamiltonian can be modified to include these interactions.

$$\mathcal{H} = g^1 B H_0 S^1 + g^2 B H_0 S^2 - \omega_n (I_z^1 + I_z^2) + \gamma I^1 A^1 S^1 + \gamma I^2 A^2 S^2 + S^1 D S^2 + J S^1 S^2$$

Here ω_n is the Larmor frequency of the nitrogen nucleus, γ is the electron gyromagnetic ratio, D is the dipolar coupling tensor, J is the isotropic spin-spin exchange factor, and number superscripts designate electron 1 and electron 2 [198]. There are two types of exchange interactions; those that occur though bonds and those that occur through space. Scalar J coupling describes through-bond interactions and is facilitated in orbital overlap or though chemical bonds. It decreases exponentially with increasing interspecies distance, contributing little beyond ~8 Å. In the case of MTSSL, the nitroxide of the spin label is separated from the protein backbone by approximately 7Å. For these reasons, J coupling is generally disregarded in spin labeled protein systems. Even in a system where spin labels are within 7Å, the dipolar interaction will be stronger than J coupling. The dipolar interaction term therefore represents spin coupling between probes which can be measured from 8-70 Å.

In the absence of dipolar and J coupling, the Hamiltonian reduces to represent the sum of two non-interacting spins. In the condition of dipolar interaction, the energy is inversely proportional to the cube of the distance and is dependent on the orientation in the external magnetic field. It can be defined according to the angle between the field and an interspecies vector, θ [198,204,205] (Figure 2.12).

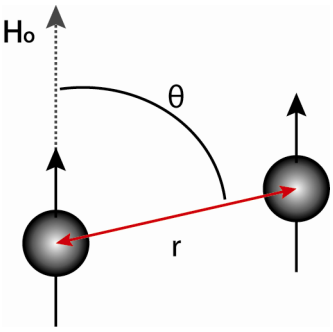

Figure 2.12† The interaction between two dipolar spins. The interaction between two magnetic dipoles is dependent on the distance between them, r, and the angle of the magnetic field, θ.

The dipolar coupling, ν_{dd}, can also be written in terms of the distance and angle. The corresponding energy of interaction between electrons, E, can be approximated with point dipoles, μ, and is described as follows.

$$\nu_{dd}(r,\theta) = \frac{\mu_1 g_1 g_2 \mu_2}{2h} \cdot (3\cos^2\theta - 1) \cdot \frac{1}{r^3}$$

$$E = \frac{\mu_1 \mu_2}{r^3} \cdot (3\cos^2\theta - 1)$$

The angular dependence of the dipolar coupling is best illustrated in the Pake pattern. This type of spectrum specifically illustrates the dipolar frequency pattern averaged over all angles with respect to the magnetic field. The Pake pattern in Figure 2.13 exhibits two prominent peaks separated by $2\nu_{dd}$ (r,90°). The frequency of separation between the two peaks of the Pake pattern is inversely proportional to the distance at θ = 90°.

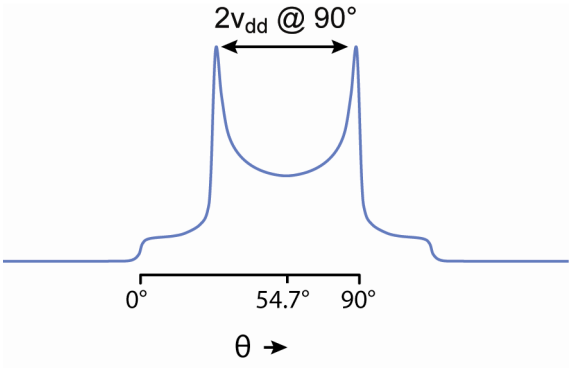

Figure 2.13[†] The Pake pattern for two dipoles. The blue trace shows two transitions with a splitting of $2\nu_{dd}$ (r,90°).

The Pake splitting can be related to the inter probe distance by the following equation where the constants are approximately correct for a nitroxide.

$$r = \sqrt[3]{\frac{52.16\ MHz}{\nu_{dd}(90°)}}\ nm$$

These relationships are the theoretical basis of distance measurements in EPR spectroscopy. At distances shorter than 20 Å, the dipolar interaction is sufficiently strong to influence the CW EPR lineshape. The lines will become broadened in a distance dependent manor, shorter distances leading to more extensive broadening. The distance can be extrapolated by a convolution/deconvolution analysis [206,207] of the spectral lineshape (Figure 2.14). This requires spectra of the singly labeled systems as well as the doubly labeled system. The spectra from the singly labeled systems are averaged to create a new spectrum referred to as the sum of singles. A Pake broadening function with variable distance values is applied to this spectrum until it converges to fit the experimental spectrum of the doubly labeled system [206,208]. The results are reported as distances with Gaussian distributions according to their relative probabilities. The distribution of distances arises from the range of the nitroxide flexibility as well as any protein conformational heterogeneity.

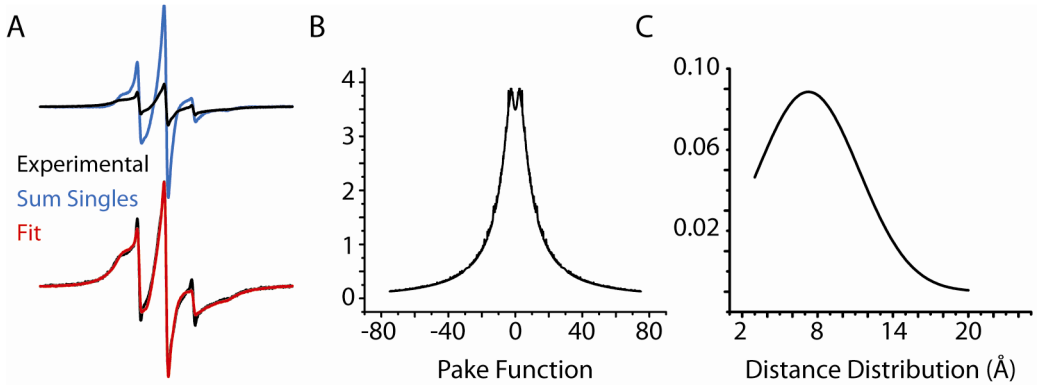

Figure 2.14 Illustration of the convolution/deconvolution method. A) The experimental spectrum of a doubly labeled protein (black) is broadened relative to the sum of singles spectrum (blue). The fit for the convolution.deconvolution method is shown in red. The Pake broadening function (B) used to obtain the fit produces the distance distribution shown in panel C.

For distances greater than 20 Å, the EPR spectrum is not broadened enough to be resolved in CW EPR. The values for ν_{dd} become very small at long distances and the inhomogeneous linewidth of the spectrum masks the dipolar interaction. Therefore,

conventional CW EPR spectroscopy can be used to measure inter-probe distances only in the range of 5-20 Å.

Time domain pulsed methods detect dipolar coupling at longer distances

A time domain EPR method called double electron-electron resonance (DEER) is used to measure dipolar interactions which are unresolved in CW spectra. This pulse technique can detect dipolar coupling up to 70 Å [206,209]. In CW experiments, the field is swept slowly under constant frequency and any resonances are detected by absorption of energy. In contrast, short and intense microwaves are applied to the system in a pulsed experiment and all the multiple resonances coming from the sample are collected in the time domain. After Fourier transformation, the various resonances are resolved and the spectrum can be reported in the frequency domain.

As previously described, the bulk magnetization, M, can be represented by a vector in a Cartesian coordinate system. It precesses at its Larmor frequency about the z axis, which is aligned with the external magnetic field (refer to Figure 2.9). This particular perspective is referred to as the lab frame. For description of the DEER experiment, it is helpful to redefine the coordinate system to rotate about the z axis so that the precessing magnetic component appears motionless. This is designated the rotating frame. The result is a stationary magnetization vector, M, aligned along the field.

The microwave resonator on the pulse instrument is designed to produce a microwave magnetic field perpendicular to the applied magnetic field. Since this dictates observation of M occurs in the x-y plane, DEER experiments must use pulses of radiation

to tip M into the x-y plane for detection. Pulses are labeled by their tip angle which depends on the strength of the field and length of the pulse. A π/2 pulse rotates M 90° into the x-y plane while a π pulse, referred to as an inversion pulse, will flip the vector 180° along the z axis (Figure 2.15).

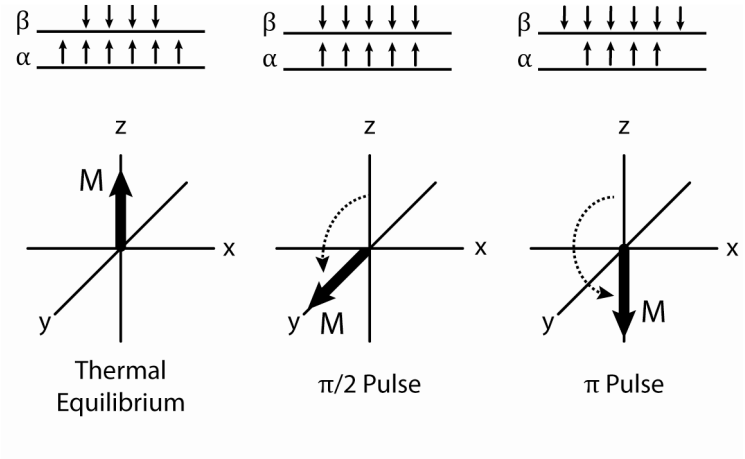

Figure 2.15† Tipped orientation of the bulk magnetization and spin population. At thermal equilibrium M is aligned with the z axis and the spin population is represented by the Boltzmann distribution. Application of a π/2 pulse equalizes the distribution and tips the magnetization into the x-y plane. A π pulse will flip M onto the negative z axis and invert the spin population.

Over time, a tipped system will return to equilibrium and realign with the z axis. The magnitude of M in the x-y plane will therefore decay over time according to the relaxation properties of the system. The spin-lattice relaxation time, T_1, describes how quickly the magnetization returns to align with the external magnetic field along the z axis. The spin-spin relaxation time, or transverse relaxation time, T_2, describes how quickly the magnetization in the x-y plane decays. For example, a π/2 pulse tips M into the x-y plane. The system is no longer in thermal equilibrium because the magnetization along the z axis goes to zero. Since this net magnetization represents the difference in spin state populations, the spin population difference is therefore zero. Interactions with its surroundings through spin-lattice relaxation will cause the system to return to thermal

equilibrium and adopt Boltzmann distribution of spin states. In the case of a π pulse, M will rotate in an antiparallel fashion to align with the negative z axis. Here the spin population is inverted and will likewise return to equilibrium by spin lattice relaxation interactions described by T_1.

The detected signal characterizes the total effect of a large number of spin packets that make up the bulk magnetization, M. The transverse relaxation time, T_2, influences the breadth of the signal either through homogeneous or inhomogeneous broadening (Figure 2.16). Homogeneous broadening describes the effect of many broad lines added together, each with the same Larmor frequency and linewidth. Inhomogeneous broadening occurs when several narrow lines of slightly varied frequencies add together to appear as one broadened peak.

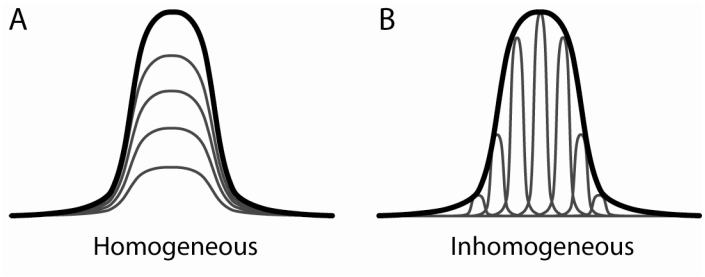

Figure 2.16[†] Homogeneous and inhomogeneous broadening of EPR lineshapes. A) Homogeneous broadening determined by relaxation processes is a sum of many lines with the same frequency and linewidth. B) Inhomogeneous broadening is caused by many narrow lines, each with a slightly different frequency.

Individually each spin packet experiences a slightly different magnetic field and has its own precession frequency due to spin-spin interactions. These interactions cause a fanning out of the spin packets throughout the x-y plane. Dephased components spread out in opposite directions to cancel each other and lead to decay of the signal in the x-y plane over time, T_2. Figure 2.17 illustrates how the signal is dependent on the decay.

After the π/2 pulse, the signal is the strongest. As the spin packets precess at their individual Larmor frequencies, they spread out through the x-y plane causing the net magnetization in the x-y plane to eventually become zero.

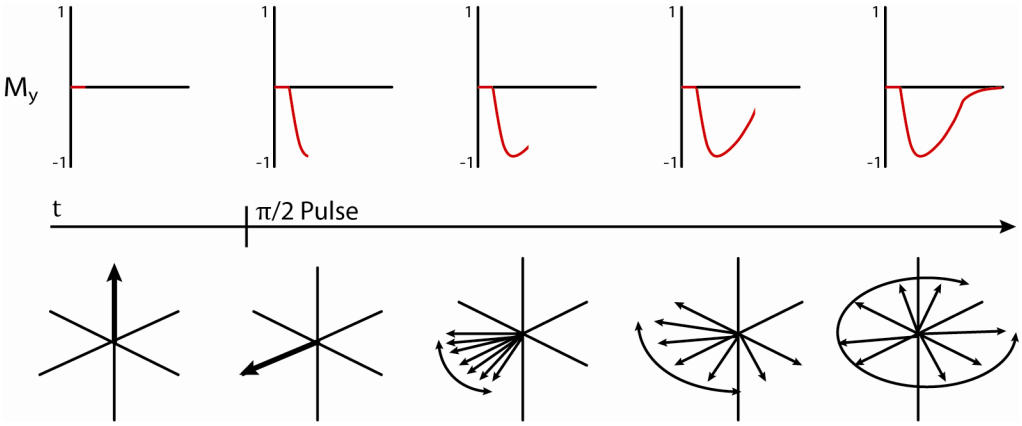

Figure 2.17† Dephasing of the transverse magnetization. After a π/2 pulse, the spins will be tipped into the x-y plane and fan out according to their individual Larmor frequencies. The spreading causes the net magnetization in the x-y plane to decay over time as a function of T_2.

DEER experiments employ a refocused echo method instead of observing the free induction decay (FID) of the π/2 pulse. The spectrometer cannot measure directly after the high power microwave pulse as the FID signal would be overwhelmed. Since most of the signal will decay in the instrument dead time, a standard four-pulse experiment is used to refocus and detect the signal after a sufficient time.

The DEER pulse sequence permits detection of the refocused echo

The pulse protocol begins with a π/2 pulse which tips spins into the x-y plane for detection (Figure 2.18). The spins will begin to diphase and produce the initial FID. After a time, τ_1, a π pulse is applied to refocus the echo. This will flip the spins 180° in the x-y plane effectively causing them to precess in the opposite direction. Spins that were separating are now converging toward the same position causing the refocused

signal. Finally an additional π pulse is applied to refocus the echo in the opposite direction. This is the observed echo and it is separated from the π pulse by τ_2.

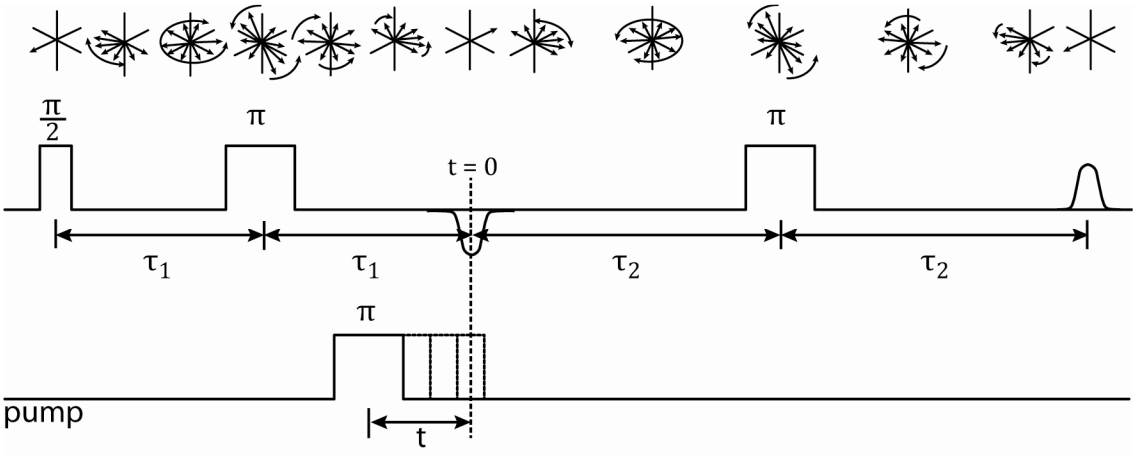

Figure 2.18[†] Four pulse protocol for a DEER experiment. The magnetization behavior is altered by a π/2 pulse, followed by a π pulse which refocuses the echo, and an additional π pulse which reorients the phase of the echo. At a separate pump frequency, a π pulse is applied to measure dipolar coupling between spins of pump frequency and spins of the observe frequency.

For the DEER experiment, it is necessary to apply two microwave frequencies to the sample, one to observe and one to pump. This protocol will allow for the detection of dipolar interactions between spins at the pump frequency and spins at the observe frequency. After the observe π pulse, a π pulse at the pump frequency is applied (Figure 2.18). This indicates that while the observe frequency spins are being refocused, the spins at the pump frequency are being flipped. Changes in the magnetization of these spins perturb the spins at the observe frequency only if they are dipolar coupled. Any of these pump frequency dependent changes in the observed frequency contribute to the EPR signal. Additionally, the start of the pump π pulse is varied by time t as the refocused echo is detected. By varying this pulse through time, the influence of the coupling on the final signal can be determined.

The oscillation of the refocused echo intensity contains the information describing the dipolar coupling. The echo will decay with T_M, the phase memory time, meaning that as the distance becomes larger oscillations become slower. T_M is primarily a function of T_2 relaxation and must be extended significantly to complete an actual experiment. This is accomplished by conducting the experiment at low temperatures around ~80 K. Since the samples are frozen at this temperature, the resulting data is a static representation of isotropically averaged spins [206,210]. The amplitude of the observe spin echo is plotted as a function of t and the periodicity of oscillations is related to the distance. The rate of signal decay to the baseline determines the width of the distance distribution (Figure 2.19).

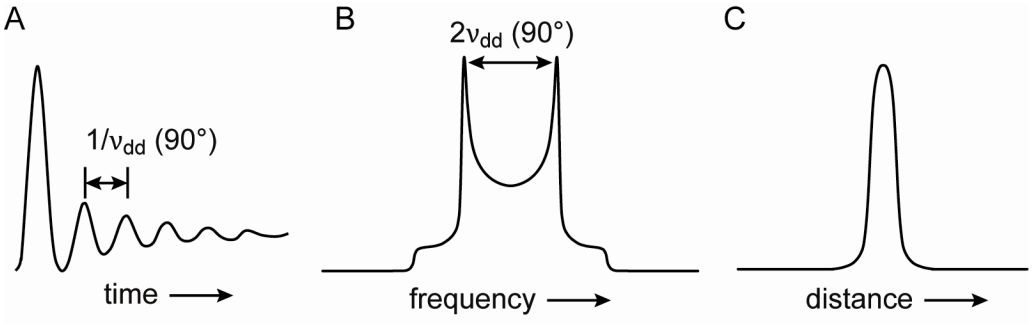

Figure 2.19 Relationship between the DEER modulation and the distance dependent dipolar coupling. A) The oscillation frequency of the DEER signal is related to the distance between paramagnetic species. B) Conversion between the time domain DEER signal and frequency domain Pake pattern can be completed with Fourier transformation. C) Distance determination can be obtained by Tikhonov regularization and is reported as distance distribution as a function of probability.

Distance information can be extracted by Fourier transforming (FFT) the signal into the frequency domain to obtain the Pake spectrum. Alternatively fitting routines like a parameterized Gaussian model or Tikhonov regularization can be used to analyze the DEER signal [210]. Tikhonov regularization simulates the time domain data to fit the experimental data and balances fit uniqueness with the smoothness of the resulting distance distribution.

Distance distributions obtained from DEER analysis facilitate interpretation of the protein conformation as well as the direction and amplitude of any conformational changes. Combined with the methods of CW EPR, these techniques provide a wealth of information on the environment, position, and motion of spin labeled side chains. In scanning experiments where spin labels are introduced sequentially along the protein sequence, the information from these parameters can also result in a structure of medium resolution at the level of backbone fold [211,212]. These methods are tried and true, as changes in the EPR parameters and distances have been shown to reflect domain movements and conformational changes in many protein systems [194,207,212,213,214,215,216]. Obtaining this type of structural information on proteins is so important because the forms and dynamics of proteins govern their functions. Since proteins of any living system are the driving forces to all biological processes, this information is essential for deciphering molecular mechanisms.

The site directed spin labeling method has experimental advantages and limitations

For the study of proteins by EPR spectroscopy, an MTSSL probe can provide the necessary unpaired electron. In this labeling technique, a probe is conjugated to a cysteine residue by disulfide linkage. Any native cysteines must be replaced with non-cysteine residues, then a cysteine at the site of choice must be introduced. Any site can be mutated to cysteine and reacted with a spin label using the site directed spin labeling (SDSL) method (Figure 2.20).

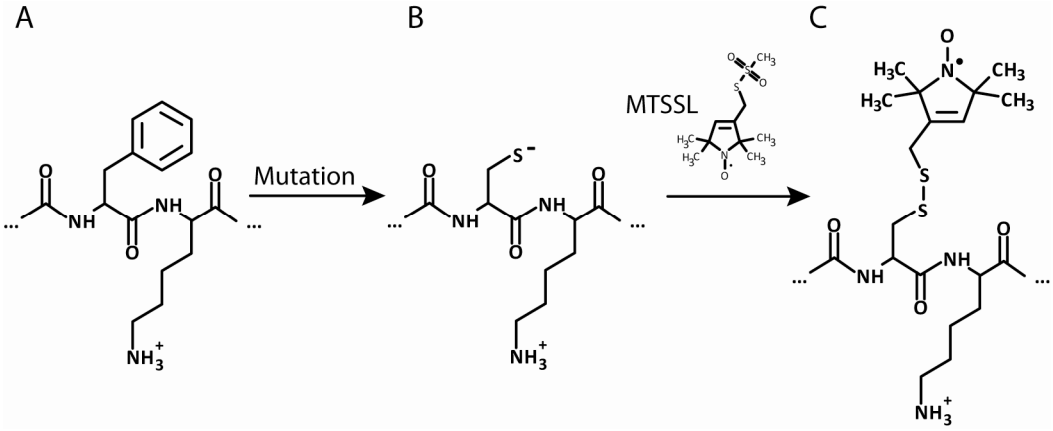

Figure 2.20 Site directed spin labeling method. A) A desired residue, in this case a phenylalanine is mutated to a cysteine by standard mutagenesis techniques. B) The sulfur in the cysteine residue reacts with the spin label. C) The resulting spin labeled side chain is linked through a disulfide bond.

Through standard mutagenesis techniques, the codon for a desired residue is changed to a cysteine codon so the expressed protein will contain the cysteine replacement. The sulfur moiety reacts with the MTSSL to produce the spin labeled side chain. The physical properties of some side chains are essential to protein fold and the spin label may perturb interactions with surrounding atoms. However, an investigation of T4 lysozyme found that only core residues are affected by labeling and that the thermodynamic perturbations were at the level of those found for natural amino acid substitutions [194]. Spin label side chains are generally well tolerated and the vast majority of sites can be labeled with this method. Because of their local environments, some sites label more efficiently than others and the labeling efficiency affects the experiment. Since the EPR spectrum reflects the total spin population, poor labeling will result in a low signal to noise ratio. In the circumstance of poor labeling, it can also be difficult to remove excess unbound label from the sample which will contribute to the EPR lineshape. For DEER measurements, excess free spin label is too dilute to be problematic, as the signal arises only from dipolar coupled spins.

Typically numerous sites on a protein need to be investigated to obtain a complete picture of protein conformation. Since each site investigated with SDSL-EPR necessitates a new protein mutant, the method requires expression and purification of many proteins. This is potentially a serious limitation for proteins which do not express in adequate yield or require extensive purification protocols. It is necessary to be able to produce purified proteins in a high throughput manner. That taken into consideration, EPR experiments only require a small amount of protein (as little as 100 pmol) compared to other structural techniques. These experiments also have the advantage of observing proteins in solution. Although the data would be considered low resolution compared to an X-ray structure, the more native-like environment allows for investigation of protein dynamics. Proteins are not static figures, they exist in multiple conformations and their movements define their molecular mechanisms. Although EPR experiments to measure interprobe distances are comparable with a FRET or homotransfer FRET method, EPR has the advantage of reporting multiple distances and their distance distributions while FRET reports a single distance that assumes an average dipole orientation of the two probes [217]. EPR also possesses advantages over other dynamic methods such as nuclear magnetic resonance (NMR) because there is no system size limitation. However EPR is synergistic with other structural methods because having a high resolution structure of the protein fundamentally expedites experimental design and interpretation. EPR data is unique in its ability to fill the gap between structural snapshots and dynamic behavior of proteins. Many model systems have been investigated with this method [194,207,212,213,214,215,216] and it is now widely used to study systems including channels, transporters, and receptors as well as soluble proteins [213,214,216]. SDSL-

EPR is ideal for CaMKII investigation because of the profound changes in backbone structure and inter-domain distances associated with its mechanism of activity.

CHAPTER III

METHODS AND BIOCHEMICAL CHARACTERIZATION

Introduction

For SDSL-EPR, it is essential to find protein expression and purifications systems which are of high yield, speed, and quality. Since a high throughput CaMKII system had not previously been developed, it was necessary to optimize the expression cell line, vector, and gene as well as the purification process. Many of the seemingly endless list of possibilities for these variables were investigated and eventually boiled down into one straightforward protocol. The final protocol is one solution for expression and purification and is certainly not unique. Although determining what will work is a trial and error method, it is the physical properties of the DNA, the translated protein, and the cellular environment which dictate success. A wealth of information was obtained in decoding the details of what worked as well as what didn't work. These details are described in this chapter. Beyond this, the rationale for mutagenesis and other alterations of the optimized protein are presented. Finally data from biochemical analyses are described to demonstrate that protein function and structure is preserved under the indicated modifications.

The mouse CaMKIIα isoform is unstable during bacterial expression

The optimization of CaMKII expression began with a mouse CaMKIIα isoform. This isoform is highly expressed in the brain and has been well characterized by the

Colbran laboratory [31,218]. If at all possible, it is preferred to work with mammalian proteins, since their physiology is the most similar to human proteins. This particular protein is extremely highly conserved, with 99.8% homology to human CaMKIIα. Previously the expression was performed in Sf9 insect cell cultures by way of baculovirus infection. Although these cultures yield sufficient amounts of active protein, they take weeks to prepare. Therefore, the first goal was to express the protein in a bacterial cell line, in which expression takes mere hours. The protein was cloned into two pET system vectors, pET28b+, which contains codons for an N-terminal six histidine affinity tag, and a tagless pET21a. These vectors were chosen because of their superior T7 promoter system. The T7 promoter tightly regulates foreign protein production and prevents any toxicity from uninduced expression of the protein during basal cell growth. Induction by IPTG then turns on expression when the culture is at a desired density. These vectors were expressed in several cells types and the growth and induction were varied in attempt to find the best expression conditions. Many conditions were tried, and all resulted in substantial protein degradation during expression. Figure 3.1 illustrates the protein cleavage for just two representative expression trials for mouse CaMKIIα.

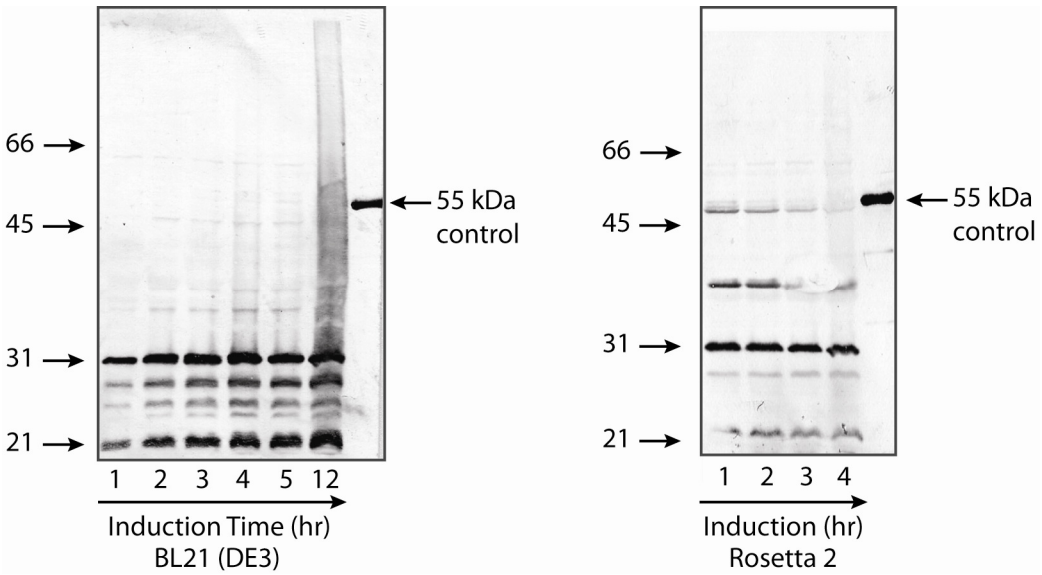

Figure 3.1 Western blot of mouse CaMKIIα expression. This figure illustrates western blots of two separate expressions, one in BL21(DE3) cells (left panel) and the other in Rosetta 2 cells (right). The lanes feature time points taken after a 1 mM IPTG induction. Numbers on the left side of the blots indicate positioning for molecular weight markers. The 55 kDa CaMKII control is purified protein expressed in Sf9 cells.

Full length CaMKII protein will be observed at a molecular weight of 55 kDa on a protein gel. When comparing the expression in BL21(DE3) cells to the 55 kDa control lane, virtually none of the expressed protein is uncleaved (Figure 3.1, left panel). Although Rosetta 2 cells, which are deficient in *lon* and *ompT* proteases, had significantly more full length protein than BL21(DE3), the yield was still too low for SDSL-EPR (right panel). For a complete list of CaMKII expression trials of all tried cell types and vector varients, see Appendix A.

Proteins can be truncated because of a natural abundance of a compatible protease, the efficiency of which can be increased if there is also a toxic effect of the expressed protein, instability of the protein, or a combination thereof. Several cell lines with reduced proteases were tried and protease inhibitors were even added to the expression media. These measures seemed to be inconsequential indicating protease activity could not be controlled. To reduce susceptibility to cleavage, we addressed

possible toxicity toward native *E. coli* proteins by this promiscuous enzyme's phosphorylation potential. The previously used technique of knocking out catalytic activity with a D135N mutation was employed [138], however truncation was not reduced. This indicated any toxicity was not relieved by inactivating the enzyme. Finally several truncated variants were engineered to intentionally omit the C-terminal association domain and its connecting flexible linker, where a large portion of proteolysis was believed to be occurring. The expectation was that CaMKII would not be recognized by proteases without this unfolded portion. Omission of this domain also simplifies the system to a monomer protein instead of the oligomer holoenzyme. The advantages for completing EPR experiments in this system will be described later in this chapter. During expression of this monomer protein, the degradation was somewhat decreased but the activity was poor. Activity was determined by the protein's ability to incorporate a radioactive gamma phosphate from [γ^{32}P] ATP onto either syntide-2, a synthetic peptide based on the glycogen synthase phosphorylation site, or autocamtide-2 (AC-2), a peptide based on the regulatory domain (see Appendix B for experimental method details). Since the protein was not easily purified, assays were completed on lysed bacterial expression culture. The activity values obtained were indistinguishable from blank samples which contained buffer instead of cellular lysate. Extensive truncation and lack of activity indicated there may have been structural instabilities within the protein and we speculate that the protein was not able to fold properly in bacterial expression cells. The cellular response to such a problem would likely be degradation of the unfolded proteins to prevent protein aggregation.

10 histidine C. elegans CaMKII is the most efficient expression construct

Since the truncated *C. elegans* CaMKII homolog consisting of catalytic and regulatory domains was crystallized, it was a good candidate for stability. The catalytic and regulatory domains of this protein are 78% identical to human CaMKIIα, meaning its structure is highly conserved. In attempt to express an uncleaved protein, the *C. elegans* gene representing these domains was inserted into the pGEX vector which contains codons for an N-terminal glutathione S transferase (GST) tag. The high solubility of this tag was expected to make CaMKII a less attractive target for degradation. Simultaneously a 6 histidine-GST tagged construct was also created to give multiple options for protein purification. Paradoxically SDS-PAGE (sodium dodecyl sulfate polyacrylamide gel electrophoresis) analysis of this system suggests that the tag itself gets cleaved from the protein during expression, rendering it completely useless. On the other hand, the expression of GST-CaMKII was very high and the protein was uncleaved, however the tag removal proved to be an impractical catch twenty two. EPR experiments necessitate the removal of this tag, as it contains several native cysteines which will label and contribute to EPR signals. Removal of the tag requires temperatures non-permissive for retention of CaMKII activity. Lowering temperatures to retain protein folding prevented thrombin cleavage of the GST tag. This avenue was quickly abandoned, and a histidine tagged CaMKII expression was investigated. The gene was cloned into pET28b+ and expression was carried out similarly as described [138] except for a modified 16 hour induction. Expression was high and truncation was reduced, showing only minor cleavage products in addition to the proper length protein. For this protein it is not necessary to remove the histidine tag because it is relatively small and contains no

labeling sites. Ni affinity was used to carry out protein purification in combination with gel filtration chromatography. This straightforward protocol requires only two chromatography steps and allows for labeling in between (Figure 3.2).

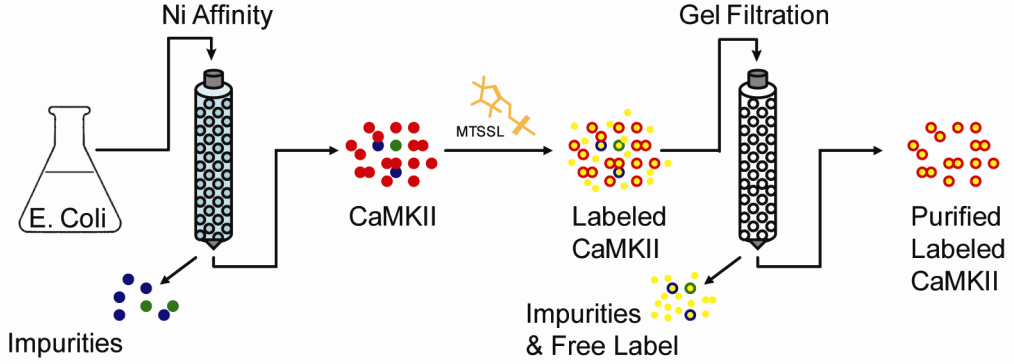

Figure 3.2 Protein purification method. For purification of histidine tagged *C. elegans* CaMKII, culture lysis is first applied to a Ni affinity column. The eluted proteins can be labeled with MTSSL and further purified by gel filtration. For complete details on the protocol, refer to experimental methods.

While this protocol yielded reasonably pure protein, a sharp mobile component was present in several EPR spectra which was feared to be a labeled impurity. To increase selectivity, a 10 histidine (10His) tag was introduced to the N-terminus of the CaMKII gene by a Quik change protocol. This was successful in increasing protein purity (Figure 3.3)

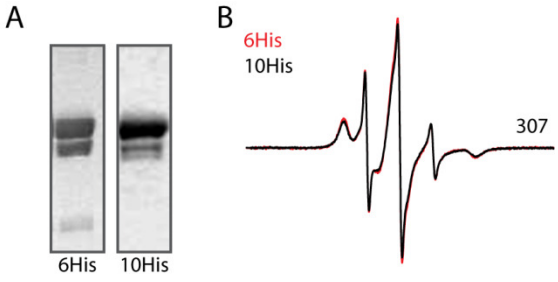

Figure 3.3 Comparison of protein purity of 6His and 10His CaMKII proteins. A) Proteins for the 307 EPR mutant were cloned into constructs containing either a 6His or 10His N-terminal tag. SDS-PAGE analysis of protein purification shows cleavage of CaMKII and extra impurities in the 6His purification. B) Overlaid spectra from show only minor changes in line shape indicating the presence of extra impurities has little effect on the EPR signal.

SDS PAGE and western analysis of the 6- and 10-His tagged *C. elegans* proteins revealed two CaMKII bands, one at the appropriate size of 42 kDa and a slightly smaller cleavage product. The purification of the 6His protein also resulted in the copurification of a small impurity which was not observed in 10His protein purification. With the initial concern that impurities were causing the sharp mobile portion of the spectrum, we compared the EPR spectra of 6 and 10His proteins. We found that the impurity actually contributes very little to the spectrum. Spectra for 6 and 10His proteins are overlaid showing that only very minor differences between their lineshapes exist (Figure 3.3B). This indicated that the mobile portion of the spectrum is contributed by CaMKII and not the impurity. Nevertheless, the 10His protein was preferred over the 6His because of its superior performance during purification.

Protein cleaved during expression is not easily separated by purification techniques

Although the 10His proteins are more easily purified, they do undergo cleavage during expression at a site near the C-terminus. C-terminal truncation of CaMKII has been established previously in *E. coli* expression [219] and analysis by mass spectrometry reveals cleavage is occurring at end of the regulatory domain near residue 318 (Figure 3.4, see Appendix B for method details).

Figure 3.4 SDS-PAGE and mass spectrometry of analysis of purified *C. elegans* CaMKII. A) A Coomassie stained gel of purified C. elegans CaMKII catalytic and regulatory domains shows a minor truncated product copurifies with the appropriately sized 1-340 protein. B) Sequence of CaMKII 1-340. The red fragments were recovered from mass spectrometry analysis of the truncated band excised from the gel while the underlined peptides were recovered from mass spectrometry analysis of the major band corresponding to CaMKII 1-340.

The detected peptide fragment corresponding to the most C-terminal sequence from the truncated protein band ended at residue 318. Because the crystal structure of this same protein is not resolved beyond residue 318 [138], this region is likely unstructured making it difficult to solve and prone to proteolysis. Additional analysis of these two purification products was completed using light scattering. During gel filtration, the truncated product peak overlaps significantly with the 1-340 peak but is slightly shifted to a longer retention time because of its smaller size. We intentionally selected for the truncated peak by collecting accordingly, and obtained a sample with a significant amount of truncated product relative to the 340 product. Analysis by light scattering revealed the two overlapping peaks with experimental molecular weights of 41010 and 34440 Da. These correspond well to weights calculated for residues 1-340 and 1-318 respectively.

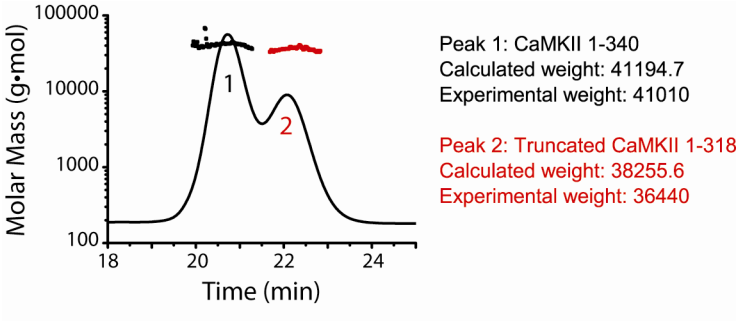

Figure 3.5 Light scattering analysis of CaMKII truncation. The truncated CaMKII protein and the appropriately sized protein are revealed as two overlapping peaks in gel filtration (black line). The scatter plots represent the average particle size as determined by light scattering for the 1-340 protein (peak 1) and the truncated protein (peak 2). The average molecular weight was determined and compared to the calculated weight for each protein (right).

Instead of trying to prevent cleavage, efforts were turned toward finding a method to separate the cleavage products. In order to attempt to obtain a purified protein without cleavage products, a His tag was introduced onto the C-terminus. The principle behind this idea was that the cleavage site was close to the C-terminus. The Ni affinity would therefore select for the uncleaved desired protein as well as the extremely short C-terminal cleavage product. Since the difference in size of these two polypeptides is substantial, they should be easily separated with sizing chromatography. Unfortunately not all good ideas come to fruition, as the dynamics of the C-terminal region were influenced by the tag. EPR spectra for site 296 are shown in Figure 3.6 for N- and C-terminal His tagged proteins. Comparison of lineshapes reveals subtle differences in the probe dynamics of these two labeled proteins. Regardless, this protein was not suitable for EPR studies due to its low expression.

Figure 3.6 Comparison of N- and C-terminal histidine tags on EPR spectra at site 296. Constructs of EPR mutant 296 were created with either an N-terminal 10 histidine affinity tag or a C-terminal 6 histidine tag in attempt to purify protein from its cleavage product. The proteins were expressed, purified, labeled and analyzed with EPR. The differences seen in spectra indicate the C-terminal tag (red) influences protein dynamics at this site.

For many protein systems, additional chromatography steps can be performed in attempt to separate unwanted products from the desired protein. Unfortunately, other chromatography techniques such as ion exchange could not be considered in this case because of the almost identical biochemical properties of the 1-340 and 1-318 proteins. At last the fact that cleavage could not be prevented during expression and could not be separated with standard ionic exchange or sizing chromatography was accepted. Figure 3.7 summarizes all of the constructs made for the optimization of protein expression and purification.

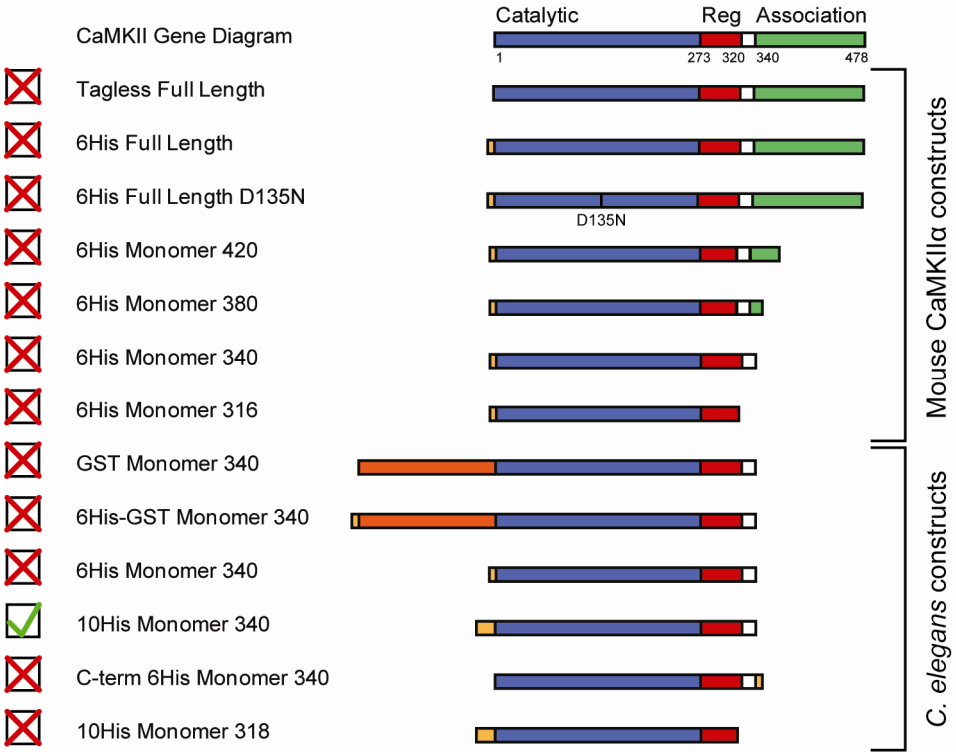

Figure 3.7 CaMKII construct diagram. Expression optimization required the investigation of many different constructs to yield abundant high quality protein. The most successful was *C. elegans* 10 histidine CaMKII, residues 1-340.

Truncation of CaMKII during expression does not alter protein dynamics

Efforts were returned to the N-terminal 10His tagged *C. elegans* protein as it was the best for expression and purification. Assessment of the consequences of having the truncation in our experimental system began. We observed that the degree of cleavage varied between mutants from virtually none up to ~15%. The truncated residues (~319-340) make up a variable linker region connecting regulatory and association domains. Although the truncation products retained the entire regulatory domain, we sought out to determine whether or not truncation would change features observed in our EPR spectra. In particular, we wanted to determine that the truncation was not causative for highly mobile components observed in all of our spectra for sites 302-309. Using engineered

constructs consisting of residues 1-318, we verified that the truncation does not affect the EPR lineshapes at representative sites along the regulatory domain (Figure 3.8).

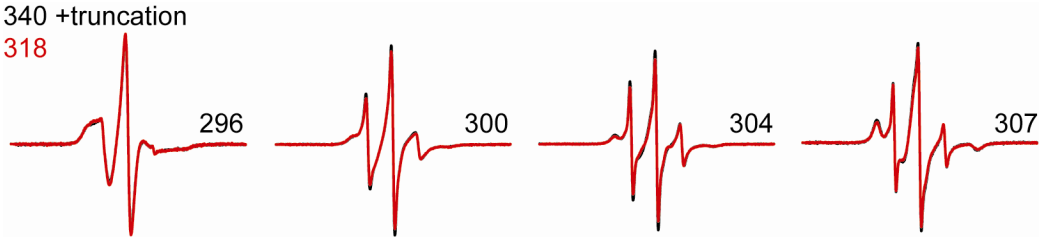

Figure 3.8 EPR spectra of representative sites introduced into the 1-340 and the 1-318 backgrounds. The superimposable lineshapes demonstrate that the truncation does not affect the dynamics of the spin label.

Spectra were nearly identical for sites 296, 300, 304, and 307 indicating cleavage of residues 319-340 does not alter the environments of the probes. At this junction of optimization, it was not reasonable to adopt the 1-318 construct as the basis for EPR studies because it did not express as well as the 1-340 construct. Therefore we completed studies with the 1-340 construct and we deemed it unnecessary to purify the 318-truncated protein from the 340 desired protein.

An inactive monomer protein system was necessary for EPR experiments

The studies presented here focus on the *C. elegans* CaMKII kinase monomer, consisting of the catalytic and regulatory domains (residues 1-340), the structure of which was determined previously (PDB 2BDW) [138]. The monomer system is not just a consequence of expression system complexities and limitations, but it is a necessary starting point for EPR studies. In addition to the advantage of having high resolution crystal structures for comparison [109,138], the monomer provides a simpler model from a spectroscopic perspective because it omits the complexities of holoenzyme intersubunit interactions. For example, each singly labeled subunit in the twelve subunit holoenzyme has the potential for dipolar coupling with other labels. Since the positioning of the

domains was unknown, experiments could not have been designed to avoid spin-spin coupling. Spin label mobility will be masked by spectral broadening making it impractical to determine dynamics. Furthermore interpretations of complex distance extrapolations may be problematic as it would be difficult to decipher which of the twelve subunits are interacting. These complexities are eliminated by using the monomer system which has no potential for intersubunit interactions. Without the association domain, monomer protein has been shown to be mechanistically relevant. It successfully undergoes autophosphorylation and binds and phosphorylates substrates [31]. Since it can undergo the conformational changes associated with activation and can be expressed in a high throughput manner, the monomer system is the ideal starting point.

To enable site specific incorporation of spin labels, single cysteine mutants were introduced in a cysteine-less CaMKII background hereafter referred to as WT*. Native cysteines were replaced with residues found in homologs or with alanine; C30A, C64L, C115A, C126I, C199A, C272A, and C289A. We investigated the effects of this mutagenesis by measuring protein activity. WT* specific activity, measured by phosphorylation of peptide substrates AC-2 and syntide-2, is similar to WT monomer and is comparable to that of WT mouse CaMKII holoenzyme and monomer (Table 3.1). Therefore the cysteine substitutions do not compromise the structural and functional integrity of the enzyme.

	Activity (μmol/min/μg)	
Protein	Syntide-2	Autocamtide-2
mouse CaMKIIα holoenzyme WT	5.62 ± 0.15	5.23 ± 0.12
mouse CaMKIIα 1-380 WT	7.13 ± 0.16	7.85 ± 0.07
C.elegans 1-340 WT	6.04 ± 0.76	4.86 ± 2.80
C.elegans 1-340 WT*	4.59 ± 0.05	4.29 ± 0.10
C.elegans 1-340 D135N*	None detected	None detected

Table 3.1. Activities of CaMKII variants. Activities of CaMKII variants determined by incorporation of radio labeled phosphate from [γ^{32}P]ATP onto the peptide substrates autocamtide-2 and syntide-2 (n = 2). The variations in specific activities between the different CaMKII are within values observed previously[220]. For D135N* the levels of radioactivities were similar to control samples without added enzymes.

Furthermore, structural parameters deduced from far and near-UV circular dichroism (CD) analysis and analysis of the melting temperature are consistent with retention of secondary and tertiary structures. At far UV wavelengths, the peptide bond is detected which gives an indication of the collective secondary structure of CaMKII (Figure 3.9 A). The negative bands at 222 and 208 nm, typically used as an indicator of alpha helical structure, are unchanged when comparing WT (black) and WT* proteins (dark gray). Additionally near UV wavelengths excite the aromatic chromophores in a protein and give an overall indication of its tertiary structure. Near UV spectra for these proteins are also nearly identical. Finally, melting experiments were conducted by observing the CD signal at 222 nm under increasing temperatures. These results indicate that the stabilities of the proteins are comparable with melting temperatures around 65°C. We conclude that these proteins are properly folded and the native cysteines are non essential for protein function.

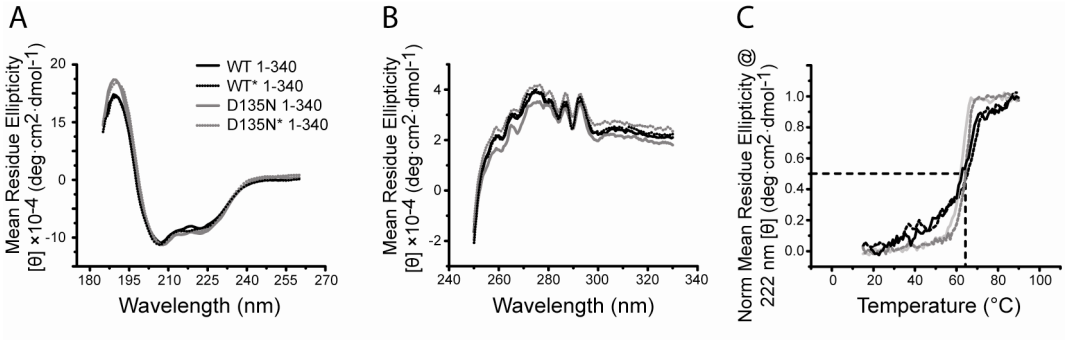

Figure 3.9 CD analysis of CaMKII mutagenesis. A) Far- UV and B) near-UV circular dichroism analysis for the wild type and cysteine-less CaMKII (WT*) along with their D135N inactivated counterparts. The spectra are almost superimposable confirming the lack of substantial structural changes due to the cysteine substitutions. C) Stability curves demonstrating the lack of substantial effects on melting temperature by the cysteine substitutions.

Among CaMKII's impressive abilities to regulate itself is the autophosphorylation capability. Autophosphorylation causes addition of negative charges and bulk at specific Thr residues, many which have been characterized and some that have only been proposed. These reactions only require the presence of Mg^{2+} and ATP to alter the conformation of the protein. Since the goal of this project is to decipher individual intermediate conformations, any heterogeneity introduced by varying states of autophosphorylation must be avoided. Since autophosphorylation has been shown to occur during bacterial expression at site 286 [109], we wanted to avoid possible phosphorylation at site 286 and/or other autophosphorylation sites such as 253, 305, and 306. To circumvent heterogeneous phosphorylation, we adopted the strategy of replacing the highly conserved D135 in the catalytic loop [221] with asparagine. This mutation inactivates WT* [138] creating a protein hereafter referred to as D135N*. Analysis by mass spectrometry confirmed the absence of detectable phosphorylation in the D135N background. Peptides spanning the regions of the well known Thr286, Thr305, and Thr306 autophosphorylation sites were abundantly represented in the analysis. No phosphorylation was observed in these peptides or at any other sites protein wide. This

analysis indicates that the D135N mutation prevents autophosphorylation and also reveals that CaMKII is not phosphorylated by a native bacterial kinase during expression. The D135N substitution does not change the CD signatures of the CaMKII monomer (Figure 3.9A,B) or the half-maximal temperature of the melting curve but increases the cooperativity of unfolding (Figure 3.9C). We speculate that the apparent non-cooperative WT unfolding reflects heterogeneous autophosphorylation leading to multiple protein populations, each with a different melting temperature.

D135N and T286E* stably bind calmodulin*

CaM binding is a requirement for substrate phosphorylation by CaMKII. Active WT and WT* proteins were able to phosphorylate substrates (see Table 3.1), meaning that they are to first bind CaM for activation. Since this type of activity cannot be observed for the D135N* inactivated protein, a cosedimentation assay was used to test the protein's ability to stably bind CaM. For this assay, purified D135N* protein was incubated with an excess of CaM-agarose resin and equilibrated in the presence of saturating Ca^{2+}. Resin was washed to remove any unbound protein and analyzed with SDS-PAGE. Figure 3.10A shows a Coomassie stained gel of the experiment. In lanes 1, 2, and 3 are the D135N* purified protein loaded as a control, the CaM-agarose pellet after incubation with D135N* and washing, and the supernatant from the incubation respectively. Lane 2 shows the presence of the D135N* protein indicating that it was able to stably bind the CaM-agarose. Lane 3 shows no D135N* protein indicating that all of it was depleted from the supernatant during the binding incubation and that complete

binding was achieved. In parallel, the same conditions were used with active wild-type mouse CaMKIIα as an assay control. Lanes 4 through 6 show similar binding results.

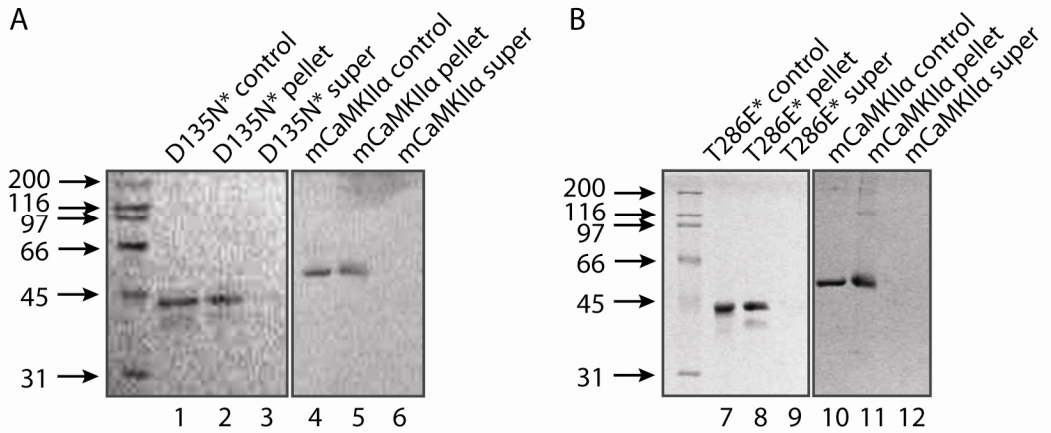

Figure 3.10 Cosedimentation assays for D135N* and T286E* engineered proteins. A) Lane 1 contains purified protein used for the cosedimentation assay to test CaMKII binding to CaM-agarose resin. Lane 2 illustrates that D135N* protein is associated with the CaM-agarose after incubating and washing in the presence of Ca2+. Depletion of the protein from the supernatant in lane 3 suggests complete binding. Lanes 4,5, and 6 show results with control mouse CaMKIIα full length wild type protein. B) The experiment in panel A was repeated with protein containing the T286E phosphorylation mimic.

To investigate the conformational changes induced by Thr286 phosphorylation, it was required to introduce in a phosphomimic T286E mutant on the D135N* background. The nomenclature used for this mutant is T286E*. This mimicry approach is necessitated by the expected heterogeneous autophosphorylation [127,222] in the WT* enzyme which would complicate interpretation of the EPR data. This approach allowed us to evade autophosphorylation at any undesired residues but also to avoid incomplete autophosphorylation of the desired site. With the T286E mutation, all proteins will have a charge at site 286 resulting in a completely homogeneous system. However, it should be noted that introduction of negative charge by the T286E mutation does not fully mimic the effects of a phosphate group, and local environment of the T286E* protein may be somewhat different from the Thr286-phosphorylated kinase. Cosedimentation assays were completed on T286E* to assess its CaM-binding abilities (Figure 3.10B). Similarily

to the D135N* protein, T286E* was able to stably bind calmodulin. These assays demonstrate that mutagenesis of native cysteines, introduction of the T286E phosphorylation mimic, and/or truncation of the protein do not significantly impair the protein's ability to stably bind CaM.

CHAPTER IV

CaMKII CONFORMATIONS OF ACTIVATION[‡]

Rationale for EPR studies

Within the deceptively short 40 amino acid stretch that makes up the regulatory domain, there is a structural basis for the regulatory capacities of CaMKII. Biochemically it is known to be involved in autoinhibition interactions with the catalytic domain and also contains a self-recognized substrate sequence which when autophosphorylated confers autonomous activity. This sequence is not phosphorylated within its own subunit, but rather by a neighboring subunit within the oligomeric holoenzyme assembly [157]. How is it that this sequence fits into the active site of a neighboring catalytic domain but not within the catalytic cleft of its own subunit? Furthermore autophosphorylation of the CaM-binding region abrogates binding and is known to occur within a single subunit. This implies an opposite effect where the CaM binding region of the regulatory domain is not recognized by a neighboring subunit. These studies raise the concept that the regulatory domain is highly promiscuous, able to interact with the catalytic domains in multiple conformations correlating to several discrete intermediates.

Even with several crystal structures of individual domains, there is no unambiguous agreement on the conformation of the autoinhibited, apo intermediate. Biochemical analysis and structures of human kinase domains consisting of catalytic and regulatory domains predict the regulatory domain contacts the catalytic cleft. In contrast

---

[‡]The majority of the text and figures described in this chapter are published in Hoffman et al., 2011 [223].

the crystal structure of the *C. elegans* kinase domain depicts regulatory domains of adjacent monomers are involved in a coiled coil dimeric interface (refer to Chapter I for a detailed description of this model). Existing crystal structures of monomeric kinase domains have also been extrapolated to mechanistic models of cooperative Ca^{2+} sensing and catalytic activation of the holoenzyme [108,109,138]. Experimental testing of these models in solution in the absence of constraints imposed by the crystal lattice is essential for an in-depth understanding of the complex landscape of holoenzyme activation.

Motivated by these conflicting models and the dearth of available information about conformational changes associated with activation, we completed the first analysis of regulatory domain dynamics in solution using systematic spin labeling and EPR spectroscopy [192,193] of monomeric *C. elegans* CaMKII [223]. The first task was to define the backbone conformation of the autoinhibited regulatory domain to confirm or refute the controversial coiled coil hypothesis and describe the mechanism of autoinhibition. This work was designed to address this and other mechanistic questions of the biochemically proposed activation pathway. What is the amplitude and nature of the conformational changes that occur upon CaM binding? What changes take place in catalytic domain induced by the release of the regulatory domain during activation? What conformational changes are required for the onset of Thr286 mediated autonomous activity? Do the Thr305/Thr306 phosphorylation charges necessary to prevent CaM binding also cause structural changes in the regulatory domain? We monitored conformational changes of the regulatory domain throughout putative biochemical intermediates; CaM bound, Thr286 phosphorylated, CaM bound and Thr286 phosphorylated, and Thr305/Thr306 phosphorylated to address these outstanding

mechanistic questions. Additionally, initial studies of the conformational rearrangements of the catalytic domain were initiated, giving preliminary evidence for the regulatory effects on the catalytic domain.

For these experiments several Cys mutants were introduced into the regulatory domain of the inactivated D135N* monomer protein. Spin labeled CaMKII mutants were analyzed by EPR spectroscopy under conditions designed to stabilize the specific intermediates on the activation pathway. Conformational changes underlying the transitions between these intermediates were deduced from analysis of spin label mobility and proximities in spin label pairs. The mobility of a spin label refers to dynamic modes on the nanosecond timescale that average the anisotropic tensors of the spin labels. These include rotation around bonds that tether the label to the backbone and large amplitude motion of the backbone [194,201,212,224] (refer to Chapter II for details). The overall tumbling of the 40 kDa CaMKII monomer has a mimimal contribution to the EPR lineshape. This chapter describes the secondary structure, tertiary interactions, and backbone dynamics of the regulatory domain in discrete catalytic intermediates. Our results reveal the structural and dynamic changes underlying activation by Ca^{2+}/CaM and Thr286 autophosphorylation and suggest a model of CaMKII holoenzyme activation which is described in Chapter V.

Dynamic equilibrium of the regulatory domain in the apo intermediate

Although the *C. elegans* autoinhibited non-phosphorylated kinase domain (referred to hereafter as the apo intermediate) crystallizes as a dimer, dimers could not be detected in solution using various analytical methods such as gel filtration and analytical

ultracentrifugation, even at moderate concentrations [109,138]. However, Rellos et al reported the detection of dimeric human CaMKII isoforms in solution at 4°C, with dissociation constants in the 200-600 μM range although the interface of this dimer does not seem to involve the regulatory domain [108]. Consistent with this observation, we found no spectroscopic evidence of regulatory domain dimerization at room temperature. Spin labels predicted to be within close proximity (Figure 4.1A) at the crystallographic coiled coil interface did not show evidence of spin-spin coupling. Site 302 of the regulatory domain directly faces its dimer counterpart in the structure with an inter-residue C_β-C_β distance 5 Å while site 307 faces outward, perpendicular to the plane of the page with a 13 Å distance.

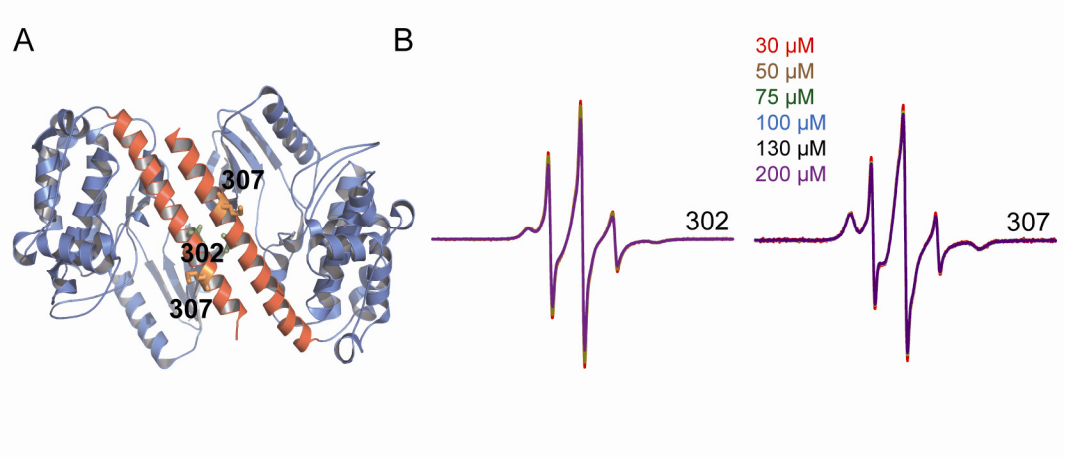

Figure 4.1 CaMKII regulatory domain is not at a dimer interface. Crystal structure of the *C. elegans* CaMKII kinase domain where two regulatory domains, each belonging to a different monomer, form a coiled coil (PDB 2BDW). Sites 302 and 307 are at the dimer interface separated by 5 and 13 Å respectively. The EPR spectra for CaMKII labeled at each site are shown for concentrations up to 200 μM. The absence of concentration-dependent broadening indicates that this dimer is not stable in solution.

Short range distances lead to extensive dipolar coupling between the spin labels and broadening of the CW EPR spectrum [207,214]. No such spectral broadening was observed for these sites up to concentrations of 200 μM, above which the protein aggregated nonspecifically to form an insoluble precipitate. Thus, the coiled coil

regulatory domain dimer is not stable in solution at room temperature, although we cannot exclude the possibility that higher effective subunit concentrations in the holoenzyme (estimated at 3 mM) allow for this interaction [138]. However, consistent with our data, the coiled coil dimer was not observed in the multiple crystals of human CaMKII isoforms [108]. Thus, multiple lines of evidence using different experimental approaches suggest that the regulatory domain dimeric interface is an artifact of the crystallization of *C. elegans* CaMKII.

In contrast to the rigid regulatory domain structure in the crystal, EPR lineshape analysis for a set of spin labeled mutants in this domain reveals evidence of multiple conformational states. In the R2 and R3 segments of the regulatory domain (residues 292-297 and 298-314 respectively defined previously [109], Figure 1.4B), multiple populations of spin labels with vastly distinct mobilities are detected (Figure 4.2).

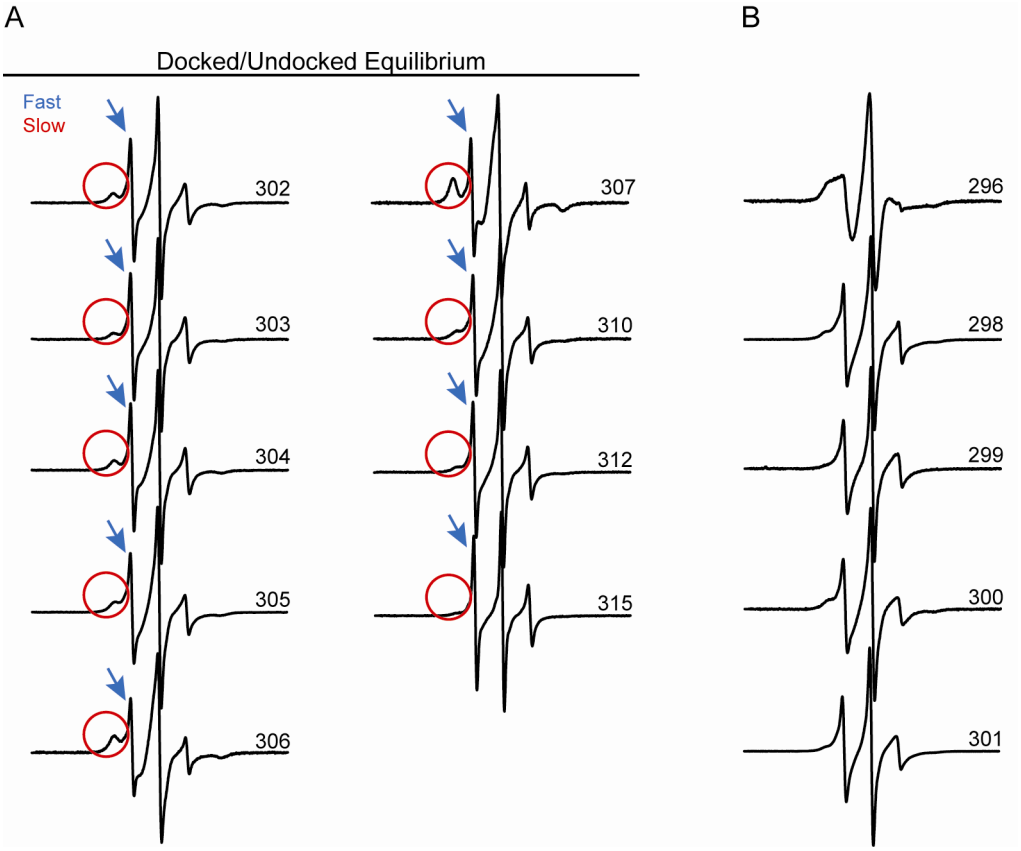

Figure 4.2 Apo state EPR spectra along the R2 and R3 segments of regulatory domain. A) and B) The lineshapes in the R2 and R3 segments show distinct evidence of at least two populations of spin labels with vastly different mobilities. A mobile population marked by the blue arrow reflects spin labels undergoing large amplitude/fast motion. Another population marked by the red circle reflects spin labels in restricted environments.

Sharp components in these spectra (indicated by arrows in Figure 4.2A) reflect spin labels undergoing fast and large amplitude motion with ~1 ns effective correlation times (Table 4.1). This type of motion is indicative of an unstructured backbone and is inconsistent with an ordered α-helical backbone. Another spectral component (indicated by circles) arises from spin labels undergoing slower motion indicative of a sterically restricted environment. This spin label population cannot arise from the putative coiled coil since there is no evidence of spin-spin coupling (Figure 4.1).

Site	Correlation Time (ns)	Classification	Prediction
278	0.97	loop	Loop
279	0.91	loop	
282	1.52	loop	
284	0.73	loop	
285	1.59	surface	Helix
286	7.05	buried	
287	7.38	buried	
289	1.48	surface	
290	6.55	buried	
291	1.17	surface	
293	9.02	buried	

	Correlation Time (ns)		
Site	τ_1 (Slow Component)	τ_2 (Fast Component)	% slow/fast
296	5.59	1.15	89/11
298	6.14	0.47	86/14
299	1.88	1.11	30/70
300	4.50	1.02	64/36
301	2.77	1.05	40/60
302	15.23	0.78	68/32
303	4.96	0.71	66/34
304	7.30	0.56	72/28
305	4.42	0.86	71/29
306	12.66	0.74	83/17
307	34.55	0.55	88/12
310	6.52	0.53	82/18
312	3.82	0.48	76/24
315	4.67	0.47	52/48

Table 4.1 Correlations times calculated from MOMD simulations (spectral fits not shown) as described in the methods section. For sites involved in the docking/undocking equilibrium correlation times are shown for the fast mobile and slow immobile populations as well as the relative percentage of each. For sites in the R1 segment, the correlation time describes the predominant motional component in the spectrum.

Rather, we interpret these results as evidence of an equilibrium between an undocked dynamic conformation (leading to fast spin label motion) and a structured conformation (leading to restricted motion), with the R2 and R3 segments docked to the catalytic domain presumably near the ATP binding site. The EPR spectra capture two extremes of this equilibrium revealing that the underlying conformational change is slow on the EPR timescale, on the order of 100 ns. Using nonlinear least-squares analysis (see Appendix B for method details), we determined the average rotational correlation time [202] and fraction of spin labels in each of the two populations (Table 4.1). For this analysis, the spectra were assumed to consist of two components, an undocked population correlating to spin labels undergoing fast isotropic motion and a docked population corresponding to labels with restricted anisotropic rotation. Simulated spectra of each component were created by varying mathematical parameters used to describe the internal rotational motion of the nitroxide. The appropriate simulated spectrum is reached when the parameters produce a simulation that converges with the features of the experimental spectrum. For each experimental spectrum, "fast" and "slow" motion component spectra were summed in varying ratios to fit the EPR spectra for sites 302-307. Figure 4.3A illustrates the "fast" (green) and "slow" (orange) motion simulated spectra corresponding to the undocked and docked populations respectively. The final simulated spectra (dotted gray line, Figure 4.3B) are made up of various percentages of each and are overlaid with the experimental spectra (black). Simulating the spectra in this manner allowed us to determine the relative percentage of the docked and undocked population for each site. We interpret these results to indicate that on average, the R3 region of the regulatory domain is docked ~80% of the time. There are differences in

percentage docked between sites which may be a result of SDSL substitutions for natural amino acids causing slight alterations in tertiary interactions.

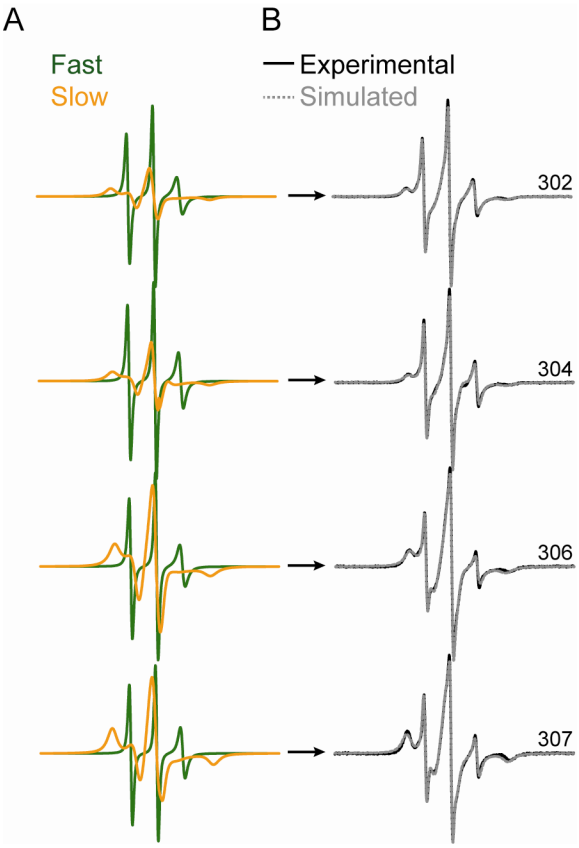

Figure 4.3 MOMD analysis of R3 docking-undocking equilibrium. The EPR linesahpes in the CaM binding region were analyzed assuming two populations of spin labels with distinct motional parameters. Non-linear least squares fits of the experimental spectra yielded two component spectra at each site. The relative fraction of each component is shown in Fig. 4.6C.

Lineshapes for spin labels in the R1 segment (residues 278-291) consist of single predominant components (Figure 4.4) demonstrating structural decoupling between R1 and the rest of the regulatory domain. In particular, the spin label environment at residues 286, 287 and 293 is restricted with lineshapes similar to those observed in protein hydrophobic cores (Table 4.1). The ordered backbone and solvent inaccessibility indicate that these residues are buried by contacts with the catalytic domain consistent with their local environments in the crystal structure (Figure 4.4C).

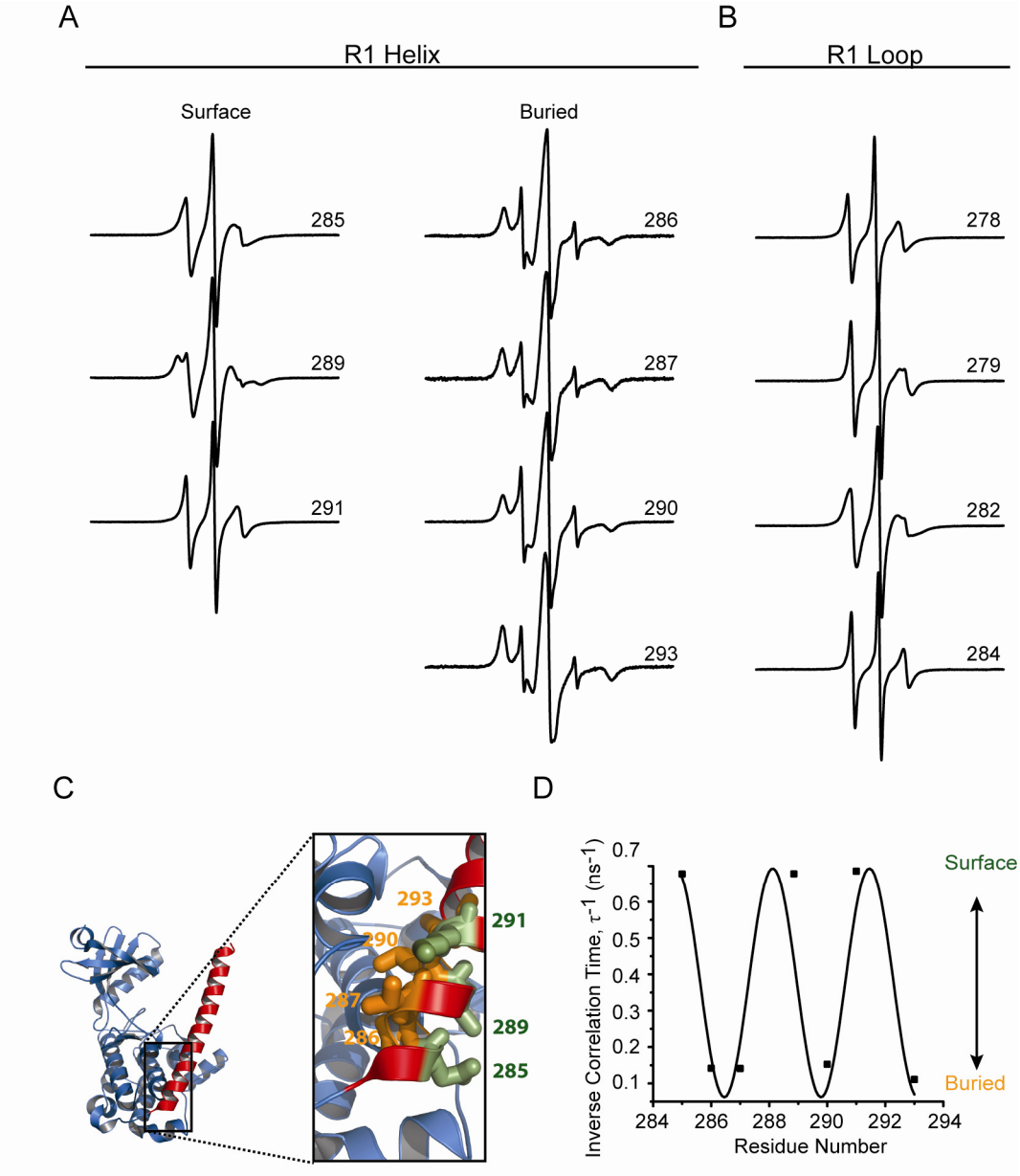

Figure 4.4 EPR spectra and correlation times of the R1 regulatory segment. A) and B) EPR lineshapes in the R1 segment seem to arise from a predominant population of spin labels. The minor sharp component has contribution from unreacted labels. In the 285-293 segment, the mobility varies with periodicity indicative of an α-helix. Uniformly mobile lineshapes in the 278-284 segment are indicative of a loop structure. C) The local environment of R1 residues in the crystal structure (PDB 2BDW) is shown to highlight the agreement with the EPR data. D) Inverse correlation times (τ^{-1}) for sites in the R1 region plotted versus residue number. The correlation time was determined from non-linear least squares analysis of the EPR spectra. The superimposed sinusoid fit to the data has a 3.7 period. Thus, residues on the surface (green) (e.g. 289) have a large τ^{-1} while those at the interface with the catalytic domain (orange) have small τ^{-1}.

Secondary structure of the regulatory domain

In segments of secondary structure, spin label mobility varies as a function of residue number [194]. Quantitative analysis of spin label dynamics along the 284-293 stretch of residues (R1 helix) reveals a periodicity strongly indicating an α-helical backbone (Figure 4.4A and Table 4.1). The phase of the helix is in concordance with the crystal structure (PDB 2BDW) [138], where the helix surface encompassing 286 and 287 is docked against the catalytic domain (Figure 4.4C). Additionally, inverse rotational correlation times, τ^{-1}, were plotted as a function of residue number and fitted with a sinusoidal function with 3.7 periodicity (Figure 4.4D). The spin labels are uniformly mobile in the preceding 278-284 (R1 loop) segment, consistent with a local loop structure (Table 4.1 and Figure 4.4B). Analysis of spin label mobility from residue 296 through residue 307 is complicated by the multicomponent nature of the EPR spectrum. However, sharp and narrow spectral components for sites 299-301 (Figure 4.2B) indicate a loop structure (Table 4.1).

The presence of helical secondary structures can also be deduced from proximities between *i*, and *i*+4 residues in consecutive helical turns. The expected 5.5 Å separation between the spin labels should result in extensive broadening of the EPR lineshape due to strong dipolar coupling and direct overlap of the unpaired electron wavefunctions [207,225]. In contrast, flexible unstructured segments are characterized by average distances greater than 13 Å and broad distance distributions. Short range coupling was evident in the spectrum of spin label pairs introduced 4 residues apart in the 285-293 region (Figure 4.5A) with a corresponding narrow distance distribution centered at 8 Å (Figure 4.5B). In contrast, (*i*, *i*+4) spin label pairs in the calmodulin binding

segment have a multimodal distance distribution consistent with a significant fraction of unstructured backbone with some α-helical characteristics (Figure 4.5C). The amount of spectral broadening can be visualized by comparing a sum of singles spectrum, which is an average of spectra from each individually labeled site (Figure 4.5A, red), to the experimental spectra (black). Gaussian distance distributions were extrapolated from a deconvolution method with the spectral fits shown in dotted gray lines. Taken together, our EPR data is consistent with a solution structure in which the R1 helix is stably docked to the C-terminal lobe of the catalytic domain and the R3 segment is in equilibrium between docked and undocked conformations, thereby inhibiting the kinase in the absence of CaM binding.

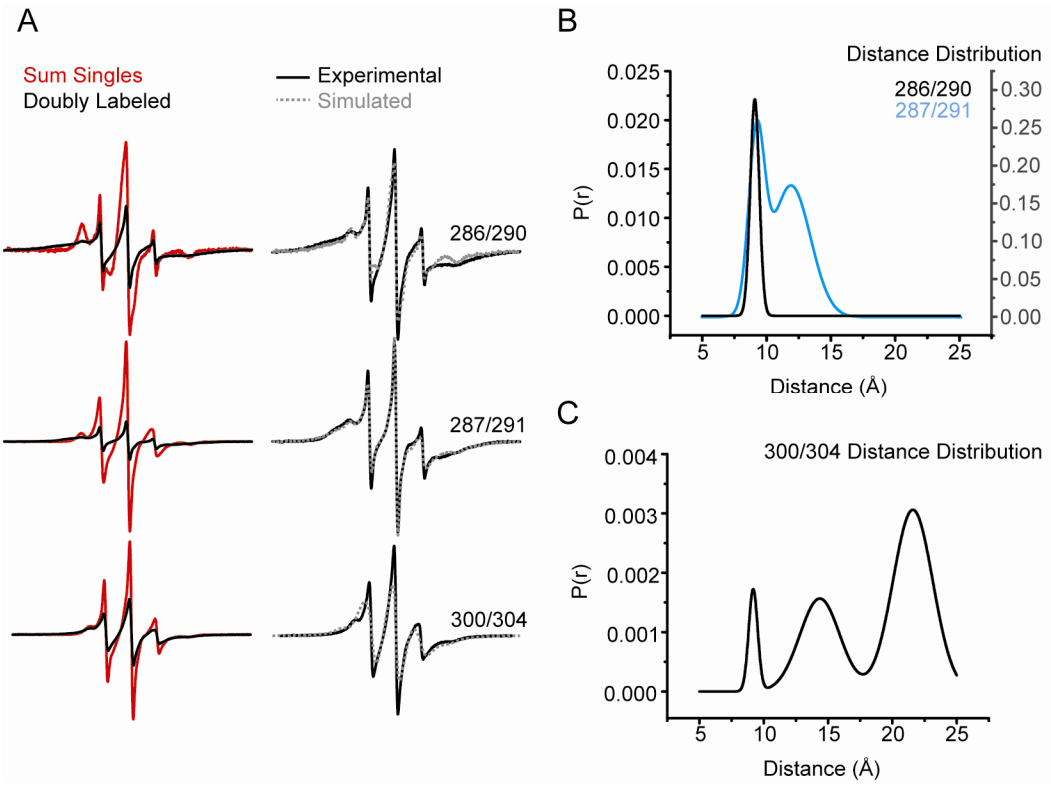

Figure 4.5 (*i, i*+4) distances in the regulatory domain. A) EPR spectra of (*i*, *i*+4) spin label pairs (black) along with the corresponding sum of singles (red) in the R1 and R3 segments. The sum of singles spectrum was obtained from a digital sum of the single sites spectra which do not contain contributions from the distance-dependent dipolar interaction. Each double mutant spectrum was fit (dashed line) as described in the methods section to a distance distribution between the two spin labels shown for the R1 (B) and R3 (C) portions of the regulatory domain.

The CaM binding segment of the regulatory domain senses ATP binding.

Since CaMKII activation is associated with increased affinity for ATP (see Chapter I), we hypothesize that the R3 dynamic equilibrium facilitates active site exposure for binding of both nucleotide and substrate. Thus, we predict ATP binding would shift the R3 equilibrium towards the undocked population. Indeed, while the addition of ATP does not change the EPR lineshapes in the R1 segment, it increases the fraction of spin labels that are in the undocked conformation in the R3 segment. Figure 4.6A compares spectra in the presence (purple) and absence (black) of ATP and illustrates an increase in the sharp mobile peaks indicative of the undocked population.

Spectra for ATP-bound protein were simulated with MOMD to reveal the relative percentages of docked and undocked populations (Figure 4.6B). When comparing to apo protein, the undocked population increases to comprise ~50% (Figure 4.6C) in the presence of ATP. This allosteric modulation by ATP suggests that the R3 segment interacts with the nucleotide-binding lobe. Furthermore, it suggests that the R3 equilibrium is not an artifact arising from the truncation of the association domain. Rather it represents a mechanism to modulate ATP affinity.

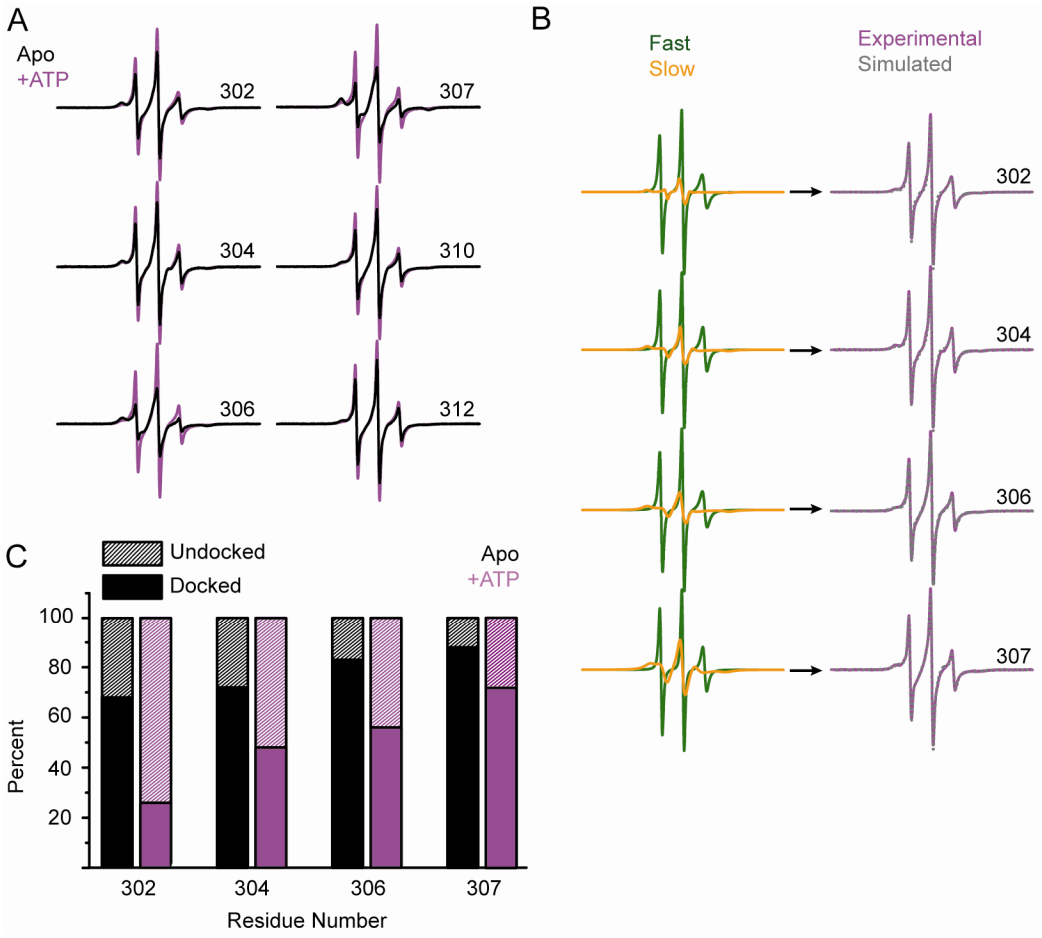

Figure 4.6 ATP modulation of the CaM binding region. A) EPR spectra of sites in the R3 segment in the presence of ATP (purple) overlaid with their corresponding apo spectra (black). B) The ATP-bound lineshapes were analyzed using the two-population model. The fast mobile component (green) and the slow immobile component (orange) for the ATP-bound spectrum are summed (gray dotted) to fit the experimental spectra (purple). C) Percentages of the fast and slow components for the apo CaMKII state (black bars) and the ATP-bound state (purple bars) for representative residues in the R3 segment

From these mobility data, we hypothesize that the R3 CaM-binding region of the regulatory domain is in a conformational equilibrium between two states. In one conformation, this region is docked against the catalytic domain presumably making contacts to the catalytic cleft. In the other, the domain is undocked and largely disordered making it accessible to solvent. We measured distances between catalytic and regulatory domains to gain insight on the position of the regulatory domain in the docked state and the amplitude of motion in the undocked state. The measurement between site 125 of the catalytic domain and site 307 of the R3 region of the regulatory domain resulted in two distances; a short distance of 25 Å with narrow distribution and a longer distance of 42 Å with a broad distribution (Figure 4.7, all raw DEER data is in Appendix A). This is in concordance with our equilibrium hypothesis. We suggest that the short, narrow distance correlates with the docked conformation since site 307 would theoretically be positioned closely and tightly to the catalytic cleft. Undocking would place this residue farther away from the catalytic domain and result in a longer distance. The distribution of the longer 42 Å distance is almost 30 Å indicating this region is quite flexible in the undocked conformation.

Additionally, DEER data indicates that ATP binding shifts the relative docked and undocked populations to favor the undocked state. In the apo state the short distance comprises 60% of the signal and in the ATP bound state it is reduced to 20% indicating a large reduction in the docked population. Percentages calculated from MOMD simulations on CW data, which were averaged over multiple residues, show the same general trend, but differ in absolute value (Table 4.2). The average percentage of the

docked population was estimated at 80% compared to 60% from the DEER data. The ATP-bound state was estimated at 50% compared to 80% from DEER.

	Apo		ATP	
	%Docked	%Undocked	%Docked	%Undocked
125/307 DEER	60	40	20	80
MOMD Ave (302,204,206,307)	80	20	50	50
MOMD 307	90	10	70	30

Table 4.2 Percentage of docked and undocked populations of R3.

In contrast, control distance measurements between catalytic site 125 and regulatory site 287 of the R1 segment show one major distance at 36 Å which does not change in the presence of ATP (Figure 4.7B). This is consistent with mobility data implying each residue resides in one conformational state which is not modified in the presence of ATP.

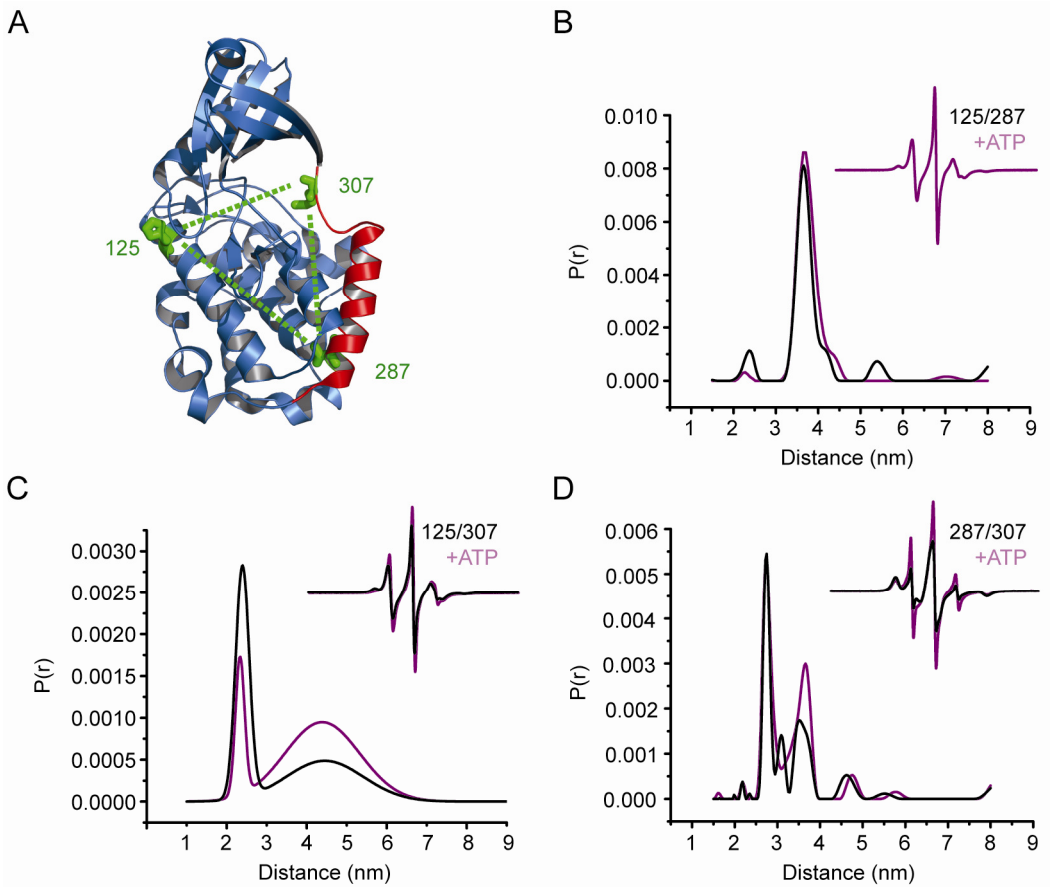

Figure 4.7 Distance measurements between catalytic and regulatory domains. A) Sites used for DEER distance measurements are highlighted in green in the crystal structure of human CaMKIIδ (PDB 2VN9). B) Distance measurements between catalytic site 125 and the R1 region of the regulatory domain from DEER experiments show little difference between apo (black) and ATP bound (purple) protein. C) Distances measurements between 125 and 307 of R3 indicate a population shift toward a longer broader distance in the presence of ATP. D) Across R1 and R3 regulatory segments, two major distances are detected and their ratio is modulated by ATP binding.

Since we predict that the R1 segment of the regulatory domain is stably docked while the R3 region is undergoing a docking/undocking conformational equilibrium, we wondered if we could capture changes in distances between R1 and R3. From mobility data we expect the undocked state to be in a flexible random coil conformation, however we do not know the conformation in the docked state. Our mobility data from the R3 region is confounded by the presence of the undocked mobile population making secondary structure predictions for the docked conformation difficult (spectra in Figure

4.2A). For the doubly labeled 287/307 protein, multiple distances were observed in the apo state (black); the two major peaks at 28 and 36 Å (Figure 4.7D). The peak at 28 Å correlates well with the distance in the crystal structure, calculated from C_β-C_β to be 29 Å. What is resolved of the R3 segment in the crystal structure of human CaMKIIδ (PDB 2VN9) is docked in a random coil conformation. Therefore, if we attribute the shorter distance to the docked conformation, the crystal conformation may be feasible for our solution protein. We speculate the longer distance may correlate with the undocked conformation because the domain presumably has the ability to "stretch out" linearly since it is not restricted by tertiary interactions. Additionally, this longer distance may be more heavily populated in the ATP bound state (red) consistent with the notion that ATP binding enhances the undocked population. Although this interpretation is somewhat speculative from the distance distribution, the CW spectra clearly indicate an increase in mobility (Figure 4.7D, inlaid spectra). Overall these results from DEER measurements serve to validate our model built from mobility data.

To confirm that the shift in equilibrium arises from ATP binding, spin labels were introduced at representative sites along the regulatory domains in a D135N*/K42M background. The Lys to Met substitution, which is expected to abolish ATP binding, eliminates the changes in the mobile component in the R3 segment. In the apo form, the mutation shifts the equilibrium towards the docked conformation (Figure 4.8). Thus, it is likely that the shift in the R3 equilibrium results from ATP competing this segment away from the nucleotide-binding lobe.

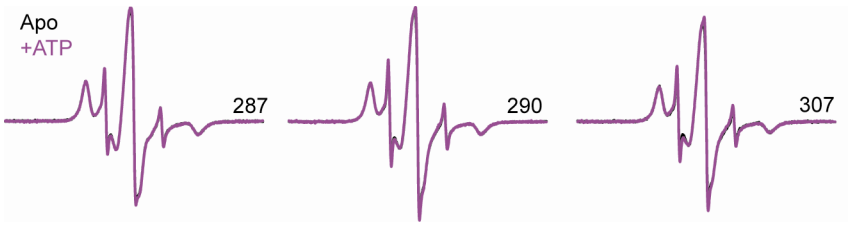

Figure 4.8 K42M control experiments. Spectra for protein containing the K42M mutation predicted to prevent ATP coordination are overlaid in the absence (black) and presence of ATP (purple). The ATP induced spectral changes are eliminated if the highly conserved Lys42 in the ATP-binding cleft is substituted by a methionine.

Ca^{2+}/CaM binding stabilizes an ordered helical conformation in the R3 segment.

The CaM binding region, which is in equilibrium between unstructured and docked conformations in the apo state, undergoes conformational transitions upon Ca^{2+}/CaM binding. For the (*i*, *i*+4) doubly labeled 300/304 mutant, binding induces spectral broadening relative to the apo state deduced from comparison of the lineshape and intensity (Figure 4.9).

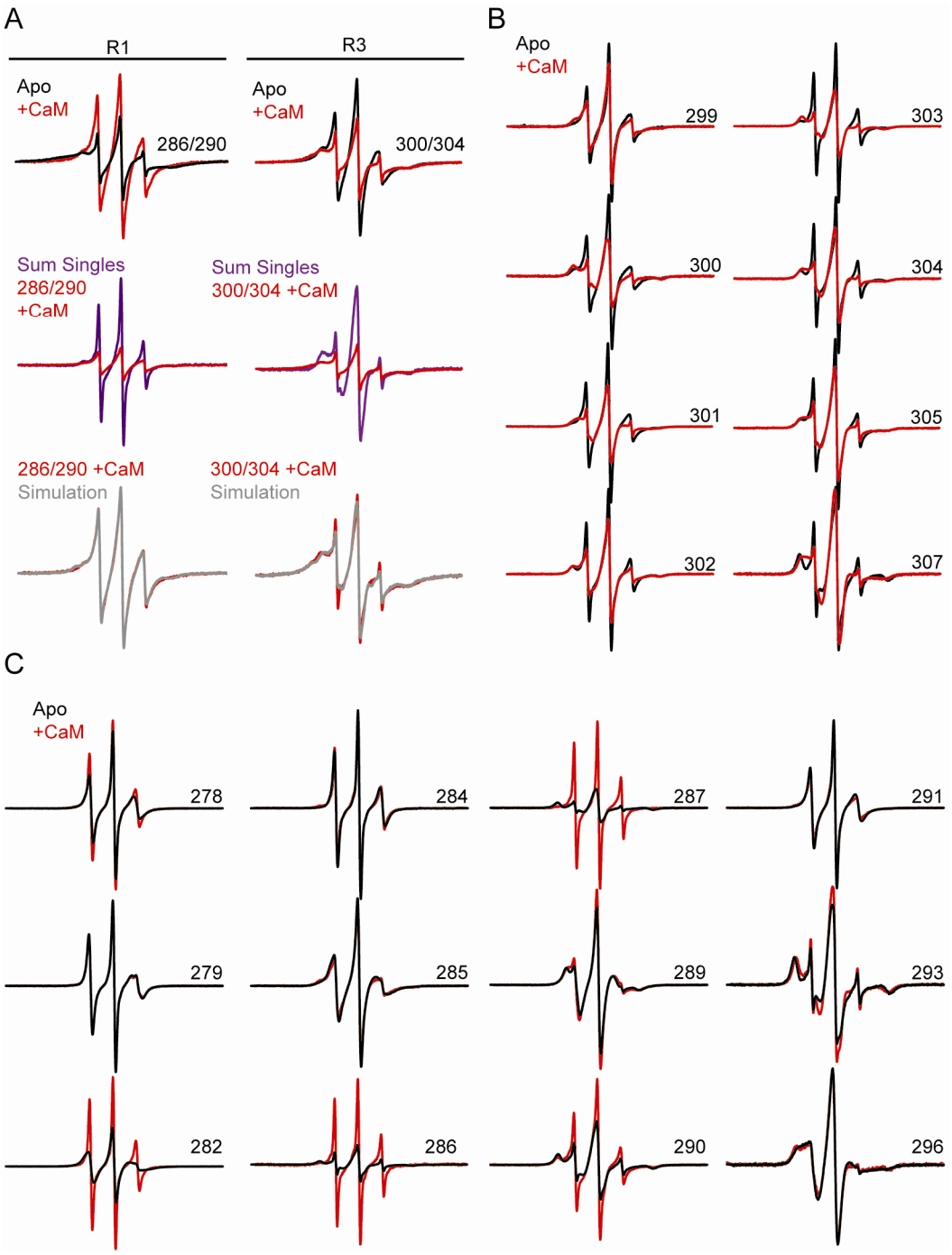

Figure 4.9 A) EPR spectra of (*i*, *i*+4) spin label pairs revealing opposite changes in distance in the R1 (286/290) and R3 (300/304) segments. Both the double mutant spectrum and that of the corresponding sum of singles are shown for the apo and CaM-bound intermediates. B) Spin label mobility changes in the R3 region (red) and C) in the R1 region upon Ca^{2+}/CaM binding.

The corresponding distance distribution shifts to shorter distance indicating stabilization of α-helical structure (Figure 4.10B). Ca^{2+}/CaM binding also leads to a reduction in the

mobile fraction of spin labels suggesting that most R3 residues are in tertiary contacts with CaM (Figure 4.9B). These changes are consistent with the crystal structure of Ca^{2+}/CaM bound to the corresponding CaMKII peptide (residues 293-310) (PDB 1CDM) [152] and a recent structure of the CaMKII/CaM complex (PDB 2WEL) [108].

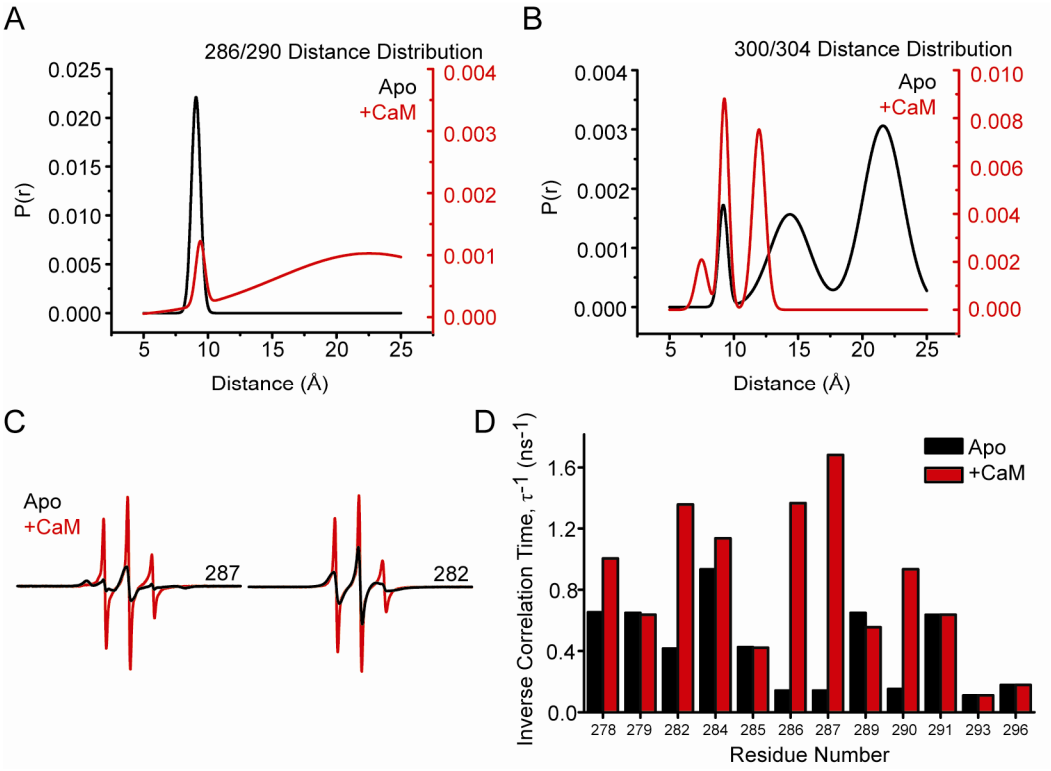

Figure 4.10 Consequences of CaM binding to the regulatory domain. Representative distance distributions between (*i*, *i*+4) spin label pairs in the R1; 286/290 (A) and R3; 300/304 (B) segments. The distributions, consisting of the probability of given a distance P(r), were obtained from fits to the EPR spectra as detailed in the methods and shown in Figures S5 and S7A. Ca^{2+}/CaM binding to R3 induces conformational changes along the entire regulatory segment evidenced by changes in average distance and breadth of the distribution (a, red trace) and increased dynamics of the R1 segment illustrated by sharper EPR lineshapes at sites 287 and 282 (C) and increases in the inverse correlation times (D).

Ca^{2+}/CaM mediated activation induces unfolding of the R1 helix.

Concomitant with the ordering of the R3 helix, spin labels at a number of sites in the R1 segment (274-291) report substantial but reversible increases in mobility upon

Ca^{2+}/CaM binding (Figure 4.9C). This is illustrated by residue 287 which in the apo state is buried at the interface with the catalytic domain (see above). Binding of Ca^{2+}/CaM leads to a 10-fold decrease in rotational correlation time (Figure 4.10C, red trace). This loss of tertiary contacts with the catalytic domain is accompanied by unfolding of the helix, as evidenced by increased distance between spin labels at (*i*, *i*+4) residues (Figure 4.10A). In addition, representative site 282 which is surface-exposed in the neighboring R1 loop reports a 3-fold increase in mobility indicating an increase in the dynamics of the backbone upon CaM binding (Figure 4.10C). The increase in backbone flexibility and loss of tertiary contacts create an expanded loop spanning residues 278-291 surrounding the Thr286 phosphorylation site (Figure 4.10D).

Unfolding in the R1 region is consistent with a recent crystal structure of CaMKII bound to Ca^{2+}/CaM (PDB 2WEL) [108], in which the R1 segment is docked at the active site of an adjacent kinase monomer in the crystal seemingly positioning Thr286 for trans-phosphorylation. Evidence of this interaction occurring in solution were also obtained from analytical ultracentrifugation at 4^0C revealing a rather moderate K_D of 50-100 μM [108]. However, the mobile EPR lineshapes in the R1 segment are inconsistent with the formation of Ca^{2+}/CaM/CaMKII dimers in solution. It is possible that these dimers are not stable at the concentrations used in the EPR experiments (50-100 μM) at 25^0C. In addition to the mobile EPR lineshapes, we failed to observe such dimers using light scattering (Figure 4.11) in disagreement with data reported previously [109].

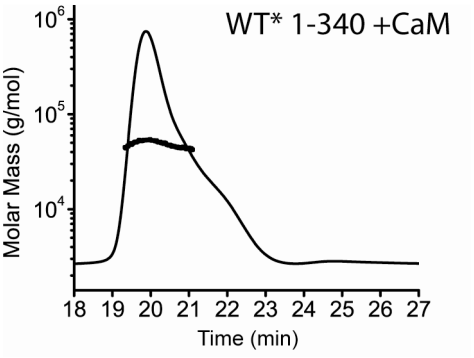

Figure 4.11 Light Scattering on CaM-bound CaMKII. Light Scattering analysis of WT* protein was analyzed in the presence of $CaCl_2$ and 6-fold excess CaM. One major peak was observed corresponding to an experimental molecular weight of 52400 Da. The expected molecular weight for the WT*/CaM complex is 58005.2 Da indicating close agreement.

DEER measurements made between the catalytic domain and the R1 segment indicate an increase in interprobe distance and distance distribution in the presence of CaM. Protein labeled at 93/287 shows two short discrete distances of narrow distribution in the apo state which are less than 30 Å (Figure 4.12, black trace). In the presence of CaM, the major distance component is centered at 45 Å with a broad 20 Å distribution (red trace). This is consistent with mobility studies which indicate an undocking and unfolding of this region upon CaM binding, a prerequisite for T286 autophosphorylation and activation.

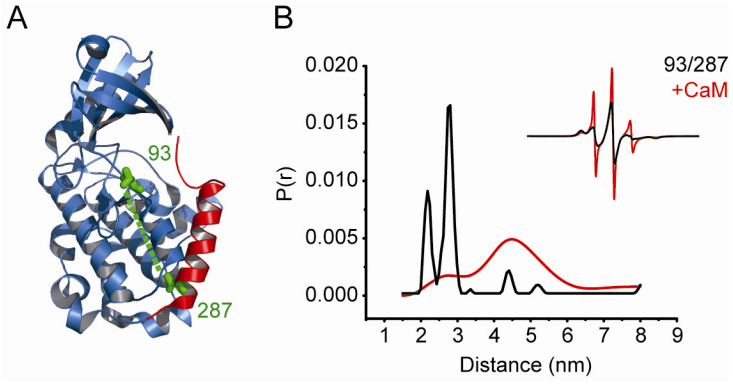

Figure 4.12 Distance measurement in the presence of CaM. A) DEER distance measurements were taken between site 93 of the catalytic domain and site 287 of the R1 regulatory segment. B) Distance distributions reveal an increase in distance length and breadth in the presence of CaM centered at 45 Å.

T286E phosphorylation mimic undergoes CaM-trapping phenomenon

Autophosphorylation of CaMKII at Thr286 increases Ca^{2+}/CaM affinity by more than a 1000 fold [147,151], and it has been established that the origin of this effect involves the transition of CaMKII-bound CaM to a high affinity "trapped" conformation [151]. Therefore, we assessed the mimicking ability of the T286E mutation by completing CaM binding and dissociation curves upon addition of EGTA chelator (see Appendix B for method details). Previous studies suggest that the on-rate for CaM is not significantly varied under trapping conditions and that the difference in binding equilibrium is almost exclusively due to changes in off rates [151]. We therefore expected to see little change in CaM binding between proteins with and without the T286E phosphorylation mimic. For these experiments, protein was not titrated to complete a binding reaction over time. Instead protein samples with varying concentrations of CaM were prepared in the presence of saturating Ca^{2+} and an EPR spectrum was collected for each condition at equilibrium (Figure 4.11). While overall changes in lineshapes are a reliable qualitative assessment, their peak heights can be used as a quantitative measure of spectral change. The mobile portion of the highfield peak was monitored in these experiments (Figure 4.13, black arrow). Here the overlaid spectra for the 287 binding experiment are shown to illustrate that the CaM binding dependent changes in EPR spectra occur in a dose-dependent manner. The peak heights were plotted as a function of the CaM to CaMKII molar ratio and were best fitted with a sigmodial dose response function when comparing R^2 values of various functions. Peak height data was normalized to span 0 to 1. It is important to note that the mobilities for the investigated sites 287 and 300 change in opposite ways; site 287 increases in mobility

with increasing concentrations of CaM as site 300 decreases in mobility. Therefore their binding curves project in opposite directions.

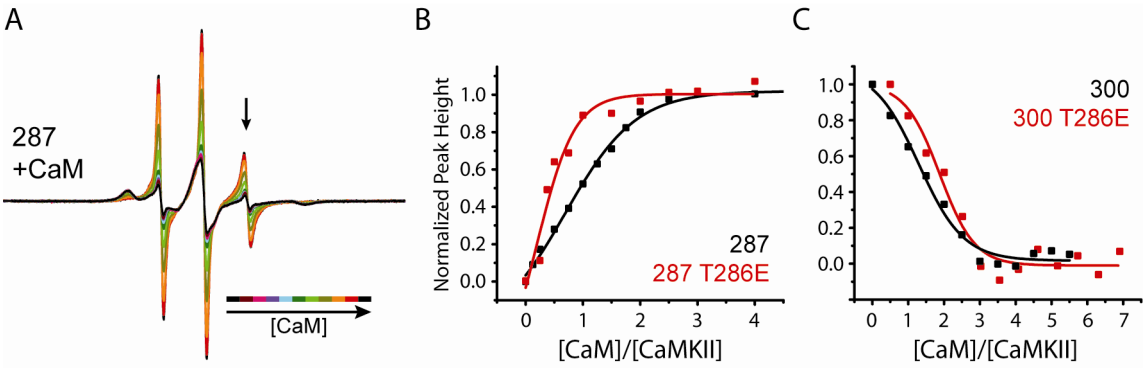

Figure 4.13 CaM-CaMKII association curves. A) The lowfield mobile peak of EPR spectra representing various concentrations of CaM was observed. The normalized height of the peak was plotted as a function of [CaM]/[CaMKII] ratio for proteins with and without the T286E phosphorylation mimic. Sites 287 (B) and 300 (C) were investigated for CaM association. Saturation for binding occurs at ~3 molar ratio.

Data for proteins labeled at site 287 indicate that CaM binding saturation occurs at a lower CaM concentration with the T286E phosphomimic than without (Figure 4.13B). Although we expected the curves to be very similar, these data indicate that the protein containing the phosphomimic has a higher apparent affinity for CaM. However we cannot rule out the possibility that the presence of the label immediately adjacent to the mimic may influence binding kinetics. Any apparent affinity effect was not as prevalent in proteins labeled at site 300. These experiments were not repeated. Only one expression and purification was prepared for each protein and validation of these experiments awaits further investigations. Nevertheless, the binding experiments show binding saturation at ~3 [CaM]/[CaMKII] for all curves indicating that saturating steady state measurements can be made above this concentration. EPR experiments for CaMKII in the presence of CaM were carried out well about this threshold, at 6 [CaM]/[CaMKII].

To investigate dissociation, CaM was added to the CaMKII proteins in the presence of Ca^{2+} for complete binding. Then samples were prepared with varying amounts of EGTA chelator which competes with CaM for Ca^{2+} binding. It has been suggested that binding of CaM to CaMKII requires several Ca^{2+} sites to be occupied [152] so stripping away of even one Ca^{2+} ion can theoretically cause CaM to dissociate from CaMKII. This would indicate that Ca^{2+} does not need to be fully chelated to have complete CaM-CaMKII dissociation. The results of EGTA dependent dissociation are illustrated in Figure 4.14.

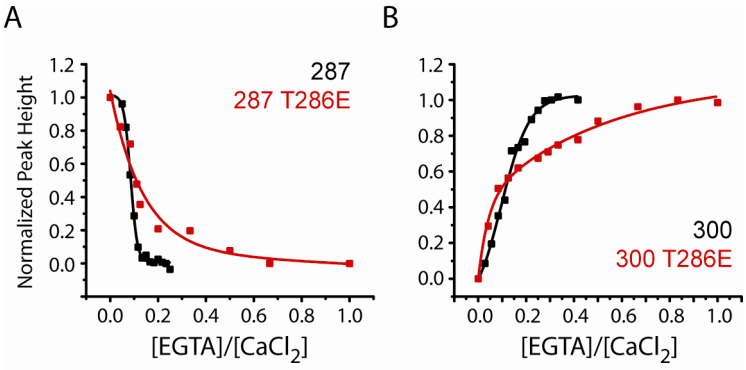

Figure 4.14 CaM-CaMKII dissociation curves. Dissociation of CaM from CaMKII was observed through changes in the low field mobile peak of EPR spectra taken under various concentrations of EGTA chelator. Peak heights are plotted as a function of [EGTA]/[$CaCl_2$] concentration for sites 287 (A) and 300 (B) with and without the T286E phosphorylation mimic.

For the proteins not containing the phosphomimic, a sigmodial dose response function was best able to fit the dissociation curves. These curves saturate at low [EGTA]/[$CaCl_2$] ratios, at approximately 0.3. The addition of the phosphomimic causes a dramatic increase in required chelator to reach the same saturation. Experimental fits for data from T286E* proteins were of exponential type. These two phase functions may indicate that CaM dissociation is occurring by a different mechanism with the phosphomimic than without. While it is difficult to speculate what mechanism is taking place, we can conclude that our mimic is indeed able to decrease the apparent dissociation of CaM.

With confirmation of CaM trapping ability, we concluded that the T286E mutation was appropriate for mimicking phosphorylation.

Autophosphorylation induces unfolding of the R1 helix.

Transition of CaMKII to the autonomously active intermediate is mediated by autophosphorylation at Thr286 which in the apo state is in a solvent inaccessible environment. To investigate the conformational changes induced by Thr286 phosphorylation, we carried out mobility analysis of spin labels introduced in a phosphomimic T286E mutant on the D135N* background. This mimicry approach is necessitated by the expected heterogeneous autophosphorylation at Thr253, Thr305 and Thr306 [127,222] in the WT* enzyme which would complicate interpretation of the EPR data. Spin labels report that the R1 helix surface buried by interactions with the catalytic domain in the autoinhibited apo D135N* monomer (i.e. residues 286, 287) becomes exposed in the T286E/D135N* mutant, with EPR lineshapes characteristic of an unstructured backbone (Figure 4.15A and Figure 4.16A).

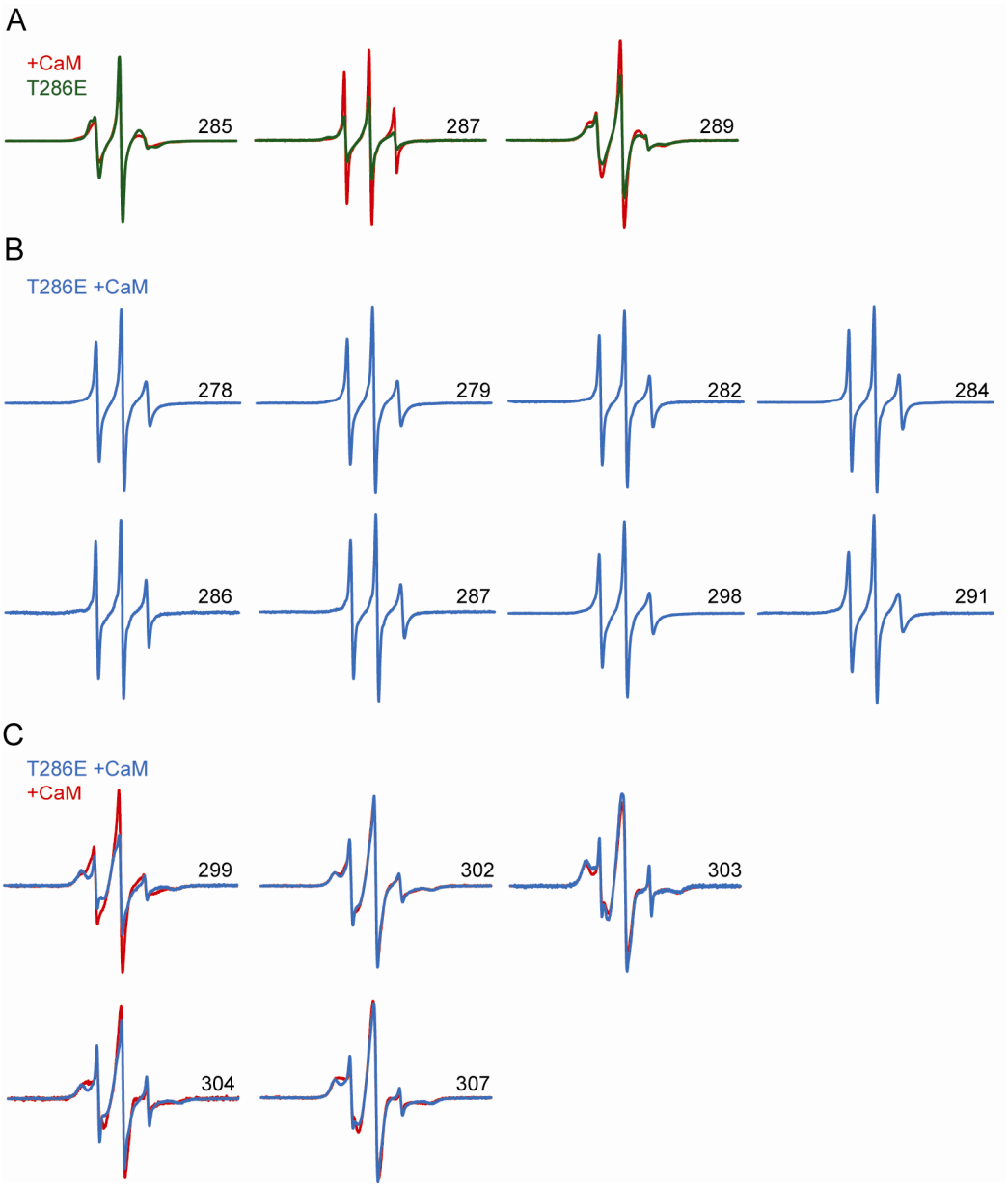

Figure 4.15 Effects of the T286E mutation on the dynamics of the regulatory domain. A) Comparison of EPR lineshapes in the T286E mutant (green) to the CaM-bound intermediate (red) in R1. B) Binding of CaM to the T286E mutant leads to EPR lineshapes in the R1 segment consisting primarily of a highly mobile component. C) EPR lineshapes in the CaM-binding region. The spectrum of site 299 is consistent with increased contact between the spin label and CaM .

Local unfolding of the helix is also manifested by increased distance between spin labels introduced at (*i*, *i*+4) residues (Figure 4.16B). Presumably, disruption of contacts between the R1 helix and the catalytic domain accounts for the lower melting temperature of CaMKII T286E/D135N* (Figure 4.16C). The similarity of the EPR parameters of the

T286E mutant to those observed in the Ca^{2+}/CaM-bound conformation is consistent with the notion that Thr286 autophosphorylation prevents docking of the 287-289 segment to the catalytic domain thereby blocking reinstatement of autoinhibition after CaM dissociates. One notable difference is that the phosphorylation-mimicking mutation leaves the conformational equilibrium of the CaM binding R3 region intact.

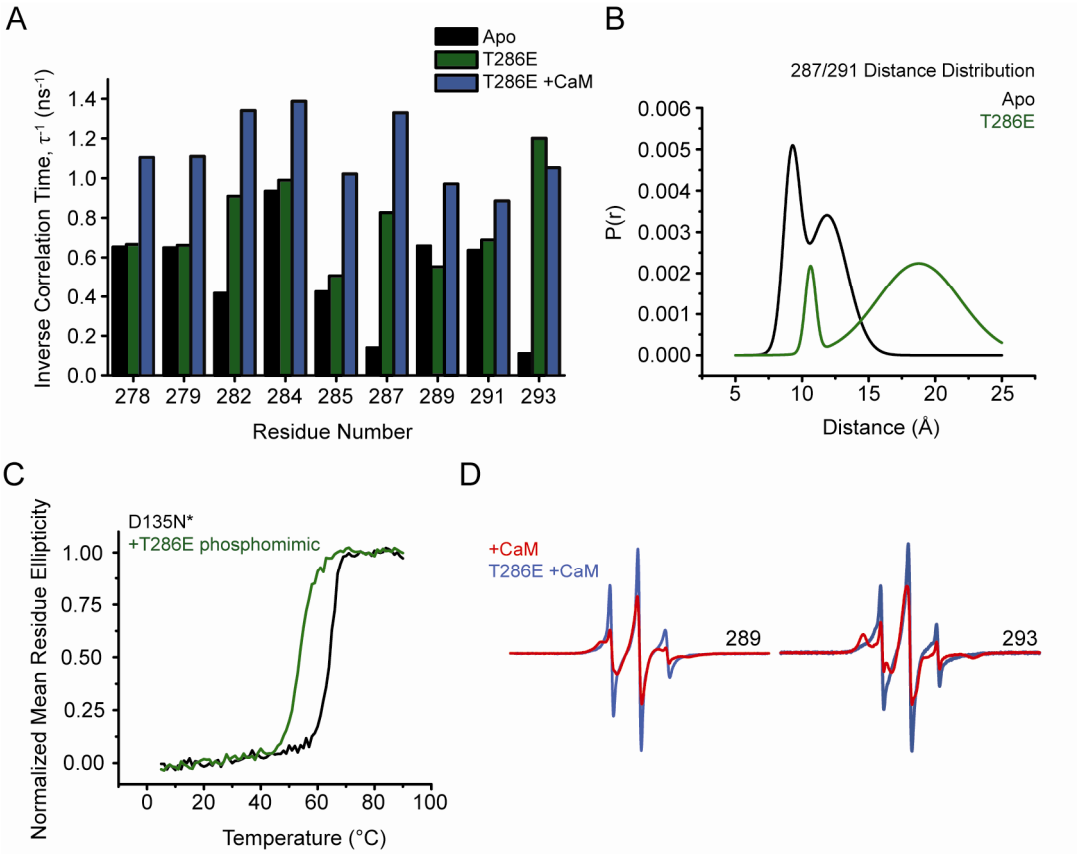

Figure 4.16 Conformational changes of T286 phosphorylation as mimicked by the T286E mutation. A) Comparison of the inverse rotational correlation time of spin labels in three CaMKII intermediates showing the increase in dynamics of the R1 and R2 segments in the presence of Ca^{2+}/CaM and in the T286E mutant. B) The phosphorylation-mimicking mutation T286E destabilizes the R1 helix leading to an increase in the width of the distance distribution between (*i*, *i*+4) spin label pairs. C) R1 helix unfolding is manifested by a shift in the melting temperature of T286E. D) Representative EPR lineshapes highlighting the increased dynamics of the regulatory domain in the CaM-bound T286E mutant.

Phosphorylation of CaM-bound CaMKII further increases the flexibility of the R1 region.

Autophosphorylation of CaMKII at Thr286 increases Ca^{2+}/CaM affinity by more

than a 1000 fold [147,151]. While it has been established that the origin of this effect involves the transition of CaMKII-bound CaM to a high affinity "trapped" conformation [151], corresponding changes in CaMKII structure have yet to be defined. We observed distinct changes in backbone order upon binding of Ca^{2+}/CaM to the T286E/D135N* mutant. EPR spectra in the R1 segment become sharper consistent with increased flexibility of the backbone (Figure 4.16D). While CaM binding alone induces an expanded loop conformation in the Thr286 region, addition of the phosphomimicking mutation causes further increases in mobility as illustrated by the spectral lineshape for site 289 (Figure 4.16D). With Ca^{2+}/CaM bound to the T286E mutant, the spectra at sites 278-291 (Figure 4.15B) are similar to those of unstructured peptides or intrinsically disordered proteins [226]. Thus we conclude the R1 helix experiences complete unfolding in the CaM-trapped intermediate (i.e. CaM-bound and Thr286 phosphorylated).

Structural changes are also observed in the region consisting of residues 291-294 that has been linked to Ca^{2+}/CaM trapping [151]. Although CaM binding has no substantial effect on EPR lineshape at residue 293 in D135N*, CaM induces a distinct increase in mobility of residues 293 in T286E/D135N* (Figure 4.16D) suggesting that disruption of the tertiary contacts with the catalytic domain are involved in the trapping phenomenon. Significant changes in the immobile components are also observed at sites 299 and 303 in the CaM-binding region (Figure 4.15C) suggesting that the T286E mutation affects the interactions between CaM and D135N* CaMKII.

Phosphorylation of Thr305 and Thr306 does not significantly alter the R3 equilibrium

Phosphorylation at T305 and T306 is known to prevent CaM binding, causing

insensitivity to calcium. While there is no specific evidence for duel phosphorylation in the cell, it is not clear if autophosphorylation of Thr305 or T306 is more physiologically relevant. To simplify the number of proteins which would need to be investigated and reduce the experiment effort, we chose to investigate both sites to determine the consequences of phosphorylation of these residues. Representative sites along the regulatory domain were therefore investigated in protein containing a T305E/T306E double phosphorylation mimic. Specifically we wanted to understand how the addition of negative charges may alter the docking/undocking equilibrium observed for this portion of the regulatory domain. Spectra for site 307 report no significant changes in the relative population of each conformation (Figure 4.17A). However, there is a small broadening of the spectrum over all, which indicates the label is experiencing a slightly different environment. Site 302 also reports an intact equilibrium with changes in tertiary contacts although the mobile and immobile populations become less discrete in this case. Site 287 of the R1 segment was also investigated and was not significantly affected by the phosphorylation mimics as expected. Lastly site 293, which is implicated in CaM trapping, shows changes in tertiary contacts but remains largely docked as in apo protein. The T305E/T306E phosphorylation mimic does not disrupt the R3 docking/undocking equilibrium but causes minor changes in docking orientation.

Figure 4.17 Effects of the T305E/T306E phosphomimics. A) Spectra for representative sites throughout the regulatory domain collected for apo protein (black), protein containing the T305E/T306E phosphomimics (magenta) and B) protein containing the T305E/T306E phosphomimics in the presence of ATP (navy).

Since ATP binding alters the docking/undocking equilibrium of the R3 regulatory segment in protein lacking any phosphorylation, we investigated whether or not protein containing the T305E/T306E mimic would behave similarly. Figure 4.17B illustrates spectra from protein containing T305E/T306E in the presence (navy blue) and absence (magenta) of ATP. Similarly to nonphosphorylated protein, ATP binding did not alter the spectra for representative sites 287 and 293 in the R1 and R2 regulatory regions respectively while sites 302 and 307 of the R3 region reported increases in the undocked population. In the presence of ATP, protein containing the T305E/T306E yielded spectra nearly identical to their nonphosphorylated counterpart proteins (data not shown). Thus we predict that phosphorylation at Thr305 and Thr306 does not cause significant conformational changes in the regulatory domain, nor does it enhance or reduce the effect of ATP binding. Because the docking/undocking equilibrium is maintained under these conditions, we predict it to be critical for protein activity.

The position of the catalytic N-lobe may be flexible relative to the C-lobe and conformational changes may be modulated by nucleotide binding.

When comparing structures of active and inactive kinase homologs, differences in positioning of the catalytic N- and C-lobes vary (see Chapter 1 for details). Therefore the conformational changes associated with activation are also thought to be accompanied by an 18˚ shift of catalytic lobes toward each other [134,181,182]. To investigate this possibility, we labeled sites in the catalytic domain and made distance measurements to anchoring site 287 using DEER. We found that the distance between 287 and 125 in the catalytic C-lobe had predominately one distance of relatively tight distance distribution in agreement with the crystal structure (shown previously in Figure 4.7B). In contrast, a distance measurement between site 17, which is located in a β strand of the N-lobe, and site 287 reports an almost 40 Å heterogeneous distribution from 2 to 6 nm (Figure 4.15B). This broad distribution may reflect side chain mobility and/or potential N-lobe movement relative to the C-lobe. Interestingly, the distance distribution for 93/287 reports two narrow, discrete distances at 22 and 27 Å (Figure 4.18C). Because site 93 resides between the N- and C-lobes of the catalytic domain, this data suggests a conformational equilibrium may exist in this hinge region between lobes. These results raise the question of whether the conformational changes in the N-lobe and hinge region are coupled, the hinge-like movement in the catalytic cleft propagating to create larger motions in the N-lobe. Additionally, ATP binding to the 93/287 protein causes a change in population of the two distances, now favoring the shorter distance. ATP also causes a shortening of the distance and tightening of the distance distribution of the 17/287 mutant, although it is still quite heterogeneous. The change in populations illustrate that

ATP binding modulates these conformational changes and begs the question of whether or not the R3 regulatory domain docking/undocking equilibrium is coincident with the proposed catalytic equilibrium.

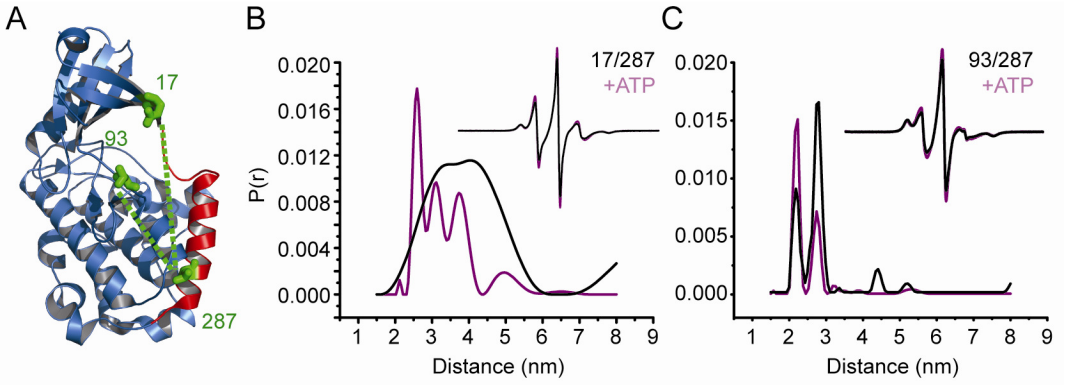

Figure 4.18 ATP effect on positioning of catalytic N-lobe. A) Sites used for DEER distance measurements are highlighted in green in the crystal structure of human CaMKIIδ (PDB 2VN9). B) Distance measurements between site 17 on the catalytic N-lobe and anchor site 287 of the regulatory domain in the apo (black) and ATP bound (purple) intermediates. C) Distance measurements between site 93 of the catalytic cleft and 287 reveal two discrete distances which invert populations in the presence of ATP.

To test the idea that the N-lobe is undergoing conformational changes relative to the C-lobe in the apo state, a series of double mutants were created that connect site 20 of the N-lobe, 134 of the catalytic cleft, and 110 of the C-lobe (Figure 4.19A). The rationale for deciding on these sites originated from a comparison of crystal structures of active PKA and inactive CaMKII. The sites chosen were anticipated to undergo large conformational changes. A 20/110 mutant measuring from the N- to C-lobe reported one narrow distance of 32 Å which does not imply conformational heterogeneity of the N-lobe. Measurement between 110 and 134 of the catalytic cleft also reports one distance of 40 Å. Interestingly, the 20/134 mutant reported distances of 22 and 45 Å which were much broader in distribution. If we think of these three sites as corners of a triangle, sides connected to site 110 do not change length while the length of the side between 20 and 134 can vary. If we interpret this data in the context of a model involving rotation of

catalytic lobes, C-lobe site 110 would be considered an anchor point since both sets of data containing site 110 show discrete, single distance distributions and the helix this residue resides on is expected to remain largely static. In this case, it is unlikely that site 134 in the catalytic cleft is part of the proposed catalytic equilibrium like site 93. Since there is only one predominant distance, site 134 may be statically associated with the C-lobe. In this case any rearrangement of lobes results in the same distance between sites 110 and 20 which is a bit difficult to reconcile.

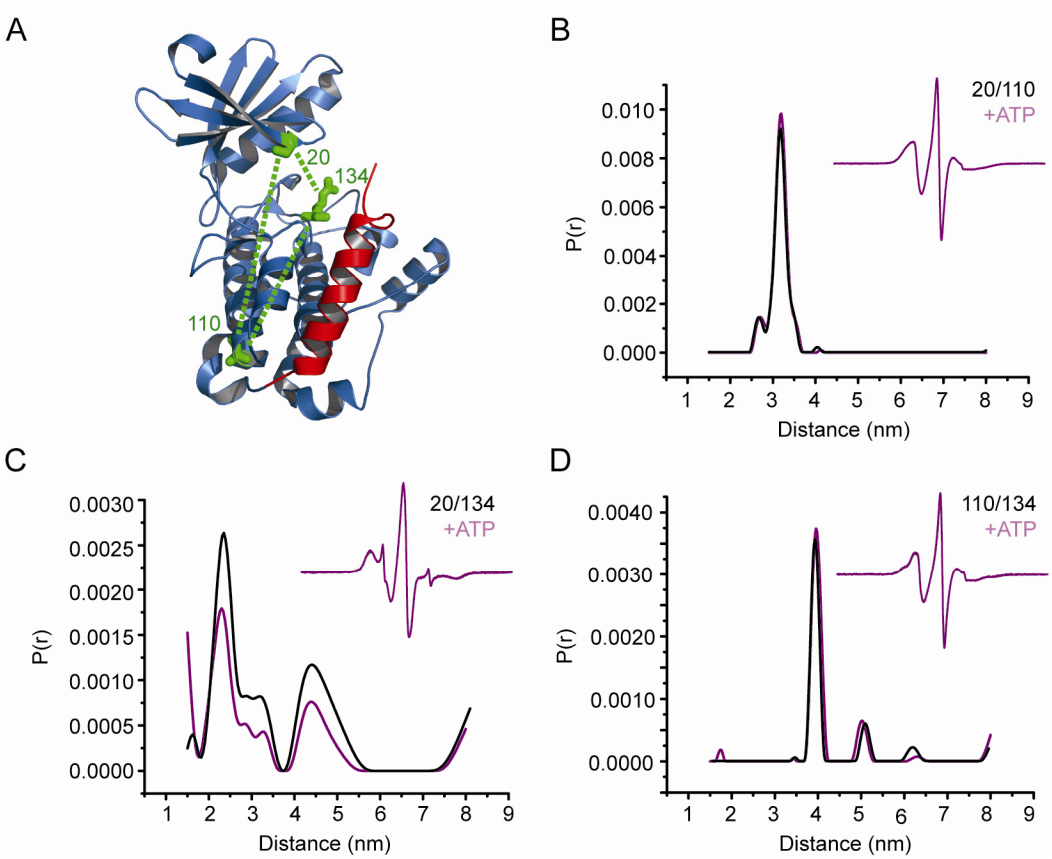

Figure 4.19 Distance measurements between catalytic lobes. A) Sites used for DEER distance measurements are highlighted in green in the crystal structure of human CaMKIIδ (PDB 2VN9) with site 20 in the catalytic N-lobe, 110 in the C-lobe, and 134 in the catalytic cleft. B) Measurements across catalytic lobes between sites 20 and 110 result in one distance unaffected by ATP. C) Measurement from the N-lobe to the catalytic cleft resulted in two broad distances while D) measurement from the C-lobe to the catalytic cleft resulted in one narrow distance distribution, neither of which were influenced in the presence of ATP.

Interestingly ATP did not modulate any of these distances as hypothesized. These results are inconsistent with data measured from 287 to the N-lobe and to the hinge region which show conformational changes upon ATP binding. Since neighboring site 135 is catalytically important, SDSL of site 134 may inhibit ATP binding. Overall these results do not serve to verify catalytic domain movements, but rather introduce mechanistic questions about lobe rotation and dynamic equilibria in the apo state. Resolution of catalytic conformational changes associated with ATP binding awaits further investigation.

While delineation of the catalytic domain conformational changes awaits future investigation, the conformational changes of the regulatory domain have been built into a model describing the structural basis for each intermediate. Additionally, the structural implications from the data reported here are united with hypotheses and data from previous biochemical research to describe a novel model of CaMKII structure-function relationships. This model is described in the next chapter.

CHAPTER V

MODEL OF CaMKII ACTIVATION[‡]

CaMKII mechanism of activation; a summary of EPR results

Our results present a novel perspective on CaMKII regulatory mechanisms revealing the link between dynamics and interactions of the regulatory domain and the activation state of the enzyme. This work was designed to investigate how this enzyme is regulated by a ~40 amino acid domain especially suited to adopt several conformations. We found that the most important feature which allows multiple and discrete intermediates is its backbone flexibility and dynamic nature. We predict that the entire domain has helical propensity, but is unstable enough such that it exists in equilibria between structured and intrinsically disordered states. It is this exchange between order and disorder that endows the regulatory domain with a conformational plasticity and makes it exceptionally sensitive to modification. The structural plasticity of this domain manifested by the conformational equilibrium described here is a central element in autoregulation, serving to modulate substrate and nucleotide access and affinity for Ca^{2+}/CaM, as well as to regulate intersubunit interactions with neighboring catalytic domains. Destabilizing phosphorylation charges or stabilizing tertiary contacts are able to shift the equilibrium, consequently producing the various conformations. Conformational changes are even coupled under some conditions, allowing a modification in one segment of the domain to communicate changes to another. From investigation of these dynamics, we have built a model of activation describing the

[‡]A portion of text and figures described in this chapter are published in Hoffman et al., 2011 [223].

conformational rearrangements that take place as the enzyme cycles from one intermediate to the next. Our findings are summarized here to illustrate how conformational changes of the regulatory domain and its multiple interactions with the kinase domain underlie transitions between CaMKII intermediates.

The cartoon illustrated in Figure 5.1 depicts our model of intermediates for one catalytic subunit. In the basal state, the R3 segment containing the CaM-binding region partitions between an undocked, dynamic conformation and one where it interacts with the catalytic domain reducing affinity for nucleotides and presumably substrate access to the active site (Figure 5.1A). The docked conformation is consistent with the structure of the human CaMKIIδ isozyme (PDB 2VN9) placing Thr306 at the catalytic cleft. The equilibrium predicts that a population of residues are undocked approximately 20% of the time, leaving the catalytic cleft open for ATP and substrate binding and the CaM binding region disordered and freely accessible. This implies mechanistic relevance for both nucleotide coordination and CaM recognition. First the equilibrium facilitates ATP binding by repeatedly exposing the active site to allow ATP access without a prior CaM-binding requirement. Additionally, we predict the undocked and unstructured state to facilitate CaM recognition.

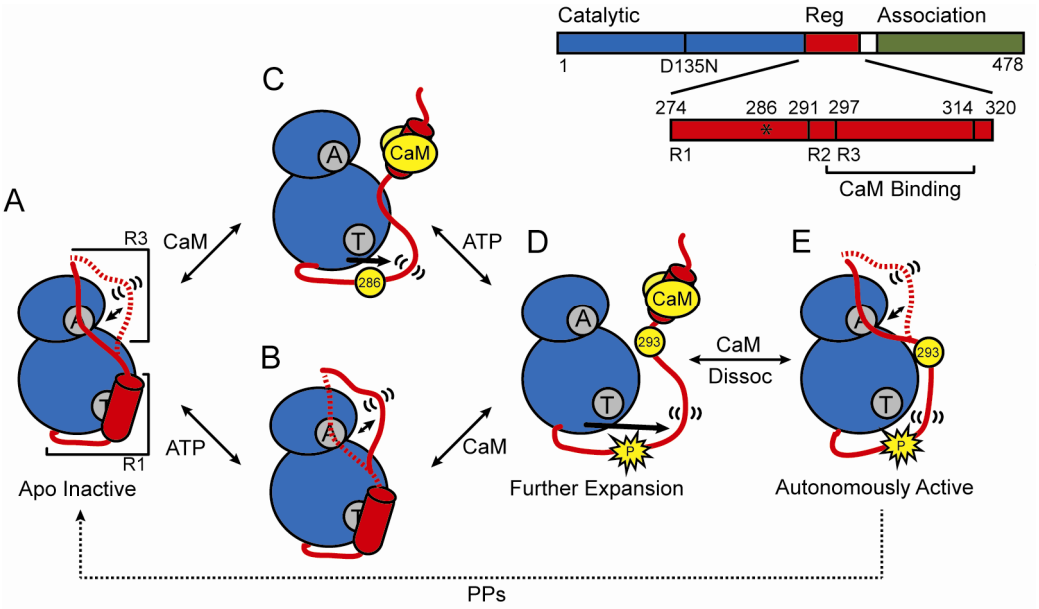

Figure 5.1 Model of the mechanism of autoinhibition and activation of CaMKII. The CaMKII monomer is represented with N- and C- lobes of the catalytic domain in blue and the regulatory domain in red. The ATP binding and Thr286 docking sites are indicated in gray with letters "A" and "T" respectively. A) In the basal, apo intermediate, the R3 segment of the regulatory domain is in a dynamic equilibrium between docked and undocked, flexible (indicated by parentheses) conformations. B) ATP binding shifts the equilibrium toward the undocked conformation facilitating exposure of the catalytic cleft. C) CaM (yellow) binding releases autoinhibition and primes the regulatory domain for phosphorylation at residue 286. D) Autophosphorylation at Thr286 causes further flexibility of the regulatory domain and exposes site 293 which is implicated in CaM trapping. E) While CaM dissociation allows for reinstatement of the R3 equilibrium, the R1 helix remains predominantly unstructured.

We found that saturating concentrations of ATP reduce, but do not eliminate, binding of R3 at or near the active site (Figure 5.1B). Thus in the docked conformation Thr306 remains proximal to the active site when ATP is bound, allowing slow basal intrasubunit autophosphorylation [122]. The event requires that nucleotide bind the autoinhibited kinase and that residue 306 fit into the active site of their own catalytic domain within the same subunit simultaneously. Since ~50% of the regulatory domain population remains catalytically docked upon ATP binding, residue 306 can occupy the active site concurrently with ATP. Maintaining the equilibrium in this manner is essential to retain the possibility for 306 autophosphorylation. This interaction also explains in a structural context previous biochemical results demonstrating that

regulatory domain peptides compete not only with substrates but also with ATP binding [110,111,132,135] and that regulatory domain peptides protect reactive arginine residues in the nucleotide-binding site from covalent modifications that inactivate CaMKII [135,186]. Because cellular concentrations of ATP are well above the K_D of binding to CaMKII, a substantial fraction of R3 is presumably in the undocked state, physiologically primed for Ca^{2+}/CaM binding.

Stable docking of the R1 helix to the catalytic domain buries Thr286, ensuring a stringent dependence on Ca^{2+} for activation. Our data supporting this proposed conformation cannot be reconciled with that of the *C. elegans* crystal structure (PDB 2BDW), which features a dimeric interface shown to be unstable in solution [138], but is consistent with structures of human kinase domains (PDBIDs 2VZ6, 3BHH, 2V7O, 2VN9) [108].

Although CaM binding does not require initial ATP coordination, our model predicts ATP binding aids in the sequestering of CaM by pushing the equilibrium to favor the undocked conformation. We predict the intrinsic disorder of this state may facilitate CaM binding by decreasing the K_d. As shown in a structure of CaM bound to a regulatory domain peptide (PDB 1CDM) [152] and a recent structure of CaM bound to CaMKII regulatory domain (PDB 1MXE) [191], CaM completely surrounds the R3 portion of the regulatory domain, stabilizing it from all sides [152]. Because its contact is so extensive, we theorize it would require less free energy for CaM to bind a freely accessible domain versus one that is catalytically docked and must dissociate from catalytic contacts. This also sheds light on previous work which showed nucleotide binding was able to stabilize the CaM-CaMKII complex and that ATP increased the CaM

affinity for CaMKII [122,123,143,227]. We predict ATP binding serves to lower the regulatory domain affinity for catalytic docking, causing an increased preference for CaM. In addition, CaMKII-bound CaM has been shown to adopt a more compact conformation in the presence of a non-hydrolyzable ATP analog [143], presumably making more extensive contacts with the regulatory domain. The increased exposure of regulatory residues might explain this change in the conformation of bound CaM.

Preliminary evidence also suggests that catalytic N- and C-lobes undergo a conformational equilibrium in the apo state. We speculate this involves a twisting motion relative to one another as predicted by the 18° rotation of catalytic lobes in active and inactive structures of kinase homologs [134,181,182]. In the apo state, the catalytic lobes are predicted to be in an "open" conformation with larger inter-lobe distance predominantly. According to the equilibrium, the minor population is in a "closed" conformation with a smaller inter-lobe distance. Interestingly this equilibrium is modulated by ATP binding which may suggest the movement is concurrent with the R3 regulatory docking/undocking equilibrium (Figure 5.2). This model predicts that ATP binding serves to switch the populations to favor the "closed" catalytic lobe conformation and the undocked R3 regulatory segment.

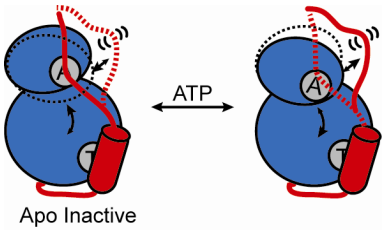

Figure 5.2 Catalytic equilibrium hypothesis. The N- and C-lobes are predicted to undergo an 18° twisting motion relative to one another. In the apo state (left), the domains are predominantly held in an "open" conformation with the R3 regulatory segment docked. The minor population is predicted to be in a closed conformation (dotted lines). ATP binding shifts the populations to favor a "closed" catalytic conformation with undocked R3 segment (right).

Our data directly demonstrates that binding of Ca^{2+}/CaM to the R3 segment induces significant changes in the backbone structure and interaction of the regulatory/catalytic domains that cause activation. The R3 equilibrium is shifted to the undocked conformation fully releasing the catalytic cleft for nucleotide binding (Figure 5.1C). The CaM-binding region is stabilized in a helical conformation consistent with crystal structures of Ca^{2+}/CaM bound to the R3 regulatory segment (PDB 1CDM, 2WEL) [108,152]. This conformational change propagates to the R1 regulatory helix (residues 285-293) exposing Thr286 to the solvent. We predict this separation of regulatory and catalytic domains abolishes autoinhibition, which is necessary for the enzyme to become active. Our results are consistent with previous data illustrating that deletion or mutation of certain residues in the extended R1 loop produces constitutive activity [126,130,144,228]. The regulatory-catalytic separation presumably exposes the active site as well as the T-site on the catalytic domain, which has been identified as the site where Thr286 docks against the catalytic domain. The T-site is also a binding site for several substrates including the NR2B subunit of the NMDA receptor. Interestingly this substrate can only bind the active enzyme [169] in which the T-site is expected to be accessible. The fact that the stabilization of the CaM-binding region coupled to the destabilization of the T286 phosphorylation region is mechanistically important; i.e. CaM binding exposes the catalytic domain for substrate binding.

The catalytic separation is preparatory for T286 autophosphorylation as well. It has been shown that T286 autophosphorylation is an intersubunit reaction in the holoenzyme and that CaM must be bound to both subunits simultaneously for autophosphorylation to occur [157,229,230,231]. This requires that the regulatory

domain of the "substrate" subunit must enter the active site of the neighboring "kinase" domain [109]. The unfolding of the R1 helix effectively expands the length of the R1 region, presumably enabling the binding of Thr286 at the active site of a neighboring subunit in the holoenzyme, a prerequisite for trans-phosphorylation and transition to the autonomously active intermediate. It also exposes the "kinase" active site for "substrate" regulatory domain binding. It is important to note that intersubunit catalytic-regulatory binding for T286 phosphorylation is structurally distinct from intrasubunit binding for autoinhibition. For autophosphorylation, the T286 residue must be in the active site of its neighboring subunit (as shown in a recent structure [109]), ready to accept the phosphate transfer. In contrast, T286 is catalytically docked in the T-site, away from the active site in the autoinhibited conformation. The promiscuous nature of the regulatory domain must allow it to adopt both conformations, and we speculate the disorder created by CaM-binding is necessary to change its affinity to prefer intersubunit binding over intrasubunit autoinhibition. In addition, undocking of the R1 segment disrupts interactions with helix D which was proposed to stabilize an inactive conformation of the catalytic domain [138]. In the CaMKIIδ/CaM structure, the orientation of the highly conserved E97 is altered to coordinate the sugar moiety of ATP, as seen in glycogen phosphorylase kinase [232]. In combination, these structural changes likely mediate the 10-fold increase in nucleotide affinity following activation by Ca^{2+}/CaM [122,187,188].

Thr286 phosphorylation is thought to generate the autonomously-active form by blocking reinstatement of autoinhibition upon dissociation of Ca^{2+}/CaM [121,153]. Indeed, we find that the phosphomimic T286E maintains the R1 helix in a predominantly unfolded and undocked conformation (Figure 5.1E). Although the T286 region is

unstructured, it is flexible to a lesser degree than CaM-bound CaMKII because the R1 loop region is shorter. The T-site may consequently be exposed to a lesser degree. The other significant difference is that in this intermediate, the T286 region is not coupled to the CaM-binding region. However, in contrast to the CaM-bound intermediate, the R3 conformational equilibrium is restored allowing contacts with the catalytic cleft. Therefore the active site is occluded 80% of the time despite the availability of the catalytic T-site. For enzymatic phosphorylation, substrates must either enter the active site while the equilibrium is undocked or alternatively bind the T-site and sterically induce undocking at the active site. This implies that the energy barrier for substrate phosphorylation is higher in the T286 autophosphorylated intermediate than in the CaM-bound intermediate. This may explain the lower activity of autophosphorylated CaMKII, which is 30-70% that of fully activated CaM-bound CaMKII [230]. The relative autonomous activity of CaMKII holenzymes can be increased by using higher concentrations of ATP and peptide substrates [135], supporting the restoration of a competitive R3 interaction with the nucleotide-binding site. However, binding of Ca^{2+}/CaM to the autonomously active Thr286 phosphorylated form fully activates CaMKII. In support of this conclusion, we found that the R1 segment is most strongly disordered in Ca^{2+}/CaM-bound/T286E CaMKII, indicative of essentially complete disruption of interactions between regulatory and catalytic domains (Figure 5.1D). Both the active site and T-site are predicted to be completely available indicating that substrates can bind more easily. This suggests there is direct correlation between the catalytic exposure resultant for regulatory domain disorder and enzymatic activity. The region between residues 291 and 294 previously implicated in the CaM-trapping

phenomenon [147,151] also shows conformational changes unique to this intermediate. It has been shown that these residues, although not known to have significant CaM contact [152], aid in establishing electrostatic contacts at residues 296-298 [151]. Interestingly sites 291 and 293 do not experience conformational changes with CaM binding alone, but become accessible when T286 is phosphorylated.

The R3 equilibrium is also maintained in protein containing T305E/T306E phosphomimics. We conclude the function of these charges is merely to prevent Ca^{2+}/CaM binding without changing affinity for ATP or disrupting regulatory-catalytic interactions. However, introduction of negative charge by the T286E, T305E, or T306E mutations do not fully mimic the effects of a phosphate group, and details of the local dynamics may be somewhat different in phosphorylated kinase.

CaMKII activation model in the context of the holoenzyme

Assembly and interaction of the CaMKII subunits in holoenzymes allow for trans-phosphorylation of one subunit by a neighboring one and mediates cooperative CaM binding and substrate phosphorylation. A model was proposed on the basis of the crystal structure of the autoinhibited kinase domain and extensive analysis of cooperative substrate phosphorylation in the holoenzyme [109]. A central element in this model is dimerization of the auto-regulatory domain which locks the enzyme in an inactive conformation. Binding of Ca^{2+}/CaM disrupts the dimer simultaneously activating the kinase domain of one subunit and releasing the CaM-binding region of the other subunit. However, we found no evidence for regulatory domain dimerization, and this model cannot rationalize cooperative CaMKII activation. Explanation for the experimental Hill

coefficient of 3 to 4 as estimated previously [109] requires the postulation of additional interactions between kinase domains. Moreover, the coiled-coil motif was not detected in a recent structure of human CaMKII kinase domains bound to ATP inhibitors (PDB 2VN9) [108]. In this structure, part of the R3 segment of the regulatory domain was folded back onto the catalytic cleft consistent with our data.

The results presented here can be extrapolated to propose an alternative model of autoinhibition and activation of the CaMKII holoenzyme. Rather than forming the coiled-coil, the R3 segment is in an equilibrium that involves interactions with the catalytic domain partially blocking the nucleotide binding region. Although the dynamics of the R3 segment are likely to be modified by its linkage to the association domain in the holoenzyme, the effects of ATP on the R3 equilibrium demonstrate its role in activation. Binding of CaM disrupts the autoregulatory/catalytic domain interactions at the R3 and R1 segments through concomitant but opposite structural changes of the backbone. Our model is also consistent with previous work showing that Ca^{2+}/CaM binding to CaMKII holenzymes enhances affinities for nucleotides [122,187,188].

How is cooperativity achieved in the context of this model? We propose that upon unfolding, the R1 segment becomes available for binding at the active site of a neighboring kinase domain effectively competing with the R3 segment and displacing it. The shift in equilibrium would increase the apparent affinity to Ca^{2+}/CaM hence accounting for the positive cooperativity with respect to Ca^{2+}/CaM binding. Figure 5.3 illustrates the hypothesis starting in the apo intermediate, where autoinhibition is instated. When Ca^{2+}/CaM binds to one subunit, autoinhibition is released, inducing unfolding of the R1 regulatory segment. This unfolding causes the R1 segment to have higher affinity

for its neighboring subunits active site (Figure 5.3B). The increased affinity allows it to compete with the neighbor's own R3 element which is undergoing docking and undocking. Once the R1 segment is bound to the neighbor's catalytic cleft, the neighbor's R3 segment is pushed to the undocked conformation, effectively increasing it's affinity for Ca^{2+}/CaM (Figure 5.3C).

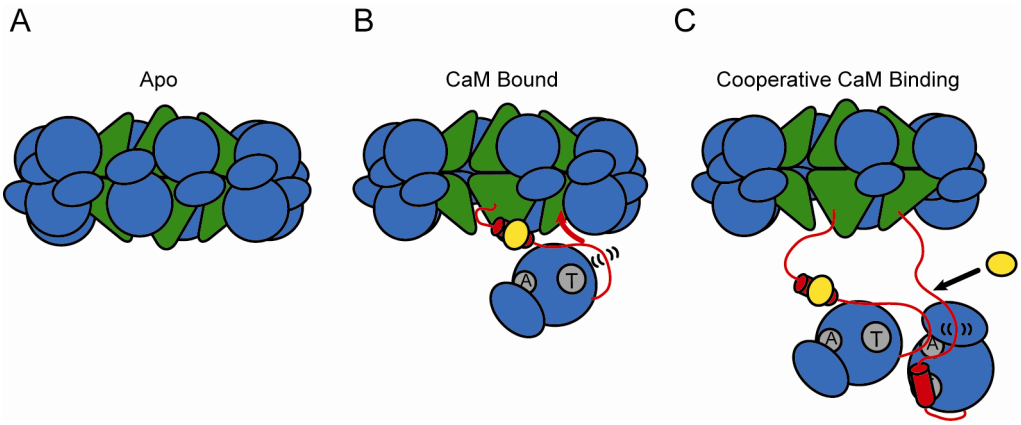

Figure 5.3 Holoenzyme model of cooperative activation. CaM binding to one subunit causes undocking and unfolding of R1. The released R1 can displace the R3 segment of a neighboring kinase subunit from the catalytic cleft. This R3 is undocked and primed for CaM association.

Experimental testing of the holoenzyme model

To experimentally test this model, we monitored the R3 equilibrium in the presence of a peptide corresponding to the autoregulatory domain, referred to as autocamtide-2 (AC-2). AC-2 mimics the unfolded and flexible R1 segment in the Ca^{2+}/CaM-bound state which contains the T286 autophosphorylation region. According to our model this sequence can extend over to a neighboring kinase domain and compete with its R3 segment of the regulatory domain for binding to the catalytic cleft. Consequently, we expect displacement of the R3 segment, now having a preference for the undocked conformation. Consistent with the model's prediction, peptide binding shifts the equilibrium towards the undocked state reflected by the sharp population in the

EPR spectrum. Figure 5.4 shows data collected for site 307 in the R3 regulatory segment in the apo state (black) and under the conditions of T286E phosphomimic (green) and in the presence of AC-2 (gold). Titrations using various concentrations of AC-2 were carried out; however only two representative data points for each protein are shown in this figure for the sake of simplicity. For the complete data set of the titrations, refer to Supplementary Figure 3 (Appendix A). In the presence of AC-2, there is an increase in the mobile population of the spectrum which correlates to the undocked conformation. When added to apo protein, 64-fold excess peptide was added to achieve a ~3 fold increase in the mobility. The high concentrations of peptide required in the case of monomeric kinase suggest a low binding affinity. However, this interaction will be potentiated in the holoenzyme which concentrates subunits to an unusual extent. In contrast, a 10-fold peptide excess correlated to a ~4.5 fold increase in mobility when added to protein containing the phosphomimic. Therefore the AC-2 concentration threshold for undocking R3 is reduced in the T286E mutant consistent with higher affinity for substrate in this intermediate.

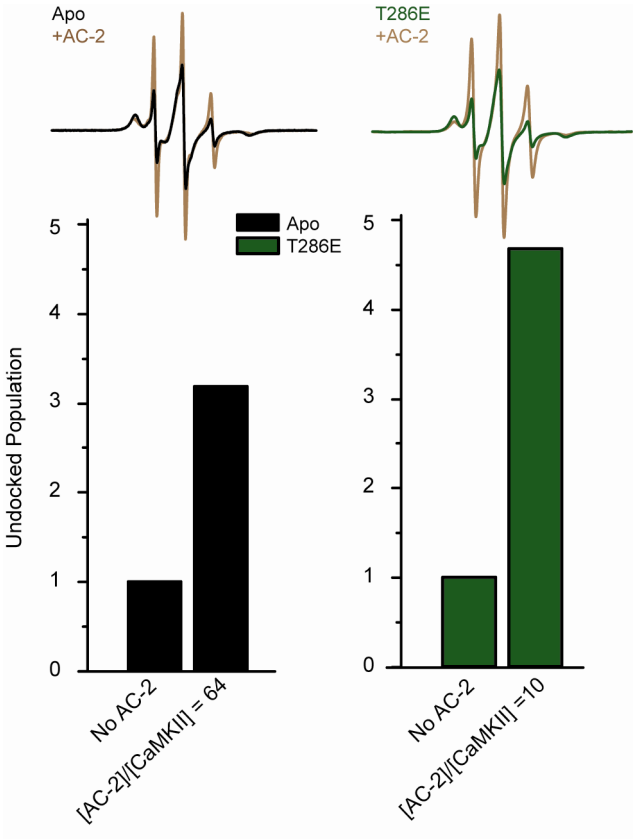

Figure 5.4 Shifts in the R3 equilibrium induced by binding of autocamtide-2 (AC-2). EPR spectra for site 307 show that the level of the mobile spectral component arising from undocked conformation of the R3 segment increases in the presence of AC-2. The T286E mutation increases the apparent affinity of this interaction as evidenced by the lower molar ratio of peptide to CaMKII (x-axis) required to increase the mobile spin label fraction.

Thus, although autophosphorylation does not perturb the R3 equilibrium, phosphorylated kinase domains are more likely to capture the unfolded R1 segment of a neighboring subunit allowing the propagation of autophosphorylation. These results are in line with recent studies demonstrating that addition of an inactivated kinase monomer lacking the regulatory domain ("decoy" kinase) leads to apparent cooperativity in the activation of an intact kinase monomer with respect to Ca^{2+}/CaM [109]. The interpretation of Figure 5.4 is consistent with a previous suggestion that CaM binding releases and unfolds the R1 segment to act as a "molecular grappling hook" that can be captured by the decoy

enzyme [109].

Inhibition of CaMKII

Similar conformational changes in the regulatory domain could be induced using a peptide based on the CaMKIIN sequence, a natural inhibitor of CaMKII [233,234]. Structural evidence, as highlighted in the structural alignment in Figure 5.5, predicts this to be the case. The trans-autophoshorylated kinase domain (green) features the R1 regulatory segment of a separate kinase domain (red) bound to its catalytic cleft (PDB 3KK8) [109]. Since these R1 residues are homologous to the AC-2 peptide, we assume AC-2 would bind in an analogous fashion. A crystal structure of the kinase domain (blue) bound to CaMKIIN inhibitor (magenta) is overlaid to demonstrate how binding of CaMKIIN is similar the R1 segment corresponding to AC-2 (PDB 3KL8) [109].

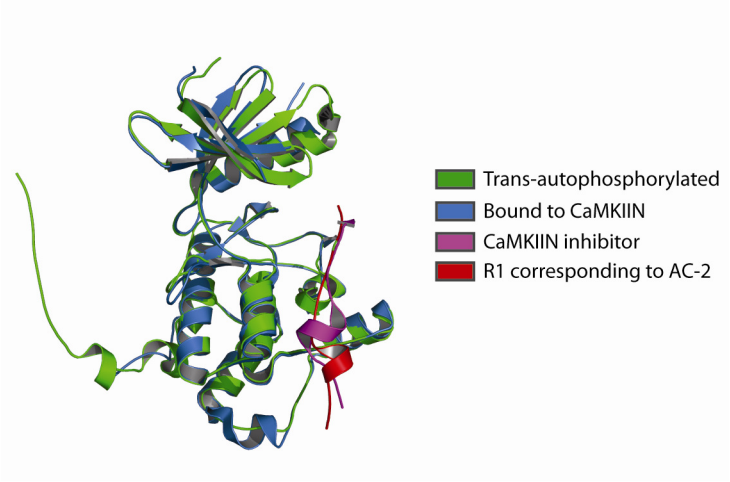

Figure 5.5 Structural alignment of trans-autophosphorylated kinase with CaMKIIN-bound kinase. Crystal structures reveal that CaMKIIN inhibitor binds similarly to the R1 regulatory segment.

The structures were interpreted to suggest CaMKIIN will block the capture of adjacent subunits' R1 elements to inhibit activity [109]. This notion is consistent with previous evidence demonstrating that CaMKIIN competes with autocamtide binding [235].

Additionally CaMKIIN contains a potential pseudosubstrate sequence, RVVIED, where the Ile position in CaMKII substrates is a phosphorylatable Ser or Thr residue. This peptide is poorly phosphorylated when Ile is mutated to Ser [234]. However, CaMKIIN has been shown to block Thr305 phosphorylation, but not trans-autophsophorylation at Thr286 [235]. This raises the conceptual question of how Thr286 becomes phosphorylated in the presence of CaMKIIN. Perhaps the unphosphorylated R1 segment, by proximity and affinity is a better competitor for the catalytic cleft. Once phosphorylated the R1 segment has lower affinity and is released, increasing the probability of inhibitor binding. Since CaMKIIN was found to inhibit autonomous activity but not Thr286 phosphorylation [236], it may occupy the catalytic cleft only after Thr286 phosphorylation is complete. Once bound, it acts as a nonphosphorylatable pseudosubstrate to prevent other substrates from binding. This hypothesis is consistent with our results revealing a higher apparent CaMKIIN affinity for protein containing the T286E phosphomimic (Figure 5.4).

Interestingly, our results demonstrate that in the absence of Thr286 phosphorylation, AC-2 and CaMKIIN are able to displace the R1 elements at low concentrations, presumably competing for T-site binding (Figure 5.6A). At only five fold molar excess of peptide to protein without the phosphomimic, sites in the R1 region show increases in mobility consistent with undocking, while the R3 equilibrium is maintained (Figure 5.6B). However, when CaMKIIN is added to protein containing the T286E phosphomimic, 5-fold excess peptide is sufficient to induce a significant increase in the undocked population of R3 (Figure 5.6B)

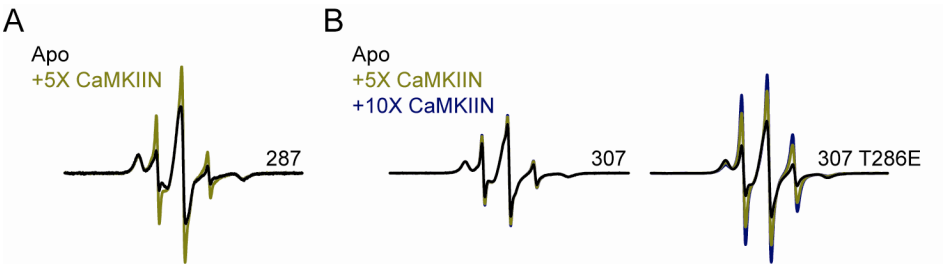

Figure 5.6 Concentration effects of CaMKIIN inhibitor on R1 and R3 regulatory elements. A) Five fold excess CaMKIIN peptide is sufficient to displace a significant portion of the R1 regulatory segment from association with the catalytic domain. B) Low concentrations of peptide are not sufficient to displace the R3 regulatory element in the absence of the T286E phosphorylation mimic.

These results suggest that high peptide concentrations or autophosphorylation at Thr286 are necessary for AC-2 or CaMKIIN competition with the R3 regulatory segment for catalytic cleft occupation. There may be mechanistic relevance for concentration dependent binding. For example, CaMKIIN has been shown to inhibit NR2B binding which requires T-site occupation [169,235,237]. Therefore at low concentrations the inhibitor may selectively inhibit phosphorylation of specific substrates which require T-site binding. The inhibitor has also been demonstrated to trap CaM [235], suggesting its binding releases the 291-295 trapping residues. In fact, the CaMKIINβ isoform, but not CaMKIINα, requires continuous presence of CaM to bind CaMKIIα [236]. This may suggest that CaM induced undocking of R3 is required for efficient CaMKIINα inhibition.

While grounded in analysis of solution dynamics under well defined biochemical conditions, the ultimate test of the veracity of our model awaits structural and dynamic analyses of the holoenzyme. This will be especially pertinent because crystals of monomeric human CaMKII bound to inhibitors (PDB 2VZ6, 3BHH, 2V7O, 2VN9) [108] suggest an interface between kinase domains different than the one originally observed (PDB 2BDW) [138]. Intersubunit communications predicted by cooperative CaM binding

and autophosphorylation have been observed by FRET studies of catalytic domain "pairs" which separate upon activation [190]. Given the strong amino acid sequence identity between catalytic/regulatory domains of the *C. elegans* protein studied here and the four mammalian CaMKII isoforms [96], it seems likely that the conformational dynamics defined here will represent core regulatory properties of all CaMKII isoforms. However, variable linker domains that couple catalytic/regulatory domains to the central "hub" of the dodecameric holoenzyme likely modify these dynamics in unique ways. For example, activation properties of CaMKIIβ holoenzymes are modulated by the length and sequence of the linker [107,116]. Elucidating the conformational dynamics associated with activation of various CaMKII holoenzymes is the next frontier in understanding CaMKII activation.

CHAPTER VI

FIELD PERSPECTIVES AND FUTURE DIRECTIONS

Introduction

CaMKII has been studied for decades and over the years the work of many groups has significantly contributed to the understanding of this enzyme. Historically, the contributions have been mainly biochemical in nature, revealing its role in complex functions but only deriving predictions of what the structural architecture might be. In the past few years however, the structural exploration of the protein has begun [108,109,112,138,155,156] and now the ground work has been laid for determining structure-function relationships. Fortuitously, the dynamic nature of CaMKII, its flexibility and large amplitude domain movements, makes it ideal for EPR studies. The effort summarized here represents the first phase of EPR studies of CaMKII structural dynamics. This work reveals significant insight into the activation mechanism and importantly, rationalizes a wealth of biochemical research. While this work advances the understanding of CaMKII activation mechanism, there are still many unanswered questions that can be investigated with EPR.

Continuing studies of conformational changes in the catalytic lobes in the monomer kinase domain

From the studies presented here, we suggest the catalytic N- and C-lobes may be undergoing a rotational twisting motion that coincides with the R3 docking-undocking

equilibrium. This hypothesis needs to be tested to determine what conformational changes are taking place. Although the sites chosen for the initial investigation, sites 20, 110, and 134, were believed to undergo the largest conformational changes based on the structures of active and inactive kinases, they did not unambiguously detect a conformational equilibrium in the apo state (refer to Figure 4.16). As suggested in the previous chapter, ATP binding may be inhibited by cysteine mutation and/or spin label attachment at site 134 in the conserved catalytic loop making it inappropriate for these experiments. Therefore, an alternative set of sites may be better suited. It may be more productive to triangulate sites 17, 93, and 111 since sites 17 and 93 experience the equilibrium and site 111 is largely static (Figure6.1).

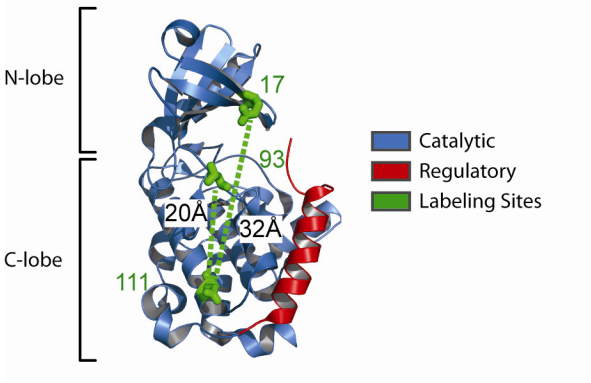

Figure 6.1 Labeling sites for DEER analysis of the catalytic domain. The CaMKIIδ isoform is illustrated with catalytic domain in blue, regulatory domain in red and labeling sites in green. The inter-residue distances are plotted in black.

Additionally, spin labels at sites 17 and 93 report conformational changes upon ATP binding, which has been shown to modulate the docking-undocking equilibrium of the R3 regulatory segment. Depending on the results of these experiments, there will likely be some trial and error in choosing additional sites to complete a set of data that confirms the twisting model.

Determining where the R3 segment is docking to the catalytic domain

Since the R3 regulatory segment is undergoing a conformational equilibrium between an undocked unstructured state and a docked state, it is unlikely that a crystal structure will capture the position of the regulatory domain. Therefore other types of experiments must be completed to determine the docked conformation. When designing initial experiments for DEER studies, the regulatory domain in its docked conformation was hypothesized to be positioned similarly to CaMKI. From sequence and structural comparisons of CaMKI with CaMKII, site 93 was expected to be in ~5 Å close proximity to site 307 of the R3 regulatory segment. However, spectral broadening in CW experiments of this double mutant was not detected and DEER analysis revealed a broad inter-probe distance centered at ~32 Å. Therefore, the regulatory domain is likely positioned somewhat differently in CaMKII. This leaves open the question of where the regulatory domain is docking. In order to decipher the position, several other sites should be investigated throughout the catalytic cleft and distances determined. An ensemble of data will be necessary to position the regulatory domain.

Conformational changes upon substrate binding

While EPR studies so far have been focused on regulation and activation of the enzyme, it is also of interest to understand the conformational changes that occur upon substrate binding. Studies of AC-2 give insight into the regulatory domain conformational changes when a substrate enters the active site of the protein. AC-2 is able to displace the R1 or R3 regulatory segments depending on its concentration and whether or not the phosphorylation mimic at site 286 is present (refer to Figure 5.4).

However, it is unknown whether or not other substrates employ the same mechanism. It would be interesting to investigate NR2B for example, which was shown to require T-site binding [238]. Therefore, we hypothesize the R1 regulatory segment must be released for NR2B binding. It is likely that this induces unfolding of the R1 segment, similar to AC-2 binding or Thr286 phosphorylation. Studies have shown that dephosphorylation of T286 is attenuated when NR2B is bound [239] and binding of CaMKII to NR2B enables it to remain autonomously active [169]. These evidences support the notion that R1 has an extended conformation upon NR2B binding, allowing a rapid 286 phosphorylation by a neighboring subunit. Since NR2B is a substrate, it must also contact the catalytic cleft for phospho transfer and may consequently cause undocking of the R3 regulatory segment as well. Interestingly, when NR2B binds to CaMKII, the affinity for the ATP analogue ATPγS increases by 11-fold [239] suggesting that the modification of the R3 equilibrium enables binding at the catalytic cleft. Additionally, NR2B has been shown to competitively inhibit CaMKII phosphorylation of AC-2, suggesting NR2B and AC-2 bind to CaMKII in a similar manner [220]. CaMKIIN has also been shown to compete with NR2B and AC-2, and our results show CaMKIIN and AC-2 induce similar conformational changes in the regulatory domain. We would therefore expect similar EPR results for NR2B. To investigate these possibilities, the monomer system would be best to insure saturated binding as NR2B binding to all subunits in the holoenzyme may not be sterically favored. Sites representative of the R1 and R3 segments, for example 287 and 307, would be ideal for monitoring undocking with mobility studies.

Syntide-2, a peptide substrate based on the glycogen synthase phosphorylation site, has not been shown to require T-site binding. Interestingly CaMKII phosphorylation

of this substrate is non-competitively inhibited by NR2B [220]. We hypothesized that syntide-2 would bind to the catalytic cleft and promote undocking of R3; however, preliminary EPR studies of syntide-2 binding did not show changes in the regulatory domain conformation, even under established phosphorylation conditions where the sample is incubated at 37˚C for 10 minutes [122]. It is currently unclear whether 1) this substrate is able to bind the D135N *C. elegans* CaMKII protein, 2) if syntide-2 has a high enough affinity to effectively compete with R3 for the catalytic cleft at the concentrations used (up to 40-fold excess), or 3) if binding of syntide-2 does not induce conformational changes in the regulatory domain. Because we obtained a negative result for several sites, the studies were abandoned but may warrant further investigation. Binding must be established first, and then conformational changes of the regulatory and/or catalytic domains can be investigated to determine the substrate's effect on the R3 equilibrium. Additionally, there are approximately 40 known substrates and counting as well as scaffolding partners, any of which could be investigated with mobility studies.

Comments on modeling of the R3 equilibrium

The ultimate goal of deciphering all the conformational changes of CaMKII is to have an atomic resolution model of each intermediate. This is inherently challenging due to difficulties in resolving flexible segments of the protein by crystallography and capturing the enzyme in all of its states. Although the cartoons of conformational changes depicted here are descriptive, they lack the resolution needed for future goals, such as rational drug design. While development of computational modeling with incorporation of EPR restraints is underway for Rosetta [211,240], there is an intrinsic

problem with modeling flexibility. Rosetta rotamers are based largely on fragments from high resolution crystal structures in which unstructured regions are not resolved. Therefore unfolded and flexible conformations are not sampled. The sampling can be skewed to select for random coil conformations but we found that because the R3 region has helical propensity, the resulting models rarely adopt an unstructured conformation. However, models of the structured docked conformation may be useful for generating hypotheses about where the regulatory domain is docked to the catalytic domain. It is possible in theory to model the flexibility and exchange between docked and undocked conformations with molecular dynamics simulations; however, the exchange is slow on the EPR timescale, on the order of 100 ns. This would require a considerable computational resource, but is possible for a monomer study. While currently it is difficult to model CaMKII's intermediates because of their disorder and slow scale dyanmics, these challenges present an opportunity for future programming development that can accommodate flexible proteins.

Validating mobility in the context of the holoenzyme

In the work presented here, monomer protein was used to avoid the complexities of studying the twelve subunit holoenzyme. As it has been shown previously, the kinase does not require the association domain or linker region to recognize and phosphorylate substrates [31]. Therefore we speculate that the conformational changes and dynamics observed in the monomer system will translate to the holoenzyme where association domains are intact. However, the monomer model proposed here has yet to be validated in the context of the holoenzyme. This is an essential next step. While preparing this

document, a new structure featuring the human CaMKIIβ oligomeric holoenzyme was determined (PDB 3SOA) [176]. This is the first higher resolution (4.0 Å) structure of the intact protein, although an inhibitor was bound to the catalytic cleft and some modifications were made (Figure 6.2). The enzyme was mutated to be inactive by K42M and D135N substitutions and also the Thr306 autophosphorylation site was converted to a valine. Additionally this construct has a shortened linker, which can be up to 50 additional amino acids in other isoforms. The crystallized protein was a hybrid consisting of the human alpha protein where the linker region is replaced with β7 linker.

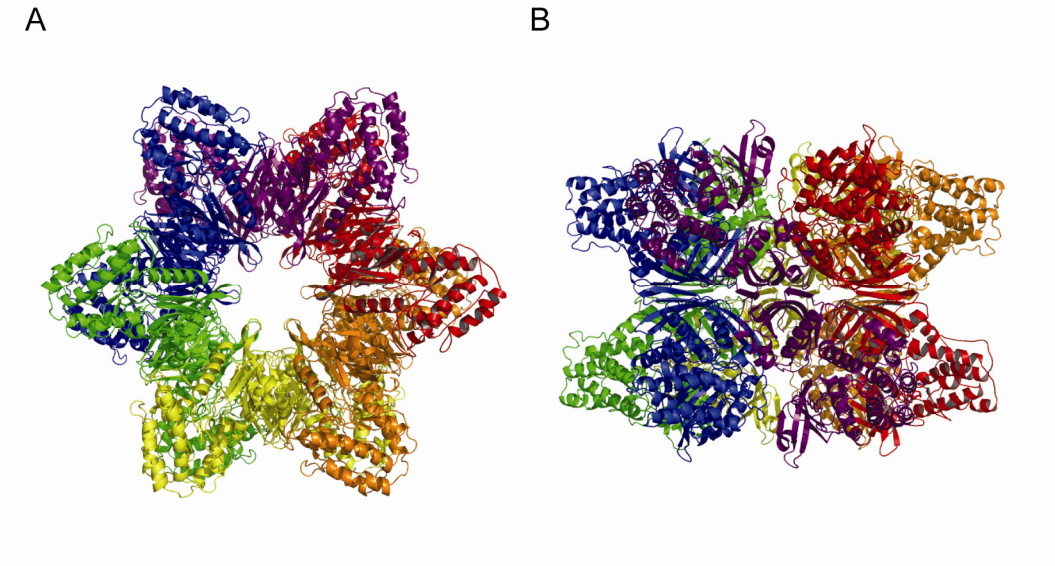

Figure 6.2 Crystal structure of the human CaMKIIβ holoenzyme. The structure is illustrated from the "top" (A) and "side" (B) views with expected dodecameric assembly (PDB 3SOA). Interacting pairs of domains, one from each ring, are colored similarly.

This structure will facilitate EPR studies in the holoenzyme by providing the spatial relationship between domains. Labeling sites can now be designed to account for spin-spin coupling between labels conjugated to different subunits. Additionally, with the advent of a bacterial holoenzyme expression solution [176], studies of the intact oligomer are potentially more straightforward assuming the method produces a sufficient protein

yield. For validation of the model, several sites initially investigated in monomer studies will have to be reexamined in the holoenzyme. Choosing the most informative sites to be representative is key. For example sites 287, 293, and 306, are good representatives for probing the R1 regulatory segment, the CaM trapping region, and the dynamic equilibrium of the R3 region.

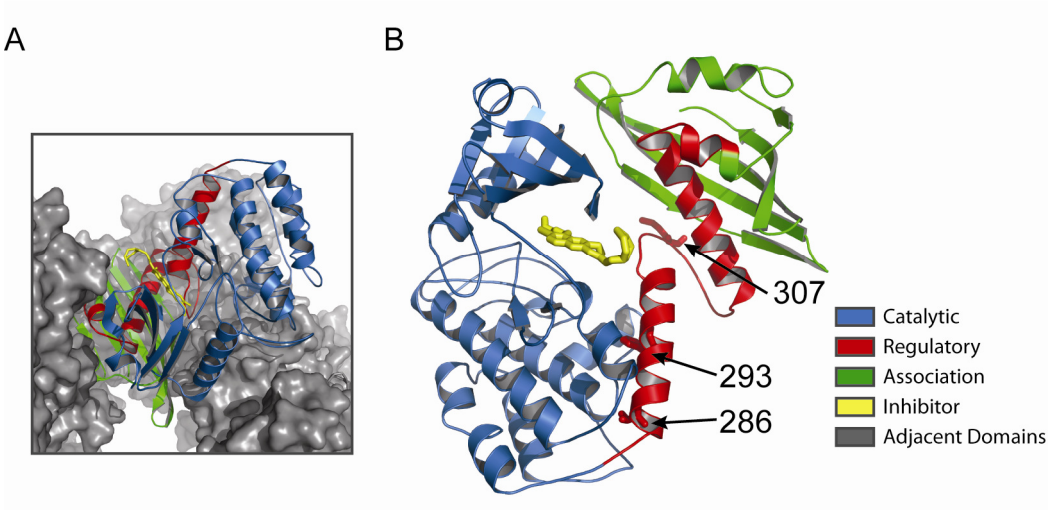

Figure 6.3 Crystal structure of isolated CaMKIIβ domain. A) The structure of one domain (ribbon outline) is highlighted in the context of adjacent domains (gray). B) The regulatory domain (red) adopts a helix loop helix conformation, making contacts with the association domain (green).

Interestingly, this structure reveals a novel conformation for the modeled regulatory domain, with the R3 segment in a loop conformation but not in contact with the catalytic domain as predicted by our model (Figure 6.3). However the conformation of the R3 segment may be confounded by the presence of the active site inhibitor, bosutinib [241,242]. One unexpected feature of this particular construct of CaMKII is the R3 regulatory domain contact with the association domain. The isoform crystallized lacks the extended linker region which is variable in sequence between various isoforms of CaMKII and can be as long as 50 additional amino acids (see Figure 1.3 for isoform diversity). The linker is the predominant difference between isoforms, as the kinase

domains share 95% sequence identity and association domains share 80% identity. Specifically, the *C. elegans* protein used in the studies presented here has 30 additional amino acids in the linker than the crystallized protein. This raises the question of how the presence of the linker region will affect the interaction between the regulatory and association domains. The authors speculate that since the region where the linker would be inserted is located on the surface of the protein, the linker could be readily accommodated without disrupting the interaction of R3 residues 304-308 with the association domain. It is difficult to conceptualize where and how the linker would be positioned without affecting this interaction observed in the crystal. In this aspect, the structure is not consistent with our model which places the R3 element in a dynamic equilibrium docking and undocking with the catalytic cleft. Since the association domain was not present in our studies, an R3-association domain interaction cannot account for the tertiary interactions evidenced by the immobilized component in the EPR lineshape observed for regulatory sites 304-308 (refer to Figure 4.2). Furthermore the regulatory-catalytic interactions are modulated by ATP binding in our model. This is difficult to reconcile with the R3 positioning in the structure, where it is not in contact with the catalytic cleft. It is unknown if this interaction exists in solution and whether or not crystallization and or inhibition of this construct have imposed this interaction. Therefore it is essential to confirm the R3 equilibrium exists in the context of the holoenzyme with mobility studies. Additionally, CW distance measurements on residues at the crystallographic R3-association domain interface could be measured to determine if this interface is stable in solution.

For mobility studies, the possibility of spin-spin coupling between labels on neighboring subunits must be considered. Although many interprobe distances will be outside of the detectable range for CW EPR, sites close to the ring-ring interface may have spectra which exhibit dipolar coupling. For example, site 309 of the regulatory domain is predicted to have an inter-residue distance of just 5 Å between neighboring subunits on adjacent rings. A 5 Å interprobe distance would result in extensive spectral broadening and would impede interpretation of the lineshape for mobility comparison with monomer data. Site 307, which is a good representative of the R3 regulatory segment, is predicted to be 18 Å and may or may not show spectral broadening depending on the orientation of the probes and how similar the solution structure is compared to the crystal structure. These sites must therefore be chosen with care. Other regulatory sites will be well beyond the ~20 Å CW EPR range for detection of dipolar coupling, evading this issue. Figure 6.4 shows an example of inter-residue distances for a hypothetical experiment with labels at site 293.

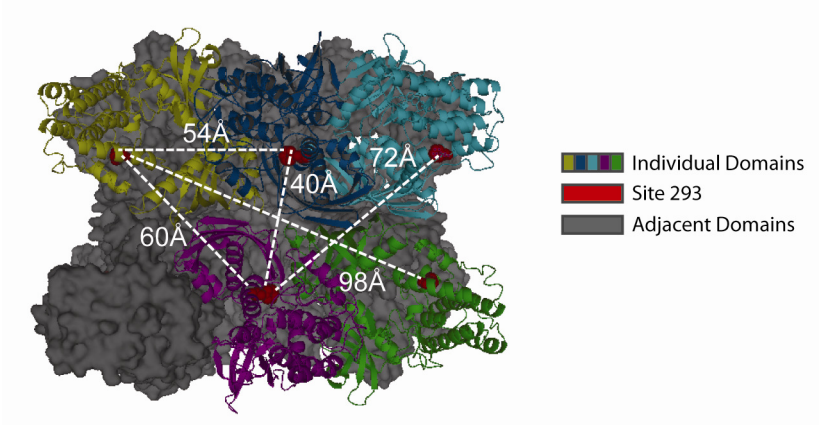

Figure 6.4 Inter-domain distances of CaMKII holoenzyme. The CaMKIIβ holoenzyme structure is depicted with five individual domains highlighted in gold, navy blue, cyan, purple, and green. The remaining adjacent domains are colored in gray and shown by surface representation. Site 293 is highlighted in red with inter-residue distances in white.

Five domains are colored individually to illustrate their positioning from the "side" view of the holoenzyme. In white are the inter-residue distances which are well beyond the dipolar coupling range for CW EPR (up to ~20 Å). Therefore, mobility for site 293 will not be masked by spectal broadening caused by dipolar coupling.

Conformational equilibrium between compact and extended holoenzyme states

Previous structural studies of CaMKII holoenzyme reveal two conformations; one cylindrical with catalytic domains protruding outward above and below the plane of the association domains and the other in a disk like conformation with catalytic and association domains residing in the same plane [112,138,155,156]. The difference in height is on the order of 150 Å and it has been hypothesized that the cylindrical and disk structures represent active and inactive conformations of CaMKII respectively. The disruption of contacts between regulatory and catalytic domains we observe combined with the lengthening of the regulatory domain may make this type of conformational change possible. The recent publication featuring the crystal structure of the holoenzyme predicts a dynamic equilibrium between a compact conformation of 100 Å height and an extended state with height of 150 Å in the apo autoinhibited state [176]. This implies at least a 50 Å change in height. The authors carried out SAXS analysis of various holoenzymes and argue that because the dimensions of the molecules agree with the crystal structure dimensions, the crystal structure likely represents a solution structure. When the length of the linker was varied, SAXS analysis resulted in observation of an extended conformation. From a kinetics computational model for CaMKII, the authors

purposed a dynamic equilibrium between compact and extended forms, the equilibrium of which is tunable by isoform.

This raises the question of whether or not their proposed equilibrium is concurrent with the docking-undocking R3 equilibrium we observe. Although there is no discussion of this concept in the manuscript perhaps due to the fact that the R3 region does not contact the catalytic domain in the structure, it remains a plausible hypothesis. One interesting aspect of their model is that the extended conformation of the protein is proposed to retain autoinhibitory interactions. If the proposed compact-extended equilibrium is a consequence of the R3 equilibrium we observe, then retention of autoinhibition is in line with our data where R1 is not is not perturbed in the apo state. Additionally, the compacted and extended equilibrium should be modified by the addition of ATP. Our model also predicts the regulatory domain will have increased flexibility when activated by CaM. We could therefore possibly observe a more extended conformation under this condition. It is not clear what conformational changes would occur following Thr286 phosphorylation. Since our model predicts that Thr286 phosphorylation does not affect the R3 equilibrium, it would be interesting to determine whether or not the compact-extended equilibrium is modified. Additionally, since Thr305 and Thr306 autophosphorylation sites are predicted to be in contact with the association domain even with an extended linker present in their model, it would be necessary to confirm that phosphorylation of these sites does not perturb the equilibrium. In our monomer system, phosphomimics at these sites slightly alter tertiary interactions, but do not significantly affect the R3 equilibrium. Finally their analysis also discovered that various isoforms may have preferences for either the compact or extended

conformations. If these equilibria are indeed able to be observed with EPR, it would be interesting to compare isoform differences and determine if there is any correlation to activity.

Initially, it is not clear if the predicted conformational exchange will be easily observed with EPR studies. When considering using EPR to monitor this kind of change, the sites must be chosen with care as the limit on DEER distance measurements is ~70 Å. Additionally since there are twelve subunits that have the potential for interprobe spin-spin coupling, multiple distances corresponding to both the compact and extended conformations will be detected. Holoenzyme domain arrangement is symmetric and domains are large enough that a label will likely have detectable dipolar coupling potential only with two adjacent neighbors resulting in three interprobe distances. To explain the complexities of these experiments, it is helpful to consider specific examples.

Several sites in the regulatory domain are in relatively close proximity with interdomain residue distances around 30-60 Å, a readily detectable range for DEER experiments. Site 293 for instance, illustrated in Figure 6.4, exhibits detectable inter-residue distances of 54 Å between subunits of the same ring and 40 and 60 Å between rings. Distances between other subunits are too far to be detected by DEER. If the structure indeed represents the compact conformation we would expect to detect these three distances in a DEER experiment of apo protein. If distances distributions are broad, resolution may be an issue. The extended conformation however is unknown. It may also produce multiple distances confounding observation of the compact conformation. Alternatively, the extended conformation may place labels outside the detectable spin-spin coupling range and which would diminish the DEER signals. This expected

negative result, while it does indicate lack of spin-spin coupling, is hardly an ideal observable. It is also unknown if the spatial relationship between subunits within the same ring changes in the extended conformation.

Shorter distances between probes near the ring interface may be more straightforward to monitor with EPR. For example site 220 of the catalytic domain is predicted to have an inter-residue distance of ~20 Å in the compact state (Figure 6.5A). The extended state will hypothetically produce a larger interprobe distance which can likely be monitored with DEER experiments.

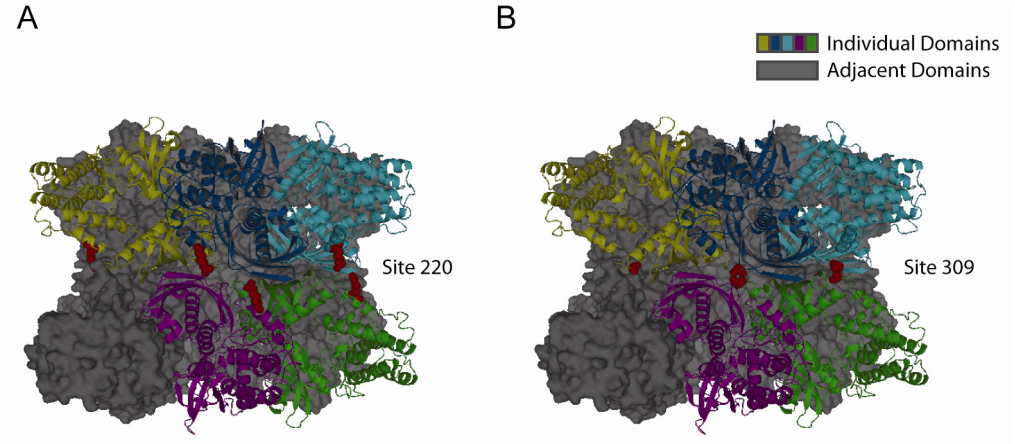

Figure 6.5 Position of residues in the holoenzyme. A) Site 220 is predicted to be ~20 Å from its nearest neighbor while B) site 309 is ~5 Å, well within the range for CW EPR.

Sites less than 20 Å, such as site 309, can also be observed with CW spectral broadening (Figure 6.5B show proximity of sites). In this case if the extended state is above 20 Å, the resultant spectrum will consist of a broadened population and an unbroadened population which reflects the sum of singles. In this manner, it may be possible to delineate what percentage is in each conformation. If ATP increases the population of the extended conformation, it may be possible to assign specific distances to the extended and compact states.

To understand the proposed conformational exchange between compact and extended forms, a bit of trial and error will be required to find the residues that best describe conformational changes. Distances must be well resolved and undergo conformational changes within a detectable range. While the holoenzyme structure provides a spatial understanding of the position of residues, subtle differences may exist in solution and between isoforms. Studies of this nature will provide insight on the apo state equilibrium as well as what conformation the holoenzyme adopts under activated conditions. Additionally, differences between isoforms that underlie the mechanism by which frequency is decoded may provide evidence to relate structure to function. There is still much to understand about how the holoenzyme structure facilitates the function of CaMKII. Investigation of the oligomer structure is at the forefront of the next frontier in CaMKII exploration.

An important aspect of defining the structures and dynamics of the biochemical intermediates is to aid in the rational drug design of inhibitors as inhibition has been shown to be a promising therapeutic strategy for diseases such as cardiac disease [75]. However, since CaMKII is implicated in many physiological processes, it is advantageous to selectively inhibit particular forms of CaMKII at specific times and places for precise regulation. The goal is therefore to rationally design CaMKII inhibitors which specifically inhibit particular intermediates associated with various states of activation, specific substrates, as well as subcellular localization. For example, the CaMKIIN inhibitor has been shown to interfere with many regulatory mechanisms involving specific intermediates including translocation, localization, and autophosphorylation [161,171]. Because it competes with NR2B binding [235,243] and

activity [233,234,235,243] as well as Thr305/Thr306 autophosphorylation [235], scientists are currently working toward increasing the selectivity of this inhibitor [244]. With a complete picture of each intermediate, inhibitors, via their amino acid composition and their localization, can be modified to have increased affinity for particular intermediates and particular isoforms. Inhibitor design relies on the available structural knowledge of the target and the work presented in this document has contributed to an understanding of the dynamics and indentified equilibria for several of CaMKII which were not previously known. These findings have allowed us to form a more accurate and complete understand of CaMKII activity and have also laid the groundwork for further exploration of additional intermediates, intermediates in the context of the holoenzyme supramolecular structure, and interactions with protein binding partners.

APPENDIX A

				Growth			Induction				
	Protein	Vector	Cell Type	Temp	Speed	OD	Type	Time	Temp	Speed	Result
1	CaMKIIα Full length	pET28b+	BL21 (DE3)	37	250	0.8	1 mM IPTG	5 hr	37	250	Truncated
2	CaMKIIα Full length	pET28b+	BL21 (DE3)	37	250	0.8	1 mM IPTG	4 hr	32	200	Truncated
3	CaMKIIα Full length	pET28b+	BL21 (DE3)	37	250	0.8	1 mM IPTG	5	18	250	Truncated
4	CaMKIIα Full length	pET28b+	BL21 (DE3)	37	250	1	1 mM IPTG	12 hr	18	200	Truncated
5	CaMKIIα Full length	pET28b+	BL21 (DE3)	32	250	N/A	Autoinduction	4 hr	32	200	Truncated
6	CaMKIIα Full length	pET28b+	BL21 (DE3)	18	250	N/A	Autoinduction	18	18	250	Truncated
7	CaMKIIα Full length	pET28b+	Rosetta 2	37	250	0.8	1 mM IPTG	4 hr	37	250	Truncated
8	CaMKIIα Full length	pET28b+	Rosetta 2	37	250	0.8	1 mM IPTG	4 hr	32	250	Truncated
9	CaMKIIα Full length	pET28b+	Rosetta 2	37	250	0.8	0.4 mM IPTG	4 hr	32	200	Truncated
10	CaMKIIα Full length	pET28b+	Rosetta 2	37	250	0.8	1 mM IPTG	5 hr	18	250	Truncated
11	CaMKIIα Full length	pET28b+	Rosetta 2	32	250	N/A	Autoinduction	4 hr	32	200	Truncated
12	CaMKIIα Full length	pET28b+	Rosetta 2	18	250	N/A	Autoinduction	18	18	250	Truncated
13	CaMKIIα Full length	pET21a	BL21 (DE3)	37	250	0.8	1 mM IPTG	4 hr	32	200	Truncated
14	CaMKIIα Full length	pET21a	BL21 (DE3)	32	250	N/A	Autoinduction	4 hr	32	200	Truncated
15	CaMKIIα Full length	pET21a	BL21 (DE3)	37	250	0.8	1 mM IPTG	5	18	250	Truncated
16	CaMKIIα Full length	pET21a	BL21 (DE3)	18	250	N/A	Autoinduction	18	18	250	Truncated
17	CaMKIIα Full length	pET21a	Rosetta 2	37	250	0.8	0.4 mM IPTG	4 hr	32	200	Truncated
18	CaMKIIα Full length	pET21a	Rosetta 2	32	250	N/A	Autoinduction	4 hr	32	200	Truncated
19	CaMKIIα 316 D135N	pET21a	Rosetta 2	37	250	0.8	1 mM IPTG	4 hr	37	250	Truncated
20	CaMKIIα 316 D135N	pET21a	Rosetta 2	32	250	N/A	Autoinduction	18	32	330	Truncated
21	CaMKIIα 340 D135N	pET21a	Rosetta 2	37	250	0.8	1 mM IPTG	4 hr	37	250	Truncated
22	CaMKIIα 340 D135N	pET21a	Rosetta 2	32	250	N/A	Autoinduction	18	32	330	Truncated
23	CaMKIIα 340 D135N	pET28b+	PR 1031	32	250	N/A	Autoinduction	18	32	330	No Expression
24	CaMKIIα 340 D135N	pET28b+	UT 5600	32	250	N/A	Autoinduction	18	32	330	No Expression
25	CaMKIIα 340 D135N	pET28b+	KS 1000	32	250	N/A	Autoinduction	18	32	330	No Expression
26	CaMKIIα 340 D135N	pET21a	PR 1031	32	250	N/A	Autoinduction	18	32	330	No Expression
27	CaMKIIα 340 D135N	pET21a	UT 5600	32	250	N/A	Autoinduction	18	32	330	No Expression
28	CaMKIIα 340 D135N	pET21a	KS 1000	32	250	N/A	Autoinduction	18	32	330	No Expression
29	CaMKIIα 380 D135N	pET21a	Rosetta 2	37	250	0.8	1 mM IPTG	4 hr	37	250	Truncated
30	CaMKIIα 380 D135N	pET21a	Rosetta 2	32	250	N/A	Autoinduction	18	32	330	Truncated
31	CaMKIIα 420 D135N	pET21a	Rosetta 2	37	250	0.8	1 mM IPTG	4 hr	37	250	Truncated
32	CaMKIIα 420 D135N	pET21a	Rosetta 2	32	250	N/A	Autoinduction	18	32	330	Truncated

Supplementary Table 1 Mouse CaMKIIα expression trials

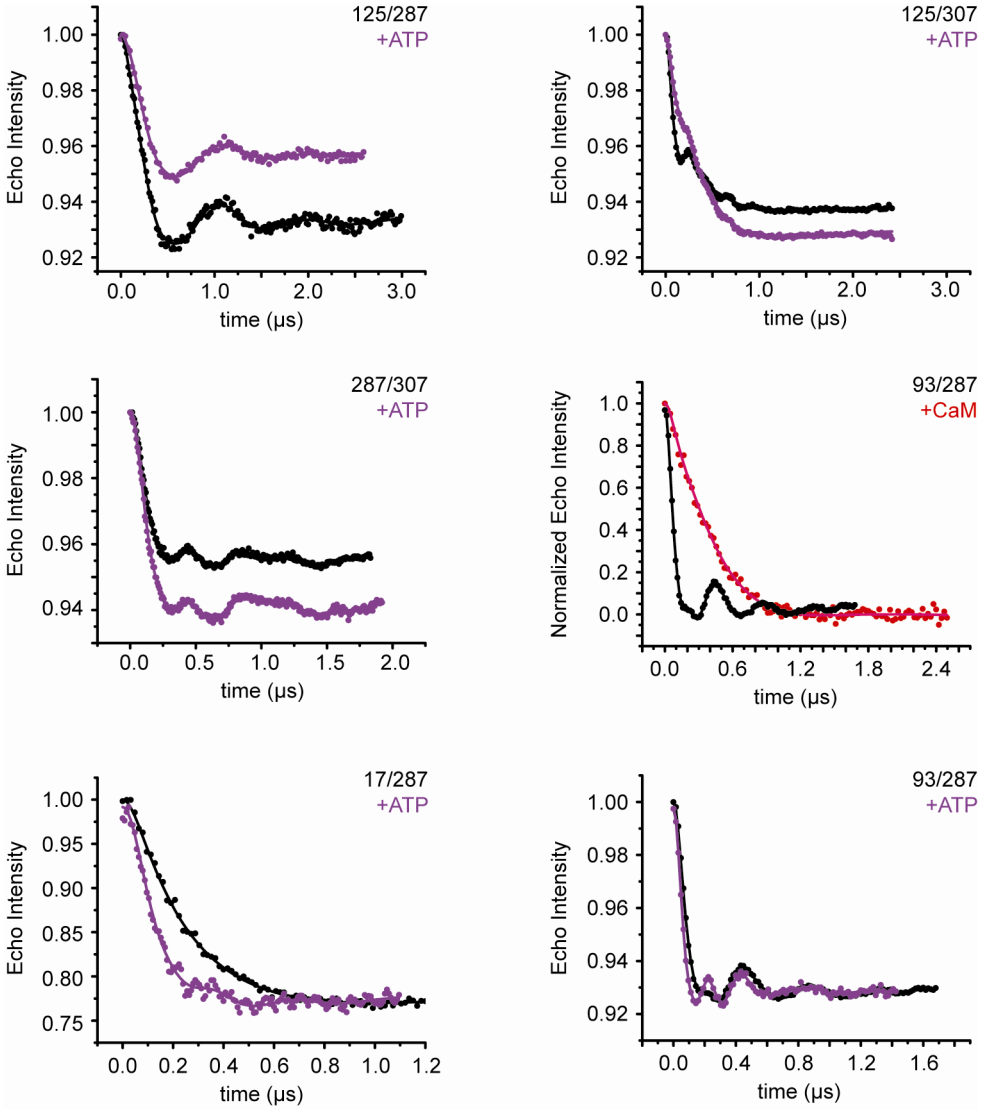

Supplementary Figure 1 Raw DEER data.

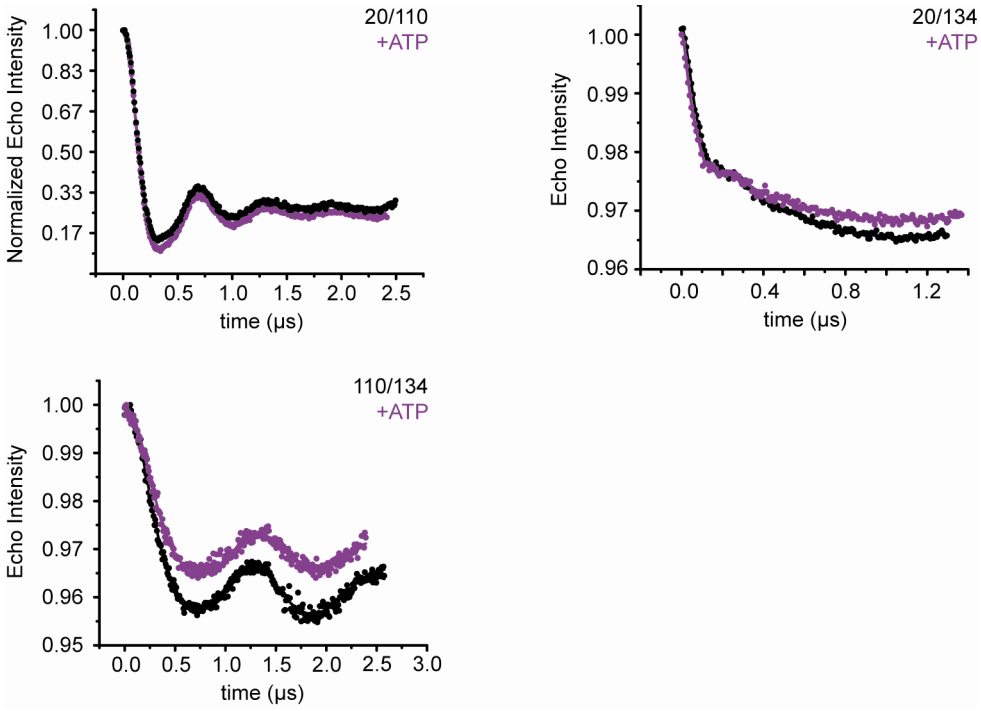

Supplementary Figure 2 Raw DEER data continued.

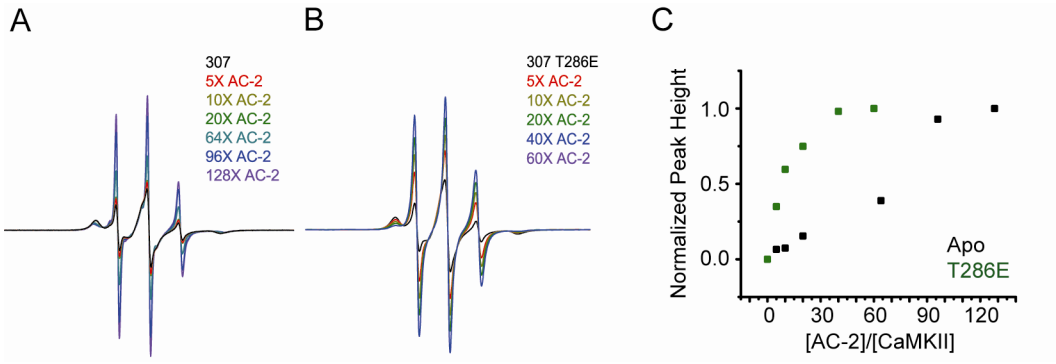

Supplementary Figure 3 Titrations of AC-2. Spectra for site 307 in the presence of varying concentrations of AC-2 are overlaid for the A) apo and B) T286E phosphomimicked proteins. C) The normalized high field peak height is plotted as a function of [AC-2]/[CaMKII] to illustrate that the T286E protein (green) has a higher apparent affinity for AC-2 than the apo protein (black).

APPENDIX B

SUPPLEMENTARY METHODS

CaMKII expression, purification, and labeling

C. elegans CaMKII (unc-43) cDNA derived from the splice variant K11E8.d with codons representing residues 1-340 and an N-terminal 10 histidine sequence was cloned into the pET28b vector controlled by the T7 promoter. All mutants were introduced using a modified Quikchange protocol and verified with DNA sequencing. A D135N inactivating mutant was introduced to prevent heterogeneous autophosphorylation during expression [138]. Native cysteines were replaced with residues found in homologs or with alanine; C30A, C64L, C115A, C126I, C199A, C272A, and C289A. Protein expression was carried out in *E. coli* BL21(DE3) as described previously except for a 16 hour induction protocol [138]. Harvested cell pellets were resuspended in buffer containing 50 mM HEPES, 150 mM NaCl, 10 mM imidazole, 1 mM DTT, 0.1 mM PMSF, 10% (vol/vol) glycerol, pH8 and lysed by sonication. CaMKII was purified from the lysate supernatant by Ni^{2+} affinity chromatography (Qiagen) by washing with 30 mM imidazole then eluting with 250 mM imidazole. Upon elution, a 20-fold excess of (1-oxyl-2,2,5,5-tetramethylpyrrolinyl-3-methyl)-methanethiosulfonate spin label (MTSSL; Toronto Research Chemicals, Inc) was added and the mixture incubated on ice for at least 15 hours. Labeled CaMKII was further purified by size exclusion chromatography on a Superdex 75 column (GE Healthcare) in 50 mM HEPES, 100 mM NaCl, 2.5 mM EDTA, 0.02% azide, pH 7.5. For these studies, the N-terminal His tag was not cleaved. Spin labeled CaMKII mutants were washed 3 times immediately before experiments with the

same buffer to remove residual free spin label. Protein concentration was determined using a calculated extinction coefficient of 1.065 M^{-1} cm^{-1} at 280 nm.

The WT holenzyme and monomeric 1-380 truncation mutant of mouse CaMKIIα were expressed in Sf9 cells and purified in the Colbran laboratory as described previously [163].

SDS-PAGE and western blot analysis

SDS-PAGE was carried out for protein expression and purity assessment as well as for cosedimentation assays. All proteins were boiled and loaded onto a 12% SDS polyacrylamide gel with bromphenyl blue loading buffer. Gels were run at 70 volts for 10 minutes through stacking and at 170 volts for 1 hour through the separating gel. Gels not undergoing western blot analysis were stained with coomassie blue stain.

For western blots, gels were transferred onto a nitrocellulose at 25 volts for 25 minutes in a BioRad Semi Dry Transfer Apparatus in transfer buffer (1 part 10X Tris-glycine, 4 parts methanol, 5 parts H_2O). Membranes were rinsed in deionized water then stained with ponceau until protein bands were visible for an analysis of total protein. For immunoblotting, membranes were blocked in TTBS buffer (50 mM Tris-HCl pH 7.5, 0.1% (v/v) Tween-20, 150 mM NaCl) containing 5% milk powder (Carnation nonfat milk) for 1 hour. Then membranes were incubated with goat anti-CaMKIIα polyclonal primary antibody (purified in Colbran laboratory) diluted into TTBS with 5% milk for 2 hours at room temperature. After 5 washes with TTBS, membranes were incubated for 1 hour at room temperature with rabbit anti-goat secondary antibody conjugated to alkaline phosphatases (Jackson ImmunoResearch). Following another 5 washes in TTBS,

membranes were developed in development buffer with 1 part BCIP and 2 parts NBT. The reaction was stopped by washing with 1X TTBS and proteins were imaged by chemiluminescence on a BioRad Gel Doc EZ apparatus.

Calmodulin expression and purification

Calmodulin was cloned into pET3a containing a T7 promoter and expressed in *E. coli* BL21(DE3) cells. Protein expression was induced with 0.4 mM IPTG and incubated at 30° and 250 rpm for 3 hours. Harvested cell pellets were resuspended in 50 mM MOPS, 100 mM KCl, 1 mM EDTA, 1 mM DTT, 0.1 mM PMSF, pH 7.5 and lysed by sonication. 5 mM $CaCl_2$ was added to lysis supernatant and loaded on a High Trap Phenyl HP column (GE Healthcare) with 50 mM Tris-HCl, 1 mM $CaCl_2$, pH 7.5. The protein was washed with 50 mM Tris-HCl, 1 mM $CaCl_2$, 0.5 M NaCl, pH7.5 and eluted with 10 mM Tris-HCl, 10 mM EDTA, pH7.5. Purified protein was then desalted into 50 mM HEPES, 100 mM NaCl, 2.5 mM EDTA, 0.02% azide, pH 7.5.

Activity assays

Specific kinase activities were determined as previously described[122] except for the buffer conditions which matched those of the EPR analysis. Activity was determined by the protein's ability to incorporate a radioactive gamma phosphate from [γ^{32}P]ATP onto either syntide-2 (PLARTLSVAGLPGKK), a synthetic peptide based on a glycogen synthase phosphorylation site, or autocamtide-2 (KKALRRQETVDAL), a peptide based on the CaMKII regulatory domain. Assays were carried out under the following conditions: 50 mM HEPES, 100 mM NaCl, 0.4 mM [γ^{32}P]ATP, 10 mM $Mg(Ac)_2$, 1 μM

CaM, 0.5 mM $CaCl_2$, 20 μM syntide-2 or 10 μM autocamtide-2, 1 mM DTT, 1 mg/mL BSA. The level of radioactive gamma phosphate was normalized relative to control samples where buffer was added instead of CaMKII.

Circular dichroism

Spectra were collected on a Jasco J-810 Spectropolarimeter in 20 mM phosphate buffer, pH 7.1. Near UV spectra (330-250 nm) were obtained using a 0.5 mg/mL protein solution at room temperature. Far UV spectra (260-185 nm) were collected at room temperature using a 0.1 mg/mL protein solution. Melting curves were obtained using 0.15 mg/mL protein solution by monitoring ellipticity at 222 nm in a temperature range between 5-95°C at a temperature slope of 60°C/hour.

Light Scattering

Molecular weight was determined by MultiAngle Laser Light Scattering (Dawn Heleos 8, Wyatt Tech) at 658 nm wavelength in tandem with size exclusion chromatography on a Superdex 75 column (GE Biosciences) equilibrated in buffer (50 mM HEPES, 100 mM NaCl, 2.5 mM EDTA, 0.02% azide, pH 7.5). Data was analyzed by Astra software package (Wyatt Tech.) and injected protein mass was estimated from refractive index detector (Agilent) assuming dn/dc to be constant 0.19. The instrument was calibrated for BSA (Sigma).

Mass Spec Analysis

Coomassie stained bands for SDS-PAGE were excised and cut into 1mm cubes and incubated in 100 mM Amic for 15 minutes. Reduction and alkylation took place by first incubating in 10 mM Amic and 100 mM DTT for 15 minutes at 50°C. To carbamidomethylate cysteines, 30 mM iodoacetamide was added to the solution and incubated at RT for 15 mins in the dark. Dehydration was completed by removing the liquid and adding a 1:1 mixture of ACN and Ambic and incubating until coomassie was removed. Then the gel was incubated with 100% ACN for 10 mins and desiccated in a speed vac. Proteins were digested with 0.01 mg/mL trypsin in 25 mM ammonium bicarbonate for 2 hours at 37°C. Peptides were extracted slices with 15-25 μL of ACN:H2O (60:40) with 0.1% formic acid then dried in a speed vac. Samples were reconstituted in in 50 μL of 2% ACN in H_2O with 0.1% formic acid and analyzed with LC-MS for sequence coverage and phosphorylation modification.

CaM Association and Dissociation Titrations

For binding experiments, the concentration of CaM was varied while CaMKII concentration was kept constant. The titration took place in 125-fold excess saturating $CaCl_2$. EPR spectra were obtained, normalized, and peak heights were determined for the mobile component of the lowfield spectral peak. These heights were then plotted against the [CaM]/[CaMKII] ratio. Dissociation experiments were completed in saturating CaM (6X) and $CaCl_2$ (25X) while EGTA concentration was varied. Peak heights were similarly determined and plotted against the [EGTA]/[$CaCl_2$] ratio. All plots were fitted using Prism software (GraphPad v. 4.0b).

Cosedimentation Assays

Binding reactions were carried out for 2 hours at 4 °C with the following reagents; 10 mM Tris HCl, 200 nM CaMKII, 5 mM $CaCl_2$ or 5 mM EGTA, 2 mM $Mg(CH_3COO)_2$, 200 mM NaCl, a 50/50 slurry of CaM-equilibrated agarose, pH 7.5. After incubation, resin was separated by centrifugation and supernatant was removed. Resin was then washed 5 times with buffer containing the same reagents except for CaMKII and resin. Protein complexes bound to resin were denatured by boiling and were then run on a 12% SDS gel and analyzed with coomassie staining.

EPR spectroscopy

EPR spectra were collected at room temperature on a Bruker EMX spectrometer (X-band) at an incident power of 10 mW and 1.6 gauss modulation amplitude. Samples contained 50 μM CaMKII unless otherwise stated and all binding molecules were added in excess; 300 μM CaM/10 mM $CaCl_2$ and/or 10 mM ATP/10 mM $Mg(CH_3COO)_2$. All proteins and reagents were prepared in the same buffer used for EPR experiments: 50 mM HEPES, 100 mM NaCl, 2.5 mM EDTA, 0.02% azide, pH 7.5.

CW Distance determinations

Dipolar coupling between spin labels was analyzed by using a modification of the deconvolution method [206]. This approach requires both the dipolar broadened spectra and unbroadened reference spectra. The unbroadened spectrum is obtained by measuring the spectrum for each mutant individually followed by digital sum of the two spectra, termed the sum of singles. The sum of singles spectra is convoluted with a broadening

function, which is a sum of Pake patterns weighted by a distribution of the distance between the two spin labels. The distribution is modeled as a sum of gaussians and the number of gaussians, up to 5, is chosen based on a statistical improvement in the fit of the broadened spectra with the experimental spectra of the double mutant [245].

DEER Distance determinations

Distance measurements were carried out on a Bruker 580 pulsed EPR spectrometer operating at either X-band or Q-band frequency using double electron electron resonance (DEER) with a standard four-pulse protocol. Glycerol was added to 30% (w/w) to all samples before freezing to 83K. Final protein concentrations were in the range of 75-150 μM. DEER signals were analyzed either by Tikhonov regularization or multiple Gaussian peak picking to yield the distance distributions.

Simulations for spectral lineshape analysis

Spectra were fit using the microscopic order/ macroscopic disorder (MOMD) model [202]. For the two component fits, the motion of one component was assumed to be effectively isotropic ($R_x = R_y = R_z$). The motion of the second component is assumed to undergo anisotropic rotation ($R_x \neq R_y \neq R_z$) within an ordering potential. The rotational correlation time, τ, for the motion is obtained from the R's: $\tau = 1/(6 (R_x + R_y + R_z)^{1/3})$. The uncertainty in the correlation time of the isotropic component is around 15% [201]. While the uncertainty is somewhat larger for the restricted component correlation time, the differences in the spectral lineshape demonstrates that difference between the two correlation times are outside the uncertainty intervals. The restriction in motion is

described by an order parameter, S, calculated from the coefficient, c_{20}, used to describe the ordering potential. In addition to the ordering potential, the axis of the nitroxide was allowed not to be co-linear with respect to the diffusion axis and this tilt is given by the angles (α_D, β_D).

REFERENCES

1. Lisman J, Schulman H, Cline H (2002) The molecular basis of CaMKII function in synaptic and behavioural memory. Nature Reviews Neuroscience 3: 175-190.
2. Cooke SF, Bliss TV (2006) Plasticity in the human central nervous system. Brain 129: 1659-1673.
3. Massey PV, Bashir ZI (2007) Long-term depression: multiple forms and implications for brain function. Trends Neurosci 30: 176-184.
4. Bliss TV, Collingridge GL (1993) A synaptic model of memory: long-term potentiation in the hippocampus. Nature 361: 31-39.
5. Malenka RC, Bear MF (2004) LTP and LTD: an embarrassment of riches. Neuron 44: 5-21.
6. Soderling TR, Stull JT (2001) Structure and regulation of calcium/calmodulin-dependent protein kinases. Chem Rev 101: 2341-2352.
7. Swulius MT, Waxham MN (2008) Ca(2+)/Calmodulin-dependent Protein Kinases. Cell Mol Life Sci.
8. Bayley PM, Findlay WA, Martin SR (1996) Target recognition by calmodulin: dissecting the kinetics and affinity of interaction using short peptide sequences. Protein Sci 5: 1215-1228.
9. Gaertner TR, Putkey JA, Waxham MN (2004) RC3/Neurogranin and Ca2+/calmodulin-dependent protein kinase II produce opposing effects on the affinity of calmodulin for calcium. J Biol Chem 279: 39374-39382.
10. Peersen OB, Madsen TS, Falke JJ (1997) Intermolecular tuning of calmodulin by target peptides and proteins: differential effects on Ca2+ binding and implications for kinase activation. Protein Sci 6: 794-807.
11. Sheng M, Hoogenraad CC (2007) The postsynaptic architecture of excitatory synapses: a more quantitative view. Annu Rev Biochem 76: 823-847.
12. Ally S, Jolly AL, Gelfand VI (2008) Motor-cargo release: CaMKII as a traffic cop. Nat Cell Biol 10: 3-5.
13. Lu W, Isozaki K, Roche KW, Nicoll RA (2011) Synaptic targeting of AMPA receptors is regulated by a CaMKII site in the first intracellular loop of GluA1. Proc Natl Acad Sci U S A 107: 22266-22271.
14. Colbran RJ, Brown AM (2004) Calcium/calmodulin-dependent protein kinase II and synaptic plasticity. Curr Opin Neurobiol 14: 318-327.
15. Elgersma Y, Sweatt JD, Giese KP (2004) Mouse genetic approaches to investigating calcium/calmodulin-dependent protein kinase II function in plasticity and cognition. J Neurosci 24: 8410-8415.
16. Schulman H (2004) Activity-dependent regulation of calcium/calmodulin-dependent protein kinase II localization. J Neurosci 24: 8399-8403.
17. Griffith LC (2004) Regulation of calcium/calmodulin-dependent protein kinase II activation by intramolecular and intermolecular interactions. J Neurosci 24: 8394-8398.
18. Elgersma Y, Fedorov NB, Ikonen S, Choi ES, Elgersma M, et al. (2002) Inhibitory autophosphorylation of CaMKII controls PSD association, plasticity, and learning. Neuron 36: 493-505.

19. Hansel C, de Jeu M, Belmeguenai A, Houtman SH, Buitendijk GH, et al. (2006) alphaCaMKII Is essential for cerebellar LTD and motor learning. Neuron 51: 835-843.
20. Weeber EJ, Jiang YH, Elgersma Y, Varga AW, Carrasquillo Y, et al. (2003) Derangements of hippocampal calcium/calmodulin-dependent protein kinase II in a mouse model for Angelman mental retardation syndrome. J Neurosci 23: 2634-2644.
21. van Woerden GM, Harris KD, Hojjati MR, Gustin RM, Qiu S, et al. (2007) Rescue of neurological deficits in a mouse model for Angelman syndrome by reduction of alphaCaMKII inhibitory phosphorylation. Nat Neurosci 10: 280-282.
22. Brown AM, Deutch AY, Colbran RJ (2005) Dopamine depletion alters phosphorylation of striatal proteins in a model of Parkinsonism. Eur J Neurosci 22: 247-256.
23. Picconi B, Gardoni F, Centonze D, Mauceri D, Cenci MA, et al. (2004) Abnormal Ca2+-calmodulin-dependent protein kinase II function mediates synaptic and motor deficits in experimental parkinsonism. J Neurosci 24: 5283-5291.
24. Bonanno G, Giambelli R, Raiteri L, Tiraboschi E, Zappettini S, et al. (2005) Chronic antidepressants reduce depolarization-evoked glutamate release and protein interactions favoring formation of SNARE complex in hippocampus. J Neurosci 25: 3270-3279.
25. Celano E, Tiraboschi E, Consogno E, D'Urso G, Mbakop MP, et al. (2003) Selective regulation of presynaptic calcium/calmodulin-dependent protein kinase II by psychotropic drugs. Biol Psychiatry 53: 442-449.
26. Tiraboschi E, Giambelli R, D'Urso G, Galietta A, Barbon A, et al. (2004) Antidepressants activate CaMKII in neuron cell body by Thr286 phosphorylation. Neuroreport 15: 2393-2396.
27. Anderson SM, Famous KR, Sadri-Vakili G, Kumaresan V, Schmidt HD, et al. (2008) CaMKII: a biochemical bridge linking accumbens dopamine and glutamate systems in cocaine seeking. Nat Neurosci.
28. Hudmon A, Schulman H (2002) Neuronal CA2+/calmodulin-dependent protein kinase II: the role of structure and autoregulation in cellular function. Annual Review of Biochemistry 71: 473-510.
29. Colbran RJ (2004) Targeting of calcium/calmodulin-dependent protein kinase II. Biochem J 378: 1-16.
30. Hudmon A, Schulman H (2002) Structure-function of the multifunctional Ca2+/calmodulin-dependent protein kinase II. Biochemical Journal 364: 593-611.
31. Robison AJ, Bass MA, Jiao Y, MacMillan LB, Carmody LC, et al. (2005) Multivalent interactions of calcium/calmodulin-dependent protein kinase II with the postsynaptic density proteins NR2B, densin-180, and alpha-actinin-2. J Biol Chem 280: 35329-35336.
32. Cooper NG, Laabich A, Fan W, Wang X (2008) The relationship between neurotrophic factors and CaMKII in the death and survival of retinal ganglion cells. Prog Brain Res 173: 521-540.
33. Choi DW (1987) Ionic dependence of glutamate neurotoxicity. J Neurosci 7: 369-379.

34. Lucas DR, Newhouse JP (1957) The toxic effect of sodium L-glutamate on the inner layers of the retina. AMA Arch Ophthalmol 58: 193-201.
35. Saido TC, Sorimachi H, Suzuki K (1994) Calpain: new perspectives in molecular diversity and physiological-pathological involvement. FASEB J 8: 814-822.
36. Chaum E (2003) Retinal neuroprotection by growth factors: a mechanistic perspective. J Cell Biochem 88: 57-75.
37. Fan W, Li, X., Cooper, N. G. F (2007) CaMKIIαB mediates a survival response in retinal ganglion cells subjected to a glutamate stimulus. Invest Ophthalmol Vis Sci 48: 3854-3863.
38. Laabich A, Li G, Cooper NG (2000) Calcium/calmodulin-dependent protein kinase II containing a nuclear localizing signal is altered in retinal neurons exposed to N-methyl-D-aspartate. Brain Res Mol Brain Res 76: 253-265.
39. Matthews RP, Guthrie CR, Wailes LM, Zhao X, Means AR, et al. (1994) Calcium/calmodulin-dependent protein kinase types II and IV differentially regulate CREB-dependent gene expression. Mol Cell Biol 14: 6107-6116.
40. Sun P, Lou L, Maurer RA (1996) Regulation of activating transcription factor-1 and the cAMP response element-binding protein by Ca2+/calmodulin-dependent protein kinases type I, II, and IV. J Biol Chem 271: 3066-3073.
41. Shimomura A, Ogawa Y, Kitani T, Fujisawa H, Hagiwara M (1996) Calmodulin-dependent protein kinase II potentiates transcriptional activation through activating transcription factor 1 but not cAMP response element-binding protein. J Biol Chem 271: 17957-17960.
42. Sun P, Enslen H, Myung PS, Maurer RA (1994) Differential activation of CREB by Ca2+/calmodulin-dependent protein kinases type II and type IV involves phosphorylation of a site that negatively regulates activity. Genes Dev 8: 2527-2539.
43. Jiang X, Zhu D, Okagaki P, Lipsky R, Wu X, et al. (2003) N-methyl-D-aspartate and TrkB receptor activation in cerebellar granule cells: an in vitro model of preconditioning to stimulate intrinsic survival pathways in neurons. Ann N Y Acad Sci 993: 134-145; discussion 159-160.
44. Benfenati F, Valtorta F, Rubenstein JL, Gorelick FS, Greengard P, et al. (1992) Synaptic vesicle-associated Ca2+/calmodulin-dependent protein kinase II is a binding protein for synapsin I. Nature 359: 417-420.
45. Hinds HL, Goussakov I, Nakazawa K, Tonegawa S, Bolshakov VY (2003) Essential function of alpha-calcium/calmodulin-dependent protein kinase II in neurotransmitter release at a glutamatergic central synapse. Proc Natl Acad Sci U S A 100: 4275-4280.
46. Acheson A, Conover JC, Fandl JP, DeChiara TM, Russell M, et al. (1995) A BDNF autocrine loop in adult sensory neurons prevents cell death. Nature 374: 450-453.
47. Bekinschtein P, Cammarota M, Katche C, Slipczuk L, Rossato JI, et al. (2008) BDNF is essential to promote persistence of long-term memory storage. Proc Natl Acad Sci U S A 105: 2711-2716.
48. Huang EJ, Reichardt LF (2001) Neurotrophins: roles in neuronal development and function. Annu Rev Neurosci 24: 677-736.
49. Yamada K, Nabeshima T (2003) Brain-derived neurotrophic factor/TrkB signaling in memory processes. J Pharmacol Sci 91: 267-270.

50. Chen J, Nagayama T, Jin K, Stetler RA, Zhu RL, et al. (1998) Induction of caspase-3-like protease may mediate delayed neuronal death in the hippocampus after transient cerebral ischemia. J Neurosci 18: 4914-4928.
51. Namura S, Zhu J, Fink K, Endres M, Srinivasan A, et al. (1998) Activation and cleavage of caspase-3 in apoptosis induced by experimental cerebral ischemia. J Neurosci 18: 3659-3668.
52. Laabich A, Cooper NG (2000) Neuroprotective effect of AIP on N-methyl-D-aspartate-induced cell death in retinal neurons. Brain Res Mol Brain Res 85: 32-40.
53. Chaudhary P, Ahmed F, Sharma SC (1998) MK801-a neuroprotectant in rat hypertensive eyes. Brain Res 792: 154-158.
54. Vorverk CK, Lipton, S.A., Zurakowski, D., Hyman, B.T., and Sabel, B.A. (1996) Chronic low-dose glutamate is toxic to retinal ganglion cells: toxicity blocked my memantine. Invest Ophthalmol Vis Sci 37: 1618-1624.
55. Olney JW (1969) Brain lesions, obesity, and other disturbances in mice treated with monosodium glutamate. Science 164: 719-721.
56. Olney JW, Sharpe LG (1969) Brain lesions in an infant rhesus monkey treated with monsodium glutamate. Science 166: 386-388.
57. Coultrap SJ, Vest RS, Ashpole NM, Hudmon A, Bayer KU (2011) CaMKII in cerebral ischemia. Acta Pharmacol Sin.
58. Liu S, Levine SR, Winn HR (2011) Targeting ischemic penumbra: part I - from pathophysiology to therapeutic strategy. J Exp Stroke Transl Med 3: 47-55.
59. Doyle KP, Simon RP, Stenzel-Poore MP (2008) Mechanisms of ischemic brain damage. Neuropharmacology 55: 310-318.
60. Hubschmann OR, Kornhauser D (1980) Cortical cellular response in acute subarachnoid hemorrhage. J Neurosurg 52: 456-462.
61. Bramlett HM, Dietrich WD (2004) Pathophysiology of cerebral ischemia and brain trauma: similarities and differences. J Cereb Blood Flow Metab 24: 133-150.
62. Greve MW, Zink BJ (2009) Pathophysiology of traumatic brain injury. Mt Sinai J Med 76: 97-104.
63. Mattson MP (2003) Excitotoxic and excitoprotective mechanisms: abundant targets for the prevention and treatment of neurodegenerative disorders. Neuromolecular Med 3: 65-94.
64. Koch-Weser J, Blinks JR (1963) The Influence of the Interval between Beats on Myocardial Contractility. Pharmacol Rev 15: 601-652.
65. Grueter CE, Abiria SA, Wu Y, Anderson ME, Colbran RJ (2008) Differential regulated interactions of calcium/calmodulin-dependent protein kinase II with isoforms of voltage-gated calcium channel beta subunits. Biochemistry 47: 1760-1767.
66. Welsby PJ, Wang H, Wolfe JT, Colbran RJ, Johnson ML, et al. (2003) A mechanism for the direct regulation of T-type calcium channels by Ca2+/calmodulin-dependent kinase II. J Neurosci 23: 10116-10121.
67. Yao J, Davies LA, Howard JD, Adney SK, Welsby PJ, et al. (2006) Molecular basis for the modulation of native T-type Ca2+ channels in vivo by Ca2+/calmodulin-dependent protein kinase II. J Clin Invest 116: 2403-2412.

68. Hudmon A, Schulman H, Kim J, Maltez JM, Tsien RW, et al. (2005) CaMKII tethers to L-type Ca2+ channels, establishing a local and dedicated integrator of Ca2+ signals for facilitation. J Cell Biol 171: 537-547.
69. Lee TS, Karl R, Moosmang S, Lenhardt P, Klugbauer N, et al. (2006) Calmodulin kinase II is involved in voltage-dependent facilitation of the L-type Cav1.2 calcium channel: Identification of the phosphorylation sites. J Biol Chem 281: 25560-25567.
70. Abiria SA, Colbran RJ (2010) CaMKII associates with CaV1.2 L-type calcium channels via selected beta subunits to enhance regulatory phosphorylation. J Neurochem 112: 150-161.
71. DeSantiago J, Maier LS, Bers DM (2002) Frequency-dependent acceleration of relaxation in the heart depends on CaMKII, but not phospholamban. J Mol Cell Cardiol 34: 975-984.
72. Marx SO, Reiken S, Hisamatsu Y, Jayaraman T, Burkhoff D, et al. (2000) PKA phosphorylation dissociates FKBP12.6 from the calcium release channel (ryanodine receptor): defective regulation in failing hearts. Cell 101: 365-376.
73. Hoch B, Meyer R, Hetzer R, Krause EG, Karczewski P (1999) Identification and expression of delta-isoforms of the multifunctional Ca2+/calmodulin-dependent protein kinase in failing and nonfailing human myocardium. Circ Res 84: 713-721.
74. Zhang T, Maier LS, Dalton ND, Miyamoto S, Ross J, Jr., et al. (2003) The deltaC isoform of CaMKII is activated in cardiac hypertrophy and induces dilated cardiomyopathy and heart failure. Circ Res 92: 912-919.
75. Zhang R, Khoo MS, Wu Y, Yang Y, Grueter CE, et al. (2005) Calmodulin kinase II inhibition protects against structural heart disease. Nat Med 11: 409-417.
76. Wayman GA, Tokumitsu H, Davare MA, Soderling TR (2011) Analysis of CaM-kinase signaling in cells. Cell Calcium.
77. Higley MJ, Sabatini BL (2008) Calcium signaling in dendrites and spines: practical and functional considerations. Neuron 59: 902-913.
78. Berridge MJ, Lipp P, Bootman MD (2000) Signal transduction. The calcium entry pas de deux. Science 287: 1604-1605.
79. Zylinska L, Kawecka I, Lachowicz L, Szemraj J (2002) The isoform- and location-dependence of the functioning of the plasma membrane calcium pump. Cell Mol Biol Lett 7: 1037-1045.
80. East JM (2000) Sarco(endo)plasmic reticulum calcium pumps: recent advances in our understanding of structure/function and biology (review). Mol Membr Biol 17: 189-200.
81. Griffith LC, Verselis LM, Aitken KM, Kyriacou CP, Danho W, et al. (1993) Inhibition of calcium/calmodulin-dependent protein kinase in Drosophila disrupts behavioral plasticity. Neuron 10: 501-509.
82. Griffith LC, Wang J, Zhong Y, Wu CF, Greenspan RJ (1994) Calcium/calmodulin-dependent protein kinase II and potassium channel subunit eag similarly affect plasticity in Drosophila. Proc Natl Acad Sci U S A 91: 10044-10048.
83. Wang J, Renger JJ, Griffith LC, Greenspan RJ, Wu CF (1994) Concomitant alterations of physiological and developmental plasticity in Drosophila CaM kinase II-inhibited synapses. Neuron 13: 1373-1384.

84. Rongo C, Kaplan JM (1999) CaMKII regulates the density of central glutamatergic synapses in vivo. Nature 402: 195-199.
85. Reiner DJ, Newton EM, Tian H, Thomas JH (1999) Diverse behavioural defects caused by mutations in Caenorhabditis elegans unc-43 CaM kinase II. Nature 402: 199-203.
86. Hanley RM, Means AR, Ono T, Kemp BE, Burgin KE, et al. (1987) Functional analysis of a complementary DNA for the 50-kilodalton subunit of calmodulin kinase II. Science 237: 293-297.
87. Lin CR, Kapiloff MS, Durgerian S, Tatemoto K, Russo AF, et al. (1987) Molecular cloning of a brain-specific calcium/calmodulin-dependent protein kinase. Proc Natl Acad Sci U S A 84: 5962-5966.
88. Srinivasan M, Edman CF, Schulman H (1994) Alternative splicing introduces a nuclear localization signal that targets multifunctional CaM kinase to the nucleus. J Cell Biol 126: 839-852.
89. Bayer KU, Lohler J, Harbers K (1996) An alternative, nonkinase product of the brain-specifically expressed Ca2+/calmodulin-dependent kinase II alpha isoform gene in skeletal muscle. Mol Cell Biol 16: 29-36.
90. Bayer KU, Harbers K, Schulman H (1998) alphaKAP is an anchoring protein for a novel CaM kinase II isoform in skeletal muscle. EMBO J 17: 5598-5605.
91. Bennett MK, Kennedy MB (1987) Deduced primary structure of the beta subunit of brain type II Ca2+/calmodulin-dependent protein kinase determined by molecular cloning. Proc Natl Acad Sci U S A 84: 1794-1798.
92. Brocke L, Srinivasan M, Schulman H (1995) Developmental and regional expression of multifunctional Ca2+/calmodulin-dependent protein kinase isoforms in rat brain. J Neurosci 15: 6797-6808.
93. Bulleit RF, Bennett MK, Molloy SS, Hurley JB, Kennedy MB (1988) Conserved and variable regions in the subunits of brain type II Ca2+/calmodulin-dependent protein kinase. Neuron 1: 63-72.
94. Karls U, Muller U, Gilbert DJ, Copeland NG, Jenkins NA, et al. (1992) Structure, expression, and chromosome location of the gene for the beta subunit of brain-specific Ca2+/calmodulin-dependent protein kinase II identified by transgene integration in an embryonic lethal mouse mutant. Mol Cell Biol 12: 3644-3652.
95. Urquidi V, Ashcroft SJ (1995) A novel pancreatic beta-cell isoform of calcium/calmodulin-dependent protein kinase II (beta 3 isoform) contains a proline-rich tandem repeat in the association domain. FEBS Lett 358: 23-26.
96. Tobimatsu T, Fujisawa H (1989) Tissue-specific expression of four types of rat calmodulin-dependent protein kinase II mRNAs. J Biol Chem 264: 17907-17912.
97. Kwiatkowski AP, McGill JM (1995) Human biliary epithelial cell line Mz-ChA-1 expresses new isoforms of calmodulin-dependent protein kinase II. Gastroenterology 109: 1316-1323.
98. Nghiem P, Saati SM, Martens CL, Gardner P, Schulman H (1993) Cloning and analysis of two new isoforms of multifunctional Ca2+/calmodulin-dependent protein kinase. Expression in multiple human tissues. J Biol Chem 268: 5471-5479.
99. Takeuchi M, Fujisawa H (1998) New alternatively spliced variants of calmodulin-dependent protein kinase II from rabbit liver. Gene 221: 107-115.

100. Tobimatsu T, Kameshita I, Fujisawa H (1988) Molecular cloning of the cDNA encoding the third polypeptide (gamma) of brain calmodulin-dependent protein kinase II. J Biol Chem 263: 16082-16086.
101. Tombes RM, Krystal GW (1997) Identification of novel human tumor cell-specific CaMK-II variants. Biochim Biophys Acta 1355: 281-292.
102. Edman CF, Schulman H (1994) Identification and characterization of delta B-CaM kinase and delta C-CaM kinase from rat heart, two new multifunctional Ca2+/calmodulin-dependent protein kinase isoforms. Biochim Biophys Acta 1221: 89-101.
103. Schworer CM, Rothblum LI, Thekkumkara TJ, Singer HA (1993) Identification of novel isoforms of the delta subunit of Ca2+/calmodulin-dependent protein kinase II. Differential expression in rat brain and aorta. J Biol Chem 268: 14443-14449.
104. Takeuchi Y, Yamamoto H, Matsumoto K, Kimura T, Katsuragi S, et al. (1999) Nuclear localization of the delta subunit of Ca2+/calmodulin-dependent protein kinase II in rat cerebellar granule cells. J Neurochem 72: 815-825.
105. Wegner M, Cao Z, Rosenfeld MG (1992) Calcium-regulated phosphorylation within the leucine zipper of C/EBP beta. Science 256: 370-373.
106. Yano S, Fukunaga K, Takiguchi M, Ushio Y, Mori M, et al. (1996) Regulation of CCAAT/enhancer-binding protein family members by stimulation of glutamate receptors in cultured rat cortical astrocytes. J Biol Chem 271: 23520-23527.
107. Bayer KU, De Koninck P, Schulman H (2002) Alternative splicing modulates the frequency-dependent response of CaMKII to Ca(2+) oscillations. EMBO J 21: 3590-3597.
108. Rellos P, Pike AC, Niesen FH, Salah E, Lee WH, et al. (2010) Structure of the CaMKIIdelta/calmodulin complex reveals the molecular mechanism of CaMKII kinase activation. PLoS Biol 8: e1000426.
109. Chao LH, Pellicena P, Deindl S, Barclay LA, Schulman H, et al. (2010) Intersubunit capture of regulatory segments is a component of cooperative CaMKII activation. Nat Struct Mol Biol 17: 264-272.
110. Payne ME, Fong YL, Ono T, Colbran RJ, Kemp BE, et al. (1988) Calcium/calmodulin-dependent protein kinase II. Characterization of distinct calmodulin binding and inhibitory domains. J Biol Chem 263: 7190-7195.
111. Kelly PT, Weinberger RP, Waxham MN (1988) Active site-directed inhibition of Ca2+/calmodulin-dependent protein kinase type II by a bifunctional calmodulin-binding peptide. Proc Natl Acad Sci U S A 85: 4991-4995.
112. Gaertner TR, Kolodziej SJ, Wang D, Kobayashi R, Koomen JM, et al. (2004) Comparative analyses of the three-dimensional structures and enzymatic properties of alpha, beta, gamma and delta isoforms of Ca2+-calmodulin-dependent protein kinase II. Journal of Biological Chemistry 279: 12484-12494.
113. Hoelz A, Nairn AC, Kuriyan J (2003) Crystal structure of a tetradecameric assembly of the association domain of Ca2+/calmodulin-dependent kinase II. Molecular Cell 11: 1241-1251.
114. Rosenberg OS, Deindl S, Comolli LR, Hoelz A, Downing KH, et al. (2006) Oligomerization states of the association domain and the holoenyzme of Ca2+/CaM kinase II. FEBS Journal 273: 682-694.

115. Kelly PT (1991) Calmodulin-dependent protein kinase II. Multifunctional roles in neuronal differentiation and synaptic plasticity. Mol Neurobiol 5: 153-177.
116. Brocke L, Chiang LW, Wagner PD, Schulman H (1999) Functional implications of the subunit composition of neuronal CaM kinase II. Journal of Biological Chemistry 274: 22713-22722.
117. Bennett MK, Erondu NE, Kennedy MB (1983) Purification and characterization of a calmodulin-dependent protein kinase that is highly concentrated in brain. J Biol Chem 258: 12735-12744.
118. Kuret J, Schulman H (1984) Purification and characterization of a Ca2+/calmodulin-dependent protein kinase from rat brain. Biochemistry 23: 5495-5504.
119. Vallano ML (1989) Separation of isozymic forms of type II calcium/calmodulin-dependent protein kinase using cation-exchange chromatography. J Neurosci Methods 30: 1-9.
120. De Koninck P, Schulman H (1998) Sensitivity of CaM kinase II to the frequency of Ca2+ oscillations. Science 279: 227-230.
121. Miller SG, Kennedy MB (1986) Regulation of brain type II Ca2+/calmodulin-dependent protein kinase by autophosphorylation: a Ca2+-triggered molecular switch. Cell 44: 861-870.
122. Colbran RJ (1993) Inactivation of Ca2+/calmodulin-dependent protein kinase II by basal autophosphorylation. J Biol Chem 268: 7163-7170.
123. Hanson PI, Schulman H (1992) Inhibitory autophosphorylation of multifunctional Ca2+/calmodulin-dependent protein kinase analyzed by site-directed mutagenesis. J Biol Chem 267: 17216-17224.
124. Robison AJ (2005) Regulated interactions of the postsynaptic density Ca2+/Calmodulin-dependent protein kinase II signalosome modulate kinase activity. Nashville, TN: Vanderbilt University. 178 p.
125. Kemp BE, Parker MW, Hu S, Tiganis T, House C (1994) Substrate and pseudosubstrate interactions with protein kinases: determinants of specificity. Trends Biochem Sci 19: 440-444.
126. Hagiwara T, Ohsako S, Yamauchi T (1991) Studies on the regulatory domain of Ca2+/calmodulin-dependent protein kinase II by expression of mutated cDNAs in Escherichia coli. J Biol Chem 266: 16401-16408.
127. Miller SG, Patton BL, Kennedy MB (1988) Sequences of autophosphorylation sites in neuronal type II CaM kinase that control Ca2(+)-independent activity. Neuron 1: 593-604.
128. Planas-Silva MD, Means AR (1992) Expression of a constitutive form of calcium/calmodulin dependent protein kinase II leads to arrest of the cell cycle in G2. EMBO J 11: 507-517.
129. Yamagata Y, Czernik AJ, Greengard P (1991) Active catalytic fragment of Ca2+/calmodulin-dependent protein kinase II. Purification, characterization, and structural analysis. J Biol Chem 266: 15391-15397.
130. Cruzalegui FH, Kapiloff MS, Morfin JP, Kemp BE, Rosenfeld MG, et al. (1992) Regulation of intrasteric inhibition of the multifunctional calcium/calmodulin-dependent protein kinase. Proc Natl Acad Sci U S A. 1992/12/15 ed. pp. 12127-12131.

131. Kemp BE, Pearson RB (1991) Intrasteric regulation of protein kinases and phosphatases. Biochim Biophys Acta 1094: 67-76.
132. Colbran RJ, Smith MK, Schworer CM, Fong YL, Soderling TR (1989) Regulatory domain of calcium/calmodulin-dependent protein kinase II. Mechanism of inhibition and regulation by phosphorylation. J Biol Chem 264: 4800-4804.
133. Hu SH, Parker MW, Lei JY, Wilce MC, Benian GM, et al. (1994) Insights into autoregulation from the crystal structure of twitchin kinase. Nature 369: 581-584.
134. Goldberg J, Nairn AC, Kuriyan J (1996) Structural basis for the autoinhibition of calcium/calmodulin-dependent protein kinase I. Cell 84: 875-887.
135. Smith MK, Colbran RJ, Brickey DA, Soderling TR (1992) Functional determinants in the autoinhibitory domain of calcium/calmodulin-dependent protein kinase II. Role of His282 and multiple basic residues. J Biol Chem 267: 1761-1768.
136. Yang E, Schulman H (1999) Structural examination of autoregulation of multifunctional calcium/calmodulin-dependent protein kinase II. Journal of Biological Chemistry 274: 26199-26208.
137. Braun AP, Schulman H (1995) The multifunctional calcium/calmodulin-dependent protein kinase: from form to function. Annu Rev Physiol 57: 417-445.
138. Rosenberg OS, Deindl S, Sung R-J, Nairn AC, Kuriyan J (2005) Structure of the autoinhibited kinase domain of CaMKII and SAXS analysis of the holoenzyme. Cell 123: 849-860.
139. Colbran RJ, Soderling TR (1990) Calcium/calmodulin-dependent protein kinase II. Curr Top Cell Regul 31: 181-221.
140. Hanson PI, Schulman H (1992) Neuronal Ca2+/calmodulin-dependent protein kinases. Annu Rev Biochem 61: 559-601.
141. Babu YS, Bugg CE, Cook WJ (1988) Structure of calmodulin refined at 2.2 A resolution. J Mol Biol 204: 191-204.
142. Hoeflich KP, Ikura M (2002) Calmodulin in action: diversity in target recognition and activation mechanisms. Cell 108: 739-742.
143. Torok K, Tzortzopoulos A, Grabarek Z, Best SL, Thorogate R (2001) Dual effect of ATP in the activation mechanism of brain Ca(2+)/calmodulin-dependent protein kinase II by Ca(2+)/calmodulin. Biochemistry 40: 14878-14890.
144. Chin D, Means AR (2002) Mechanisms for regulation of calmodulin kinase IIalpha by Ca(2+)/calmodulin and autophosphorylation of threonine 286. Biochemistry 41: 14001-14009.
145. Johnson JD, Snyder C, Walsh M, Flynn M (1996) Effects of myosin light chain kinase and peptides on Ca2+ exchange with the N- and C-terminal Ca2+ binding sites of calmodulin. J Biol Chem 271: 761-767.
146. Kranz JK, Lee EK, Nairn AC, Wand AJ (2002) A direct test of the reductionist approach to structural studies of calmodulin activity: relevance of peptide models of target proteins. J Biol Chem 277: 16351-16354.
147. Meyer T, Hanson PI, Stryer L, Schulman H (1992) Calmodulin trapping by calcium-calmodulin-dependent protein kinase. Science 256: 1199-1202.
148. Newman RA, Van Scyoc WS, Sorensen BR, Jaren OR, Shea MA (2008) Interdomain cooperativity of calmodulin bound to melittin preferentially increases calcium affinity of sites I and II. Proteins 71: 1792-1812.

149. Singla SI, Hudmon A, Goldberg JM, Smith JL, Schulman H (2001) Molecular characterization of calmodulin trapping by calcium/calmodulin-dependent protein kinase II. Journal of Biological Chemistry 276: 29353-29360.
150. Tse JKY, Giannetti AM, Bradshaw JM (2007) Thermodynamics of calmodulin trapping by Ca2+/calmodulin-dependent protein kinase II: subpicomolar Kd determined using competition titration calorimetry. Biochemistry 46: 4017-4027.
151. Waxham MN, Tsai AL, Putkey JA (1998) A mechanism for calmodulin (CaM) trapping by CaM-kinase II defined by a family of CaM-binding peptides. J Biol Chem 273: 17579-17584.
152. Meador WE, Means AR, Quiocho FA (1993) Modulation of calmodulin plasticity in molecular recognition on the basis of x-ray structures. Science 262: 1718-1721.
153. Lai Y, Nairn AC, Greengard P (1986) Autophosphorylation reversibly regulates the Ca2+/calmodulin-dependence of Ca2+/calmodulin-dependent protein kinase II. Proc Natl Acad Sci U S A 83: 4253-4257.
154. Strack S, Choi S, Lovinger DM, Colbran RJ (1997) Translocation of autophosphorylated calcium/calmodulin-dependent protein kinase II to the postsynaptic density. J Biol Chem 272: 13467-13470.
155. Kolodziej SJ, Hudmon A, Waxham MN, Stoops JK (2000) Three-dimensional reconstructions of calcium/calmodulin-dependent (CaM) kinase IIalpha and truncated CaM kinase IIalpha reveal a unique organization for its structural core and functional domains. J Biol Chem 275: 14354-14359.
156. Morris EP, Torok K (2001) Oligomeric structure of alpha-calmodulin-dependent protein kinase II. J Mol Biol 308: 1-8.
157. Mukherji S, Soderling TR (1994) Regulation of Ca2+/calmodulin-dependent protein kinase II by inter- and intrasubunit-catalyzed autophosphorylations. J Biol Chem 269: 13744-13747.
158. Bradshaw JM, Kubota, Y., Meyer, T., Schulman, H. (2003) An untrasensitive Ca2+/calmodulin-dependent protein kinase II-protein phosphatase 1 switch facilitates specificity in postsynaptic calcium signaling. Proc Natl Acad Sci U S A 100: 10512-10517.
159. Walikonis RS, Oguni, A., Khorosheva, E. M., Jeng, C. J., Asuncion, F. J., Kennedy, M. B. (2001) Densin-180 forms a ternary complex with the (alpha)-subunit of Ca2+/calmodulin-dependent protein kinase II and (alpha)-actinin. J Neuorosci 21: 423-433.
160. Pawson CT, Scott JD (2010) Signal integration through blending, bolstering and bifurcating of intracellular information. Nat Struct Mol Biol 17: 653-658.
161. Shen K, Teruel MN, Connor JH, Shenolikar S, Meyer T (2000) Molecular memory by reversible translocation of calcium/calmodulin-dependent protein kinase II. Nat Neurosci 3: 881-886.
162. Shen K, Meyer T (1998) In vivo and in vitro characterization of the sequence requirement for oligomer formation of Ca2+/calmodulin-dependent protein kinase IIalpha. J Neurochem 70: 96-104.
163. Strack S, McNeill RB, Colbran RJ (2000) Mechanism and regulation of calcium/calmodulin-dependent protein kinase II targeting to the NR2B subunit of the N-methyl-D-aspartate receptor. J Biol Chem 275: 23798-23806.

164. Strack S, Colbran RJ (1998) Autophosphorylation-dependent targeting of calcium/calmodulin-dependent protein kinase II by the NR2B subunit of the N-methyl- D-aspartate receptor. J Biol Chem 273: 20689-20692.
165. Gardoni F, Caputi A, Cimino M, Pastorino L, Cattabeni F, et al. (1998) Calcium/calmodulin-dependent protein kinase II is associated with NR2A/B subunits of NMDA receptor in postsynaptic densities. J Neurochem 71: 1733-1741.
166. Leonard AS, Lim IA, Hemsworth DE, Horne MC, Hell JW (1999) Calcium/calmodulin-dependent protein kinase II is associated with the N-methyl-D-aspartate receptor. Proc Natl Acad Sci U S A 96: 3239-3244.
167. McNeill RB, Colbran, R. J. (1995) Interaction of autophosphorylated Ca2+/calmodulin-dependent protein kinase II with neuronal cytoskeletal proteins: characterization of binding to a 190-kDa postsynaptic density protein. J Biol Chem 270: 10043-10049.
168. Gardoni F, Schrama LH, van Dalen JJ, Gispen WH, Cattabeni F, et al. (1999) AlphaCaMKII binding to the C-terminal tail of NMDA receptor subunit NR2A and its modulation by autophosphorylation. FEBS Lett 456: 394-398.
169. Bayer KU, De Koninck P, Leonard AS, Hell JW, Schulman H (2001) Interaction with the NMDA receptor locks CaMKII in an active conformation. Nature 411: 801-805.
170. Ohta Y, Nishida E, Sakai H (1986) Type II Ca2+/calmodulin-dependent protein kinase binds to actin filaments in a calmodulin-sensitive manner. FEBS Lett 208: 423-426.
171. Shen K, Meyer T (1999) Dynamic control of CaMKII translocation and localization in hippocampal neurons by NMDA receptor stimulation. Science 284: 162-166.
172. Dhavan R, Greer PL, Morabito MA, Orlando LR, Tsai LH (2002) The cyclin-dependent kinase 5 activators p35 and p39 interact with the alpha-subunit of Ca2+/calmodulin-dependent protein kinase II and alpha-actinin-1 in a calcium-dependent manner. J Neurosci 22: 7879-7891.
173. Apperson ML, Moon IS, Kennedy MB (1996) Characterization of densin-180, a new brain-specific synaptic protein of the O-sialoglycoprotein family. J Neurosci 16: 6839-6852.
174. Vallano ML, Goldenring JR, Lasher RS, Delorenzo RJ (1986) Association of calcium/calmodulin-dependent kinase with cytoskeletal preparations: phosphorylation of tubulin, neurofilament, and microtubule-associated proteins. Ann N Y Acad Sci 466: 357-374.
175. Yamauchi T, Fujisawa H (1988) Regulation of the interaction of actin filaments with microtubule-associated protein 2 by calmodulin-dependent protein kinase II. Biochim Biophys Acta 968: 77-85.
176. Chao LH, Stratton MM, Lee IH, Rosenberg OS, Levitz J, et al. (2011) A Mechanism for Tunable Autoinhibition in the Structure of a Human Ca(2+)/Calmodulin-Dependent Kinase II Holoenzyme. Cell 146: 732-745.
177. Kolb SJ, Hudmon A, Ginsberg TR, Waxham MN (1998) Identification of domains essential for the assembly of calcium/calmodulin-dependent protein kinase II holoenzymes. J Biol Chem 273: 31555-31564.

178. Hanks SK, Hunter T (1995) Protein kinases 6. The eukaryotic protein kinase superfamily: kinase (catalytic) domain structure and classification. FASEB J 9: 576-596.
179. Hanks SK, Quinn AM (1991) Protein kinase catalytic domain sequence database: identification of conserved features of primary structure and classification of family members. Methods Enzymol 200: 38-62.
180. Hanks SK, Quinn AM, Hunter T (1988) The protein kinase family: conserved features and deduced phylogeny of the catalytic domains. Science 241: 42-52.
181. Knighton DR, Zheng JH, Ten Eyck LF, Ashford VA, Xuong NH, et al. (1991) Crystal structure of the catalytic subunit of cyclic adenosine monophosphate-dependent protein kinase. Science 253: 407-414.
182. Knighton DR, Zheng JH, Ten Eyck LF, Xuong NH, Taylor SS, et al. (1991) Structure of a peptide inhibitor bound to the catalytic subunit of cyclic adenosine monophosphate-dependent protein kinase. Science 253: 414-420.
183. Zhang F, Strand A, Robbins D, Cobb MH, Goldsmith EJ (1994) Atomic structure of the MAP kinase ERK2 at 2.3 A resolution. Nature 367: 704-711.
184. Hubbard SR, Wei L, Ellis L, Hendrickson WA (1994) Crystal structure of the tyrosine kinase domain of the human insulin receptor. Nature 372: 746-754.
185. Zheng J, Knighton DR, Xuong NH, Taylor SS, Sowadski JM, et al. (1993) Crystal structures of the myristylated catalytic subunit of cAMP-dependent protein kinase reveal open and closed conformations. Protein Sci 2: 1559-1573.
186. King MM (1988) Conformation-sensitive modification of the type II calmodulin-dependent protein kinase by phenylglyoxal. J Biol Chem 263: 4754-4757.
187. King MM, Shell DJ, Kwiatkowski AP (1988) Affinity labeling of the ATP-binding site of type II calmodulin-dependent protein kinase by 5'-p-fluorosulfonylbenzoyl adenosine. Arch Biochem Biophys 267: 467-473.
188. Shields SM, Vernon PJ, Kelly PT (1984) Autophosphorylation of calmodulin-kinase II in synaptic junctions modulates endogenous kinase activity. J Neurochem 43: 1599-1609.
189. Kanaseki T, Ikeuchi Y, Sugiura H, Yamauchi T (1991) Structural features of Ca2+/calmodulin-dependent protein kinase II revealed by electron microscopy. J Cell Biol 115: 1049-1060.
190. Thaler C, Koushik SV, Puhl HL, 3rd, Blank PS, Vogel SS (2009) Structural rearrangement of CaMKIIalpha catalytic domains encodes activation. Proc Natl Acad Sci U S A 106: 6369-6374.
191. Clapperton JA, Martin SR, Smerdon SJ, Gamblin SJ, Bayley PM (2002) Structure of the complex of calmodulin with the target sequence of calmodulin-dependent protein kinase I: studies of the kinase activation mechanism. Biochemistry 41: 14669-14679.
192. Hubbell WL, Cafiso DS, Altenbach C (2000) Identifying conformational changes with site-directed spin labeling. Nat Struct Biol 7: 735-739.
193. Hubbell WL, Mchaourab HS, Altenbach C, Lietzow MA (1996) Watching proteins move using site-directed spin labeling. Structure 4: 779-783.
194. McHaourab HS, Lietzow MA, Hideg K, Hubbell WL (1996) Motion of spin-labeled side chains in T4 lysozyme. Correlation with protein structure and dynamics. Biochemistry 35: 7692-7704.

195. Budil DE, Lee S, Saxena S, Freed JH (1996) Molecular motion of spin labeled side chains in α-helices: analysis by variation of side chain structure. Biochemistry 40: 3828-3846.
196. Laukien J, Gewiese B, Roth G, Jung W-I (2011) Bruker Biospin. What is EPR? Rheinstetten, Germany.
197. Carrington A, & McLachlan, A.D. (1967) Introduction to magnetic resonance with applications to chemistry and chemical physics. New York: Harper & Row, Inc.
198. Weil JA, Bolton, J. R., and Wertz, J. E. (1994) Electron paramagnetic resonance: elementary theory and practical applications. New York: Wiley.
199. Teng Q (2005) Structural biology : practical NMR applications. New York: Springer.
200. Columbus L, Hubbell WL (2002) A new spin on protein dynamics. Trends Biochem Sci 27: 288-295.
201. Columbus L, Kalai T, Jeko J, Hideg K, Hubbell WL (2001) Molecular motion of spin labeled side chains in alpha-helices: analysis by variation of side chain structure. Biochemistry 40: 3828-3846.
202. Budil DE, Lee S, Saxena S, Freed JH (1996) Nonlinear-least-squares analysis of slow-motion EPR spectra in one and two dimensions using a modified Levenberg–Marquardt algorithm. J Mag Res Series A 120: 155-189.
203. Salwinski L, Hubbell WL (1999) Structure in the channel forming domain of colicin E1 bound to membranes: the 402-424 sequence. Protein Sci 8: 562-572.
204. Eaton SS, Eaton, G. R., and Berliner, L. J. (2004) Biomedical EPR. New York: Kluwer Academic/Plenum Publishers.
205. Berliner LJ, Eaton, G. R., and Eaton, S. S. (2000) Distance measurements in biological systems by EPR. New York: Kluwer Academic/Plenum Publishers.
206. Rabenstein MD, Shin YK (1995) Determination of the distance between two spin labels attached to a macromolecule. Proc Natl Acad Sci U S A 92: 8239-8243.
207. McHaourab HS, Oh KJ, Fang CJ, Hubbell WL (1997) Conformation of T4 lysozyme in solution. Hinge-bending motion and the substrate-induced conformational transition studied by site-directed spin labeling. Biochemistry 36: 307-316.
208. Steinhoff HJ, Radzwill N, Thevis W, Lenz V, Brandenburg D, et al. (1997) Determination of interspin distances between spin labels attached to insulin: comparison of electron paramagnetic resonance data with the X-ray structure. Biophys J 73: 3287-3298.
209. Borbat PP, Surendhran K, Bortolus M, Zou P, Freed JH, et al. (2007) Conformational motion of the ABC transporter MsbA induced by ATP hydrolysis. PLoS Biol 5: e271.
210. Jeschke G (2002) Distance measurements in the nanometer range by pulse EPR. Chemphyschem 3: 927-932.
211. Alexander N, Bortolus M, Al-Mestarihi A, McHaourab H, Meiler J (2008) De novo high-resolution protein structure determination from sparse spin-labeling EPR data. Structure 16: 181-195.
212. Hubbell WL, Gross A, Langen R, Lietzow MA (1998) Recent advances in site-directed spin labeling of proteins. Curr Opin Struct Biol 8: 649-656.

213. Cuello LG, Cortes DM, Perozo E (2004) Molecular architecture of the KvAP voltage-dependent K+ channel in a lipid bilayer. Science 306: 491-495.
214. Dong J, Yang G, Mchaourab HS (2005) Structural basis of energy transduction in the transport cycle of MsbA. Science 308: 1023-1028.
215. McHaourab HS, Kalai T, Hideg K, Hubbell WL (1999) Motion of spin-labeled side chains in T4 lysozyme: effect of side chain structure. Biochemistry 38: 2947-2955.
216. Perozo E, Cortes DM, Cuello LG (1999) Structural rearrangements underlying K+-channel activation gating. Science 285: 73-78.
217. Lakowicz JR (2006) Principles of fluorescence spectroscopy, 3rd ed. New York: Springer.
218. Brickey DA, Colbran RJ, Fong YL, Soderling TR (1990) Expression and characterization of the alpha-subunit of Ca2+/calmodulin-dependent protein kinase II using the baculovirus expression system. Biochem Biophys Res Commun 173: 578-584.
219. Praseeda M, Beena MK, Asha SJ, Omkumar RV (2004) The C-terminus of CaMKII is truncated when expressed in E. coli. Protein Pept Lett 11: 175-179.
220. Robison AJ, Bartlett RK, Bass MA, Colbran RJ (2005) Differential modulation of Ca2+/calmodulin-dependent protein kinase II activity by regulated interactions with N-methyl-D-aspartate receptor NR2B subunits and alpha-actinin. J Biol Chem 280: 39316-39323.
221. Ten Eyck LF, Taylor SS, Kornev AP (2008) Conserved spatial patterns across the protein kinase family. Biochim Biophys Acta 1784: 238-243.
222. Lou LL, Schulman H (1989) Distinct autophosphorylation sites sequentially produce autonomy and inhibition of the multifunctional Ca2+/calmodulin-dependent protein kinase. J Neurosci 9: 2020-2032.
223. Hoffman L, Stein RA, Colbran RJ, McHaourab HS (2011) Conformational changes underlying calcium/calmodulin-dependent protein kinase II activation. EMBO J 30: 1251-1262.
224. Columbus L, Hubbell WL (2004) Mapping backbone dynamics in solution with site-directed spin labeling: GCN4-58 bZip free and bound to DNA. Biochemistry 43: 7273-7287.
225. Fiori WR, Miick SM, Millhauser GL (1993) Increasing sequence length favors alpha-helix over 3(10)-helix in alanine-based peptides: evidence for a length-dependent structural transition. Biochemistry 32: 11957-11962.
226. Morin B, Bourhis JM, Belle V, Woudstra M, Carriere F, et al. (2006) Assessing induced folding of an intrinsically disordered protein by site-directed spin-labeling electron paramagnetic resonance spectroscopy. J Phys Chem B 110: 20596-20608.
227. Tzortzopoulos A, Torok K (2004) Mechanism of the T286A-mutant alphaCaMKII interactions with Ca2+/calmodulin and ATP. Biochemistry 43: 6404-6414.
228. Brickey DA, Bann JG, Fong YL, Perrino L, Brennan RG, et al. (1994) Mutational analysis of the autoinhibitory domain of calmodulin kinase II. J Biol Chem 269: 29047-29054.

229. Bradshaw JM, Hudmon A, Schulman H (2002) Chemical quenched flow kinetic studies indicate an intraholoenzyme autophosphorylation mechanism for Ca2+/calmodulin-dependent protein kinase II. J Biol Chem 277: 20991-20998.
230. Hanson PI, Meyer T, Stryer L, Schulman H (1994) Dual role of calmodulin in autophosphorylation of multifunctional CaM kinase may underlie decoding of calcium signals. Neuron 12: 943-956.
231. Rich RC, Schulman H (1998) Substrate-directed function of calmodulin in autophosphorylation of Ca2+/calmodulin-dependent protein kinase II. J Biol Chem 273: 28424-28429.
232. Huang CY, Yuan CJ, Blumenthal DK, Graves DJ (1995) Identification of the substrate and pseudosubstrate binding sites of phosphorylase kinase gamma-subunit. J Biol Chem 270: 7183-7188.
233. Chang BH, Mukherji S, Soderling TR (1998) Characterization of a calmodulin kinase II inhibitor protein in brain. Proc Natl Acad Sci U S A 95: 10890-10895.
234. Chang BH, Mukherji S, Soderling TR (2001) Calcium/calmodulin-dependent protein kinase II inhibitor protein: localization of isoforms in rat brain. Neuroscience 102: 767-777.
235. Vest RS, Davies KD, O'Leary H, Port JD, Bayer KU (2007) Dual mechanism of a natural CaMKII inhibitor. Mol Biol Cell 18: 5024-5033.
236. Lepicard EM, Mizuno K, Antunes-Martins A, von Hertzen LS, Giese KP (2006) An endogenous inhibitor of calcium/calmodulin-dependent kinase II is up-regulated during consolidation of fear memory. Eur J Neurosci 23: 3063-3070.
237. Bayer KU, LeBel E, McDonald GL, O'Leary H, Schulman H, et al. (2006) Transition from reversible to persistent binding of CaMKII to postsynaptic sites and NR2B. J Neurosci 26: 1164-1174.
238. Coultrap SJ, Buard I, Kulbe JR, Dell'Acqua ML, Bayer KU (2010) CaMKII autonomy is substrate-dependent and further stimulated by Ca2+/calmodulin. J Biol Chem 285: 17930-17937.
239. Cheriyan J, Kumar P, Mayadevi M, Surolia A, Omkumar RV (2011) Calcium/calmodulin dependent protein kinase II bound to NMDA receptor 2B subunit exhibits increased ATP affinity and attenuated dephosphorylation. PLoS One 6: e16495.
240. Kazmier K, Alexander NS, Meiler J, McHaourab HS (2010) Algorithm for selection of optimized EPR distance restraints for de novo protein structure determination. J Struct Biol 173: 549-557.
241. Puttini M, Coluccia AM, Boschelli F, Cleris L, Marchesi E, et al. (2006) In vitro and in vivo activity of SKI-606, a novel Src-Abl inhibitor, against imatinib-resistant Bcr-Abl+ neoplastic cells. Cancer Res 66: 11314-11322.
242. Rix U, Remsing Rix LL, Terker AS, Fernbach NV, Hantschel O, et al. (2010) A comprehensive target selectivity survey of the BCR-ABL kinase inhibitor INNO-406 by kinase profiling and chemical proteomics in chronic myeloid leukemia cells. Leukemia 24: 44-50.
243. Vest RS, O'Leary H, Coultrap SJ, Kindy MS, Bayer KU (2010) Effective post-insult neuroprotection by a novel Ca(2+)/ calmodulin-dependent protein kinase II (CaMKII) inhibitor. J Biol Chem 285: 20675-20682.

244. Coultrap SJ, Bayer KU (2011) Improving a natural CaMKII inhibitor by random and rational design. PLoS One 6: e25245.
245. Sen KI, Logan TM, Fajer PG (2007) Protein dynamics and monomer-monomer interactions in AntR activation by electron paramagnetic resonance and double electron-electron resonance. Biochemistry 46: 11639-11649.